

Biosynthesis of ω -Hydroxy Fatty Acid Polyesters in *Nicotiana tabacum* Stigmas

A thesis presented to

The Faculty of Graduate Studies

of

Lakehead University

by

Marc Arman Mohammadi

In partial fulfillment of requirements
for the degree of
Master of Science in Biology

May 10th, 2023

Abstract

The aerial surfaces of all land plants are covered by hydrophobic lipid barriers that contain a core structure of polyesters derived from hydroxy fatty acids and glycerol. One type of surface lipid polyester is found in the exudates of wet stigmas of *Solanaceae* species, such as *Nicotiana tabacum*. These polyesters consist of ω -hydroxy fatty acids and glycerol, are extracellular, and have the experimental advantage of being soluble in organic solvents. However, very little is known about the biosynthesis mechanisms of stigma lipid polyesters. To gain insight into the biosynthesis of stigma lipid polyesters, I have characterized their structure and composition through stigma development and monitored polyester assembly through [^{14}C]-acetate and [^{14}C]-glycerol radiolabeling. Tobacco stigma lipids accumulate estolides consisting of ester-bonded ω -hydroxy fatty acids end-capped by normal fatty acids in the form of triacylglycerol, TAG(n), diacylglycerol, DAG(n), and free estolides, FFA(n), where n denotes the estolide bond count. These are composed primarily of oleic acid, linoleic acid, 18-hydroxyoleic acid, and 18-hydroxylinoleic acid and the estolides were identified to form on any position of the glycerol backbone. Chemical characterization of stigma lipid estolides suggest that polyester assembly occurs within the glandular zone of stigmatic tissue and then exported to the stigma surface; however, no distinctions have been made whether this process is intracellular or extracellular. Phosphatidylcholine (PC) is involved in stigma glycerolipid synthesis but not in acyl hydroxylation or estolide formation. Radiolabeled substrate accumulation suggests non-estolide glycerolipids to be synthesized through a combined *de novo* and PC-derived DAG(0)/TAG(0) pathways. A precursor-product relationship was observed in TAG(n) species and suggests that TAG(n) remodeling occurs, such that estolide polymerization occurs in a stepwise manner. These oxygenated fatty acids and estolides have physiochemical properties suitable for potential industrial uses, such as biolubricants. Identifying the mechanisms involved in the production of stigma lipid polyesters will help develop alternative sources of bio-based polymers by bioengineering plant surfaces or microorganisms. The sustainable and environmentally friendly production of these polyesters by engineered organisms is expected to result in substantial economic and environmental benefits.

Lay summary

With the impending risks associated with climate change, the demand for “green” alternatives rises such that we may reduce our waste and adapt our agriculture and industrial processes to a changing environment. The goal of this research is to further our understanding of the production of naturally occurring plant-based polymers found on the surface of the reproductive sites of tobacco flowers. This work has identified key structural arrangements of these polymers and has established similarities and differences to known biochemical processes in similar plant components. These polymers contain large amounts of highly valuable chemicals that have demonstrated use as industrial biolubricants and have the potential to replace certain petroleum-based products. Understanding the series of biochemical reactions used to produce these compounds may provide alternative ways to manufacture these valuable chemicals in a more efficient, economic, and environmentally friendly manner. Moreover, further insight into plant surface biochemistry will benefit our ability to engineer better drought and insect resistant crops.

Acknowledgements

First and foremost, I would like to express my deepest appreciation to my professor and co-supervisor Dr. Isabel Molina for her invaluable time, encouragement, and feedback over the years since I first started working in her lab. Her commitment and passion to her research is what inspired me to pursue my academic endeavors. I am also very thankful to Lakehead University and my supervisor Dr. Wensheng Qin for the administrative efforts involved with allowing me to pursue my research at Algoma University and for providing me opportunities to practice and present my research. Along with my committee members Dr. Doug Reid and Dr. Heidi Schraft, as well as Dr. Mike Pollard for the knowledge, expertise, and feedback they provided throughout my thesis research.

I am extremely grateful to Dr. Richard Bourgault for all the countless help and guidance provided in the lab, as well as to all my fellow lab members at Algoma University over years, Annika, Aseel, Amanda, Desiree, Debbie, and Jessica, for all their assistance in the lab and pleasant conversations to offset the occasional monotony of research.

Lastly, I would like to thank my family for their constant support and encouragement, especially my partner Jaclyn, to whom words cannot express my gratitude and without them I could not have undertaken this journey.

Table of Contents

Abstract	i
Lay summary	ii
Acknowledgements.....	iii
Table of Contents.....	iv
List of Tables	vii
List of Figures	viii
Key to Symbols and Abbreviations.....	x
Chapter 1: Introduction and Literature Review	1
1.1 Plant glycerolipids	1
1.2 Wet stigmas and their lipid exudates.....	3
1.3 Traditional fatty acid and glycerolipid synthesis in plants.....	6
1.4 Surface lipid structure and biosynthesis	10
1.5 Secretion of lipids to plant surfaces.....	14
1.5.1 Movement through plasma membrane	14
1.5.2 Movement through cell wall	16
1.6 Objectives	19
Chapter 2: Chemical Characterization of Developing Stigma Lipids	20
2.1 Introduction	20
2.2 Materials and Methods.....	23
2.2.1 Plant material and harvesting	23
2.2.2 Stigma lipid extraction.....	24
2.2.3 Lipid fraction isolation by thin layer chromatography (TLC).....	24
2.2.4 TLC lipid recovery.....	25
2.2.5 Monomer analysis	25
2.2.6 Partial depolymerization	26
MAG(n) ladder	26
2.3 Results.....	26
2.3.1 Tobacco stigma lipids accumulate through stigma development.....	26

2.3.2 Distribution and structure of stigma lipid estolides throughout development show polyesters are formed prior to being exported to the surface.	28
2.3.3 Characterization of the TAG(n) fraction suggests that FAME(1) is the predominant estolide chain.....	36
2.3.4 Estolides are attached to all three positions of glycerol to form TAG(n).	40
2.3.5 PC provides selected acyl groups for PAG(n) synthesis.	42
Phosphatidylcholine	42
IPPE	43
2.4 Discussion	44
2.4.1 Stigma polyesters are assembled in the glandular zone prior to surface export.	45
2.4.2 TAG(n) characterization shows an underestimation of hFA content.....	47
2.4.2 Iodine-stained densitometry is not suitable for quantitative analysis.	48
2.4.3 Estolides can occur in any glycerol position.....	48
2.4.4 Phosphatidylcholine is involved in estolide acyl desaturation but not acyl hydroxylation.	49
2.5 Conclusions	51
Appendix A	52
Chapter 3: In vivo [¹⁴C]-Tracing of Wet Stigma Lipid Metabolism	55
3.1 Introduction	55
3.2 Materials and Methods.....	63
3.2.1 Development of in planta isotope labeling assay	63
3.2.2 Radiolabeling assay	63
3.2.3 Radiolabeling analysis	63
3.2.4 Radiolabeled monomer analysis.....	64
3.3 Results.....	64
3.3.1 Development of an isotope labeling assay <i>in planta</i>	64
3.3.2 Radiolabeled substrate was incorporated into all lipid fractions demonstrating a lag phase until surface accumulation.....	67

3.3.3 A portion of radiolabeled glycerol was incorporated into acyl groups.	71
3.3.4 Estolide formation showed precursor-product relationship.....	72
[¹⁴ C]-Acetate labeling	72
[¹⁴ C]-Glycerol labeling	76
3.3.5 Oleic acid was the first labeled acyl lipid.	81
3.3.6 Labeling kinetics of non-estolide species showed similarities to expected Kennedy pathway kinetics with acyl editing and multiple DAG pools.	82
3.4 Discussion	84
3.4.1 Novel <i>in planta</i> substrate incubation is an effective method for analyzing stigma lipids.	84
3.4.2 Labeling data suggests DAG(0) and TAG(0) synthesis utilizes a combined de novo DAG/TAG and PC-derived DAG/TAG pathways.	85
3.4.3 Potential impurities in α,β -DAG(n) and FFA(n) fractions.	88
3.4.4 Estolide polymerization may occur in a stepwise manner.	89
3.5 Conclusions	94
Appendix B	95
Chapter 4: Conclusions and Future Research Goals	98
4.1 Research questions	98
4.2 Summary of findings	99
4.3 Unknowns and future experiments	100
4.4 Future applications of research	103
References.....	104

List of Tables

Table 1. Total soluble lipid composition of tobacco stigmas across developmental stages.

Table 2. Measured and expected molar ratios of ω -hFAs in TAG estolides.

Table 3. TAG(n) estolide composition and molar distribution.

Table 4. Measured and expected molar ratios of ω -hFAs in TAG estolides.

Table 5. Composition ratios of fatty and ω -hFAs in TAG(n) species and PC.

Table 6. Percent label distribution across stigma lipid fractions.

Table 7. [14 C]-acetate reaction kinetics and lag times.

Table 8. [14 C]-glycerol reaction kinetics and lag times.

Table 9. Labeled and total ω -hydroxy fatty acyl content.

Table 10. Initial substrate incorporation rates and lag times for non-estolide species.

List of Figures

Figure 1. Structure of common glycerolipids.

Figure 2. Schematic representation of triacylglycerol synthesis in oilseeds.

Figure 3. Proposed TAG biosynthesis pathway in bayberry wax.

Figure 4. Possible cutin molecular structures based on monomer type.

Figure 5. Biosynthesis and regulation of cutin.

Figure 6. TEM images of tobacco stigmas.

Figure 7. Secretion of exudate in petunia stigmas.

Figure 8. General structure of a polyacylglycerol.

Figure 9. Tobacco flower developing stages.

Figure 10. Free-hand longitudinal sections of *Nicotiana tabacum*.

Figure 11. Average fresh weight and lipid content of developing stigmas.

Figure 12. Soluble stigma lipid fractions and separation.

Figure 13. Soluble lipid class and distribution.

Figure 14. TAG(n) distribution across developmental stages.

Figure 15. FFA(n) distribution across developmental stages.

Figure 16. α,β -DAG distribution across developmental stages.

Figure 17. DAG isomer ratios relative to estolide chain length.

Figure 18. Composition of TAG(n) species.

Figure 19. Overall FAME(n) composition.

Figure 20. Flowchart for positional estolide analysis of TAG(3) and TAG(4).

Figure 21. Attempted IPPE development with MAG(n) ladder.

Figure 22. Combined de novo DAG and PC-derived DAG/TAG synthesis pathways and initial [¹⁴C] labeling flux.

Figure 23. Expected precursor-product relationships for TAG synthesis in the Kennedy pathway and its variants.

Figure 24. Incorporation of [¹³C]-glycerol in stigma lipid fractions.

Figure 25. Phosphorimager display of radiolabeled stigma lipids.

Figure 26. Time course of radiolabeled substrate accumulation in tobacco stigmas.

Figure 27. Total label distribution between internal and surface stigma lipids.

Figure 28. Acyl group and glycerol backbone labeling from [¹⁴C]-glycerol incorporation.

Figure 29. Time course of TAG(n) [¹⁴C]-acetate labeling.

Figure 30. Time course of FFA(n) [¹⁴C]-acetate labeling.

Figure 31. Time course of DAG(n) [¹⁴C]-acetate labeling.

Figure 32. DAG(n) [¹⁴C]-acetate labeling distribution between α,β -DAG(n) and α,α -DAG(n) isomers.

Figure 33. Time course [¹⁴C]-glycerol labeling of TAG(n).

Figure 34. Time course [¹⁴C]-glycerol labeling of FFA(n).

Figure 35. Time course [¹⁴C]-glycerol labeling of DAG(n).

Figure 36. Proportion of α,β -DAG(n) relative to total DAG(n) fraction.

Figure 37. Labeled acyl distribution in estolide containing species.

Figure 38. Time course of non-estolide lipid labeling.

Figure 39. Proposed lipase-mediated mechanism for TAG(n) assembly.

Figure 40. Proposed acyl-remodeling mechanism for TAG(n) assembly.

Key to Symbols and Abbreviations

ABC	ATP-binding cassette
ACC	acetyl-CoA carboxylase
ACP	acyl carrier protein
BDG	bodyguard
BHT	butylated hydroxytoluene
CDP	cytidine-diphosphocholine
CHCl ₃	chloroform
CNSC	Canadian Nuclear Safety Commission
CoA	coenzyme A
CPM	counts per minute
CPT	CDP-choline:diacylglycerol cholinephosphotransferase
CUS	cutin synthase
CXT	cutin:xyloglucan transacylase
CYP	cytochrome P450 monooxygenase
DAG	diacylglycerol
DCA	dicarboxylic acid
DCF	deficient in cutin ferulate
DCR	defective in cuticular ridges
DGAT	diacylglycerol acyltransferase
DPM	disintegration per minute
ER	endoplasmic reticulum
EtOH	ethanol
FA	fatty acid
FAD	fatty acid desaturase
FAE	fatty acid elongase

FAME	fatty acid methyl ester
FAS	fatty acid synthase
FAT	fatty acid thioesterase
FFA	free fatty acid
G3P	glycerol-3-phosphate
GC-FID	gas chromatography-flame ionization detector
GC-MS	gas chromatography-mass spectroscopy
GPAT	acyl:glycerolphosphate acyltransferase
GPDH	G3P dehydrogenase
H ₂ SO ₄	sulfuric acid
hFA	hydroxy fatty acid
hFAME	hydroxy fatty acid methyl ester
IPPE	intermediate polarity polyesters
LACS	long-chain acyl-CoA synthetase
LPA	lysophosphatidic acid
LPAT	LPA-acyltransferase
LPC	lyso-phosphatidylcholine
LPCAT	acyl-CoA:lyso-phosphatidylcholine acyltransferase
LTP	lipid transfer protein
MAG	monoacylglycerol
MeOAc	methyl acetate
MeOH	methanol
MGAT	monoacylglycerol acyltransferase
MGDG	monogalactosyldiacylglycerol
NaOMe	sodium methoxide
NSCA	Nuclear Safety and Control Act
PA	phosphatidic acid

PAG	polyacylglycerol
PAP	Phosphatidic acid phosphohydrolase
PC	phosphatidylcholine
PDAT	phospholipid:diacylglycerol acyltransferase
PDCT	phosphatidylcholine:diacylglycerol cholinephosphotransferase
PE	phosphatidylethanolamine
PEP	phosphoenolpyruvate
PI	phosphatidylinositol
PL	polar lipid
Rf	retention factor
RP-TLC	reverse phase TLC
SAD	stearoyl-ACP desaturase
<i>sn</i>	stereospecific numbering
TAG	triacylglycerol
TEM	transmission electron microscopy
TLC	thin layer chromatography
TMS	trimethylsilyl
WBC	white-brown complex

Chapter 1: Introduction and Literature Review

1.1 Plant glycerolipids

Glycerolipids constitute a large group of structurally and functionally diverse molecules in plants. These consist of at least one hydrophobic chain connected through either an ester or ether bond to a glycerol backbone. In a glycerolipid, the number and the characteristics of the molecules linked to the hydroxyl groups in glycerol provides the basis for its purpose. Such molecules include a variety of fatty acyl groups (e.g. oleic acid) or non-acyl functional groups, such as carbohydrates (e.g. galactose) or charged molecules (e.g. phosphocholine; Fig.1-B). These groups affect the overall glycerolipid hydrophobicity, polarity, reactivity, and ability to form lipids bilayers. Thus, structural variations in these molecules greatly impact their functions such that triacylglycerols (TAGs) of oil bodies act as storage for energy and carbon, phospholipids of cellular membranes allow for compartmentalization of metabolism, the galactolipid-rich thylakoid membrane acts as the reactive center for photosynthesis, and released glycerolipid acyl groups can provide strong signaling for abiotic stress tolerance, pathogen defense, and reproductive development (Wang et al, 2019).

One of the key adaptations of vascular plants to life on land was the ability to produce complex, cell wall-specific macromolecule structures that interact with the external environment (Delwiche & Cooper, 2015). All aerial plant surfaces are protected by a hydrophobic lipid barrier. Such structures include two types of polymers of fatty acids (FAs) that are associated with the cell wall, cutin and suberin (Yeats & Rose, 2013). These have protective functions against biotic and abiotic factors, providing a physical barrier against pathogens and preventing drought stress through the control of water exchange. Cutin is the framework of the cuticle layer synthesized by the epidermal cells of aerial primary tissues of plants; it is deposited on the outside of the cell wall. Suberin is deposited on the internal side of (facing the plasma membrane) of cork cell walls of specialized tissues, including root, stem and tuber periderms, root endodermis and bundle sheath cells. The focus of this thesis is on a less ubiquitous lipid polyester found in the exudate of wet stigmas.

Cutin, suberin and glycerolipids of wet stigma exudates are lipid polyesters of ω -hydroxy fatty acids (ω -hFAs) and glycerol. However, cutin and suberin also contain other oxygenated FAs including dicarboxylic acids, polyhydroxy FAs, and epoxy-FAs, as well as phenolics (Kolattukudy, 1981; Pollard et al, 2008). Furthermore, suberin composition is even more complex as it contains a lignin-like polyphenolic domain in addition to the lipid polyester. The monomer composition of cutin and suberin allow for high levels of interlinking which gets presented as an insoluble, tightly knit matrix (Fig.1-D). However, wet stigma exudate polyesters consist of extractable triacylglycerides and diacylglycerides (Matsuzaki, 1983a; Han et al, 2010). Between lipid polyesters, stigma lipids are more chemically similar to cutin and are also found on the outermost side of the cell wall, thus the remainder of this chapter focuses on cutin and stigma lipid polyesters.

Studies on the metabolism of surface lipids can be challenging because they are solely synthesized by epidermal cells, which are most active in developing tissues, and because waxes and cutins are usually present in lower concentrations than membrane and storage lipids. Interpolating the fluxes intended for general lipid metabolism and for cuticular lipid secretion may therefore be difficult. Bayberry fruits were identified to be an alluring model for studying surface lipid metabolism as they contain very high amounts of lipids accumulated on their surface and these lipids are steadily synthesized on fully grown tissue which allows for prolonged time course experimentation (Simpson & Ohlrogge, 2016). The bayberry surface wax is composed almost exclusively of TAG, diacylglycerol (DAG), and monoacylglycerol (MAG) which differs from typical plant surface waxes. These glycerolipids are speculated to be synthesized in an alternate manner than acylglycerols in oilseeds.

Similarly, the lipids found in wet stigma exudates contain primarily TAG and DAG. However, a major distinction from both bayberry fruit wax and oilseeds (Fig.1-A) is that these lipids contain unusual FAs, namely 18:1 and 18:2 ω -hFA (Fig.1-C; Koiwai & Matsuzaki, 1988). Tobacco stigma lipids have been previously characterized by Matsuzaki *et al* (1983a; 1983b; 1983c; 1986) and prove to be good models to study these extracellular lipid polyesters as they accumulate in large quantities on the stigma surface, are present from early stages of development and continue to accumulate through mature stages. Furthermore, similar lipid polyesters are found in the wet stigma of petunia as well, another model organism, with much higher ω -hFA content (96% vs

56% in tobacco; Koiwai & Matsuzaki, 1988). However, petunia stigma lipids contain a much higher acyl per glycerolipid ratio than tobacco, making it difficult to experimentally manipulate these much longer polyesters. On the other hand, methods to separate and isolate multi-acyl glycerolipid fractions in tobacco stigmas have been developed (Matsuzaki *et al*, 1983b; 1986).

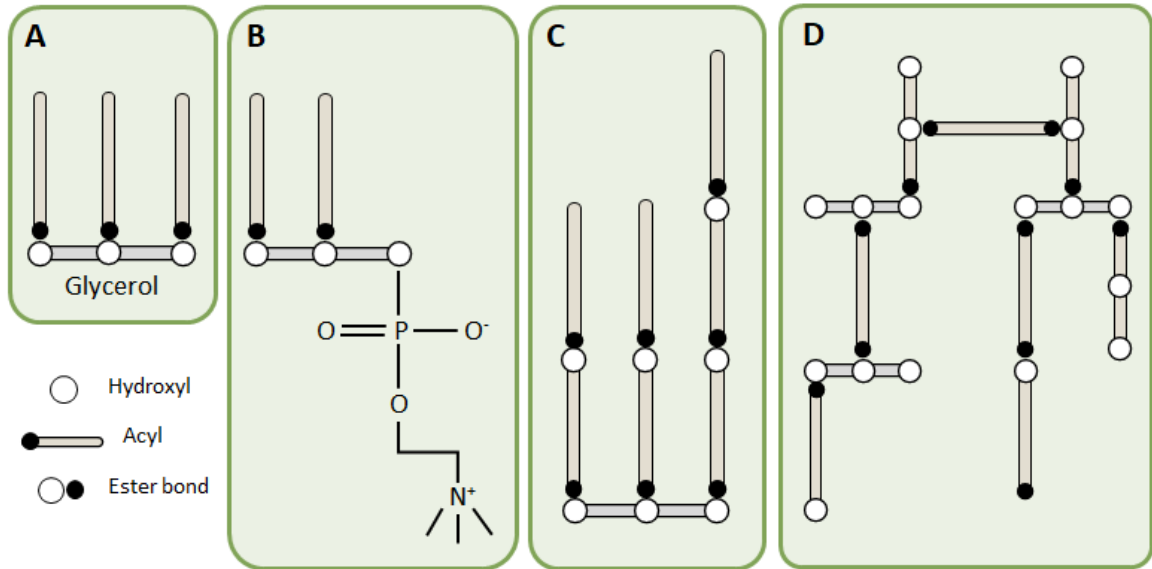


Figure 1. Structure of common glycerolipids. A: Oilseed triacylglycerol. B: Membrane lipids; phosphatidylcholine. C: Tobacco stigma polyester. D: Putative cutin polyester arrangement.

1.2 Wet stigmas and their lipid exudates

The stigma is the part of the female reproductive organ in angiosperms (flowering plants). It is located at the head of the pistil and acts as the pollen receptacle where it captures and protects pollen, helps mediate selective pollen discrimination, and promotes pollen hydration and germination. Typically, stigmas are distinguished into two major categories: wet stigmas, commonly found in Solanaceae species, which contain a free-flowing secretion, and dry stigmas which instead contain an overlaying pellicle (Heslop-Harrison & Shivanna, 1977). The exudate secretion consists of a variety of proteins, lipids, sugar, and pigments (e.g., chlorophylls) (Cresti *et al*, 1986). Stigma lipids are thought to be necessary for directing the flow of water to pollen to allow for pollen-tube growth (Wolters-Arts *et al*, 1998). These lipids are primarily polyacylglycerols, such as diacylglycerol (DAG) and triacylglycerol (TAG), which are assembled from ω -hFAs

and normal FAs in which composition varies between species (Koiwai & Matsuzaki, 1988) (Fig.1-C). In plants, generally seeds, pollen, and fruit mesocarp contain the most abundance of TAG accumulation, although such TAGs rarely contain modified FAs such as ω -hFAs.

Oilseed crops generally accumulate lipids in the form of TAG which consist primarily of normal FAs: for example, soybean (Pryde, 1980), rapeseed (Zaderimowski & Sosulski, 1978), *Arabidopsis thaliana* (Li *et al*, 2006), and *Camelina sativa* (Abramovic & Abram, 2005). The most common FAs present in seed oil TAG are palmitic acid (16:0), stearic acid (18:0), oleic acid (18:1 Δ^9), linoleic acid (18:2 $\Delta^{9,12}$), and α -linolenic acid (18:3 $\Delta^{9,12,15}$) (Miklaszewska *et al*, 2021). However, in oilseeds, many other FAs have been discovered in various oilseeds such as gondoic acid (20:1 Δ^{11}) and erucic acid (22:1 Δ^9) in the Brassicaceae family (i.e., rapeseed), or ricinoleic acid (12-OH 18:1 Δ^9) in castor oil (Binder *et al*, 1962). In contrast, jojoba seed oil stores its lipids in the form of liquid wax esters composed primarily of very long chain (20–24 carbons) monounsaturated FAs and alcohols (Miwa, 1971).

Pollen TAG seem to be constructed of the same core oilseed FAs where in both rapeseed and arabidopsis are composed primarily of 18:3 (50-65%) and 16:0 (20-25%) (Piffanelli *et al*, 1997; McDowell *et al*, 2013). Similarly, both avocado and olive fruit mesocarp TAG show very high amounts of monounsaturated FAs (65% and 75%, respectively) and low saturated FAs (20% and 15%, respectively) (Gaydou *et al*, 1987; Ollivier *et al*, 2003). However, bayberry fruit waxes contain TAG, DAG, and MAG that are distinctly composed of saturated FAs (Harlow *et al*, 1965).

The presence of ω -hFAs in plant TAG is demonstrated in both wet and certain dry species' stigmas and are composed of 18-OH 18:1 Δ^9 and 18-OH 18:2 $\Delta^{9,12}$ hFAs (Koiwai & Matsuzaki, 1988). The dry stigma species with the highest ω -hFA content was found to be the snapdragon, *Antirrhinum majus*, (33% of stigma lipid content), while that in the wet stigma species is petunia at 96% ω -hFA of total stigma lipid content (Koiwai & Matsuzaki, 1988). Studies in tobacco (56% ω -hFA content of stigma lipid fraction) have determined that the structure of these ω -hFA-containing TAG differs to that of traditional TAG (Matsuzaki *et al*, 1983a; 1983b; 1986). The ω -hFA can form estolides, such that the terminal hydroxyl group of one acyl can be esterified to the carboxyl group of another, forming a linear polyester. In stigma glycerolipids, these estolides are esterified

to the glycerol backbone and can construct a TAG composed of more than three acyl groups. Estolides have been shown to occur in both DAG and TAG species and the polyester chains have been shown to contain ω -hFAs end-capped by a normal FA (Matsuzaki *et al*, 1983b; 1986).

These estolides, however, are not unique to stigma lipid TAG. The presence of polyacylglycerols (PAG) containing more than three FAs, including hFAs, have been reported in multiple plant species, namely their seed oils. Greek thistle, *Chamaepeuce afra*, seed oil was shown to contain a pentaacyl TAG in which a 9,10,18-trihydroxyoctadec-cis-12-enoic acid (9,10,18-OH 18:1 Δ^{12}), bound to the central position of the glycerol backbone, has its terminal and one mid-chain hydroxyl groups acylated (Mikolajczak & Smith, 1968). Chinese tallow tree, *Sapium sebiferum*, seed oil was found to contain a tetraacyl TAG in which a trans-2,cis-4-decadienoic acid (10:2 $\Delta^{2,4}$) is joined in an estolide linkage to 8-hydroxy-5,6-octadienoic acid (8-OH 8:2 $\Delta^{5,6}$) in the glycerol's third position (Sprecher *et al*, 1965). The presence of tetra-ricinoleic acid (12-OH 18:1 Δ^9) TAG was identified in castor oilseeds (Lin *et al*, 2006) and ergot oilseeds, *Claviceps purpurea*, were found to contain up to hexaacyl TAG with ricinoleic acid estolides (Morris & Hall, 1966). Tetra- and pentaacyl TAG containing isoricinoleic acid (9-OH 18:1 Δ^{12}) was identified in *Apocynaceae* subfamily species *Adenium obesum* (desert rose) and *Nerium oleander* (Smith & Zhang, 2016). A variety of *Lesquerella* and related species were found to contain mono- and di-estolides derived from lesquerolic acid (14-OH 20:1 Δ^{11}) and auricollic acid (14-OH 20:2 $\Delta^{11,17}$) on the outer positions of glycerol (Hayes *et al*, 1995). Estolide-containing TAG in both kamala, *Mallotus philippinensis*, and false white teak, *Trewia nudiflora*, seed oils consist of kamlolenic acid (18-OH 18:3 $\Delta^{9,11t,13t}$) in only one position of the glycerol backbone with up to 14 total FAs, with the latter more likely to be "end-capped" by a normal FA (Rajiah *et al*, 1976; Smith *et al*, 2013). Lastly, estolides are not limited to TAG and DAG species but also seen in galactolipids: mono-, di-, tri-, and tetra-galactosyldiacylglycerol (MGDG, DGDG, TriGDG, and TetraGDG) were discovered to contain estolides in oat kernels, *Avena sativa*, with up to three additional avenoleic acid (15-OH 18:2 $\Delta^{9,12}$) molecules (Hamburg *et al*, 1998; Moreau *et al*, 2008).

Plant estolides have the potential to be used as lubricants, plasticizers, cosmetic additives, and hydraulic fluid, for example, and show many physical properties in which they outperform regular vegetable oils (Hayes & Kleiman, 1995; Isbell *et al*, 2001;

Zerkowski, 2008). Vegetable oils are generally prone to thermal oxidation and fail to maintain their desirable properties at low temperatures such that additives are used to supplement these properties but at the cost of biodegradability, toxicity, and price (Becker & Knorr, 1996; Lal & Carrick, 1994). Estolides are a cost-effective and biodegradable alternative to vegetable oils while maintaining a similar function. The authors of Isbell *et al* (2001) identify the melting points and viscosity ratings of various oils, FAs, and estolides which are important metrics in applications such as lubricants. Their results show that the viscosity of oils increases exponentially with respect to the increasing oligomerization of estolides while the pour point, the lowest temperature at which the oil remains mobile, decreases with decreasing oligomerization of estolides. Also, hydrogenation of unsaturated estolides was shown to increase the pour point but had no significant effect of the viscosity. In another study, capping the hydroxyl moiety of estolides, observed in kamala and false white teak seed oils, was shown to reduce viscosity, and increasing the acyl chain length increases viscosity (Isbell *et al*, 2006). Free acyl estolides containing both hydroxy and unsaturated FAs were shown to have great potential for a wide range of industrial lubricant applications due to their oxidative stability and useful properties at cold temperatures (Isbell, 2011).

The crucial distinction between oilseed and stigma estolides is that oilseed lipids are stored in cytosolic lipid droplets while stigma lipids accumulate extracellularly and on the stigma surface (Harlow *et al*, 1965). Surface lipids have been shown to be more resistant to deterioration than internal lipids, especially during plant senescence (Yang & Ohlrogge, 2009). Therefore, this may provide an advantage in harvesting desirable estolides for large scale production. The potential for identifying a new pathway for extracellular lipids may show important industrial applications in producing high value estolides.

1.3 Traditional fatty acid and glycerolipid synthesis in plants

Glycerolipids are composed fundamentally of a glycerol backbone and acyl groups. The glycerol backbone is derived from G3P (glycerol-3-phosphate) which can be synthesized from three potential sources: 1) glucose via glycolysis (Margolis & Vaughan, 1962), 2) pyruvate and other intermediates in the citric acid cycle through glyceroneogenesis (Reshef *et al*, 1969), and 3) glycerol through glycerol kinase (Turner *et al*, 2003).

Fatty acid biosynthesis occurs in the plastid by two enzyme systems: ACETYL-COA CARBOXYLASE (ACC) and FATTY ACID SYNTHASE (FAS) (Wakil & Stoops, 1983). A greatly simplified description of this process starts with two molecules of acetyl-CoA, one is converted to malonyl-CoA through the enzyme ACC. Acyl transferases replace the CoA portion of these two molecules with acyl carrier proteins (ACP) and then subsequent acylation of acetyl-ACP and malonyl-ACP occurs to form ACP-bound palmitic acid (16:0), stearic acid (18:0), or oleic acid (18:1). Such mechanism requires recurrent condensation, reduction of a 3-keto group, condensation, and then double bond reduction reactions for acyl chain elongation. This process is terminated by FATTY ACID THIOESTERASE proteins (FAT) by releasing the acyl groups from ACP. The release of 16:0 and shorter acyl groups is catalyzed by FATB, while 18:0 and 18:1 are catalyzed by FATA (Ohlrogge & Browse, 1995). The desaturation of 18:0 to 18:1 occurs in the plastid prior to release by STEAROYL-ACP DESATURASE (SAD). These three FAs, along with linoleic acid (18:2) and linolenic acid (18:3) make up the majority of all vegetative oil acyl chains (Töpfer *et al*, 1995). Certain species will produce shorter chain FAs, such as lauric acid (12:0), the most common medium chain FA found in coconut oil (Laureles *et al*, 2002). Plastidial FAs are then activated to form coenzyme A thioesters by LONG-CHAIN ACYL-COA SYNTHETASE (LACS; Lü *et al*, 2009; Schnurr *et al*, 2004) and transported to the endoplasmic reticulum (ER), where further FA modifications, such as elongation, reduction, or hydroxylation take place.

Various pathways exist for the biosynthesis of DAG and TAG in plants (Chapman & Ohlrogge, 2012; Bates & Browse, 2012). The simplest is known as *de novo* DAG/TAG synthesis, the Kennedy pathway, or the glycerol phosphate pathway (Fig.2-green; Weiss & Kennedy, 1956; Weiss *et al*, 1960). This process takes place in the cell ER and begins with the acylation of G3P with a fatty acyl-CoA. This occurs in the *sn*-1 position by a GLYCEROL-3-PHOSPHATE ACYLTRANSFERASE (GPAT) to form lysophosphatidic acid (LPA). Then, the *sn*-2 position is acylated by ACYL:GLYCEROPHOSPHATE ACYLTRANSFERASE (GPAT) to create phosphatidic acid (PA). The phosphate group (on *sn*-3) is then hydrolyzed by a group of PHOSPHATIDIC ACID PHOSPHOHYDROLASE (PAP) enzymes to form a DAG. Finally, one last acylation occurs in the *sn*-3 position by DIACYLGLYCEROL ACYLTRANSFERASE (DGAT) enzymes. In this pathway, only the DGAT enzymes are unique for TAG synthesis, as PA and DAG are used as precursors for membrane lipids.

The membrane lipid phosphatidylcholine (PC) is also a crucial intermediate in the biosynthesis of both TAG and other membrane lipids. Modified FAs that are most commonly found in membrane and storage lipids (i.e. 18:2 and 18:3) and rely on ER-bound enzymes that act upon FAs esterified to PC (Sperling *et al*, 1993). For example, 18:1-PC is desaturated to 18:2-PC, and again to 18:3-PC through the FATTY ACID DESATURASE FAD2 (Okuley *et al*, 1994) and FAD3 (Arondel *et al*, 1992) enzymes, respectively. Furthermore, other FAs with unusual double bond positions or functional groups can be PC-produced, such as the production of ricinoleic acid through a FA hydroxylase (Moreau & Stumpf, 1981). These modified-FAs can be incorporated in DAG/TAG synthesis through a process called “acyl editing” which involves a deacylation-reacylation cycle of PC (Fig.2-pink; Bates *et al*, 2007). The releases of an acyl group from PC forms lyso-PC (LPC) and is mediated by either the reverse reaction of ACYL-COA:LYSO-PHOSPHATIDYLCHOLINE ACYLTRANSFERASE (LPCAT; Stymne & Stobart, 1984) or phospholipase A (Chen *et al*, 2011). A new acyl group can then re-esterify to LPC through LPCAT to reform PC. The released FAs enter the acyl-CoA pool and can then be used for *de novo* DAG/TAG synthesis. Another feature of the acyl editing cycle is that PC can directly transfer its *sn*-2 acyl group to the *sn*-3 hydroxyl of DAG to generate TAG (and LPC) using the PHOSPHOLIPID:DIACYLGLYCEROL ACYLTRANSFERASE (PDAT; Dahlqvist *et al*, 2000).

Glycerolipids rich in PC-modified FAs can also be produced through a PC-derived DAG pool (Fig.2-yellow). The production of PC is derived from *de novo* DAG through CDP-CHOLINE:DIACYLGLYCEROL CHOLINEPHOSPHOTRANSFERASE (CPT; Slack *et al*, 1983; 1985; Vogel & Browse, 1996) or PHOSPHATIDYLCHOLINE:DIACYLGLYCEROL CHOLINEPHOSPHOTRANSFERASE (PDCT; Lu *et al*, 2009). The former generates a net PC production from DAG, while the latter swaps the phosphocholine and hydroxyl groups from PC and DAG respectively, resulting in no net accumulation of either species. Once PC is formed, the esterified FAs can be subjected to modification and acyl editing, then DAG can be derived from this PC molecule through the removal of the phosphocholine headgroup. PC-derived DAG can be produced through PDCT interconversion (Lu *et al*, 2009), the reverse CPT reaction (Slack *et al*, 1983; 1985), or it can be lipase mediated using phospholipase C or D (Lee *et al*, 2011) and the aforementioned PAP. The new PC-derived DAG pool can then be used for TAG synthesis. All plants may have the ability to use each of these alternative

metabolic pathways but the relative flux of *de novo* and PC-derived DAG/TAG synthesis may vary among plant species.

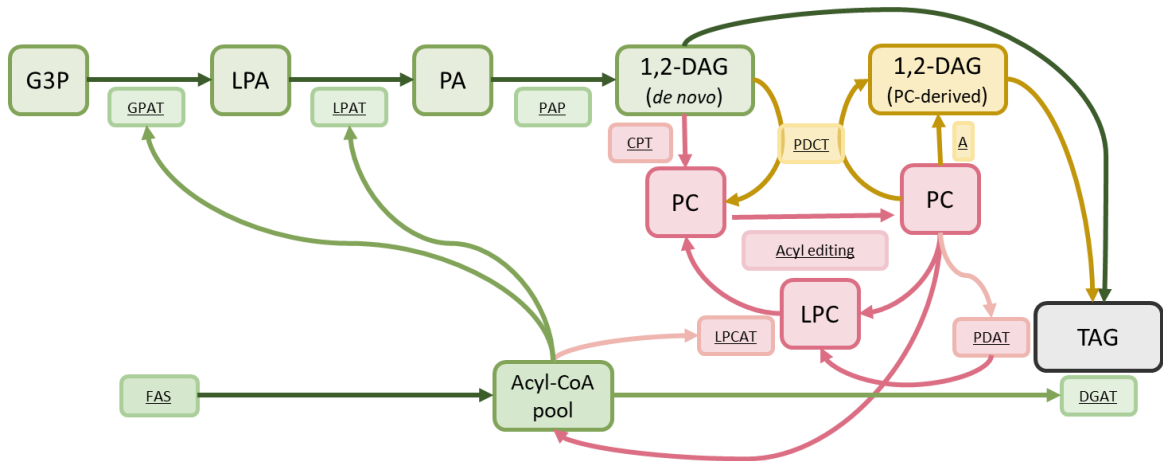


Figure 2. Schematic representation of triacylglycerol synthesis in oilseeds (Adapted from Allen *et al*, 2015). Enzymes are underlined>. *De novo* DAG/TAG synthesis pathway in green, acyl-editing cycle in pink, and PC-derived DAG/TAG synthesis in yellow. Acyl editing cycle may include reverse LPCAT or phospholipase A for acyl release and FAD2, FAD3, FA hydroxylase, etc. for acyl modification. The enzyme process marked as “A” may involve reverse CPT, PAP, or phospholipase C or D.

An alternative method for TAG biosynthesis involves using MAG as a substrate. While MONOACYLGLYCEROL ACYLTRANSFERASE (MGAT) enzymes are typically associated with lipid absorption in animal intestines (Yen *et al*, 2002; Yen & Farese, 2003), the expression of these genes in plants provided an independent and complementary pathway for TAG synthesis using MAG as a substrate (Petrie *et al*, 2012). Similarly, a natural MAG pathway has been proposed for the biosynthesis of TAG accumulating in the surface wax of bayberry fruits (Simpson & Ohlrogge, 2016). Like the Kennedy pathway, this process begins with the acylation of G3P, however such acylation occurs uniquely in the *sn*-2 position, similarly to the pathway used in cutin and suberin biosynthesis (Pollard *et al*, 2008). It is proposed that MAG intermediates can then be used to synthesize DAGs by an unidentified MAG:MAG transacylase and then transported outside the cell along with excess *sn*-2 MAG. The TAGs can then be formed by MAG:DAG transacylase, where a free *sn*-2 MAG provides the third and final acyl

chain (Fig.3). While this mechanism is still hypothetical, radiolabeling data in Bayberry wax supports this proposal (Simpson & Ohlrogge, 2016). It is possible, however, that DAG assembly may also occur outside the cell.

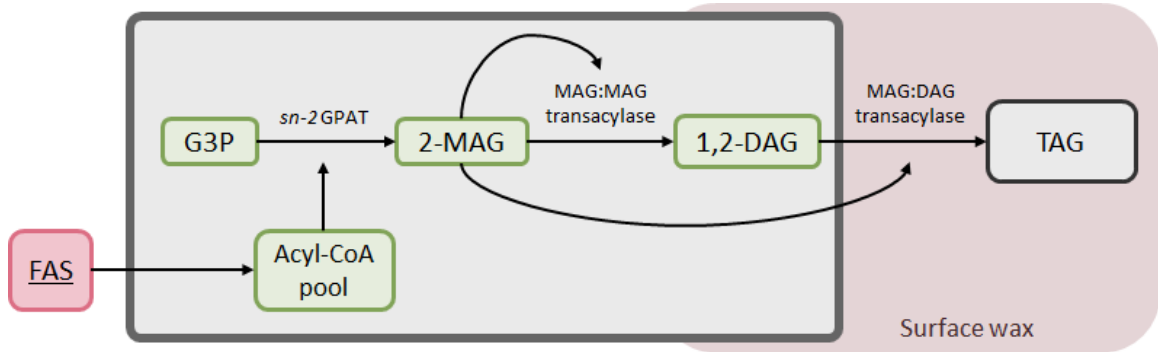


Figure 3. Proposed TAG biosynthesis pathway in bayberry wax (Adapted from Simpson & Ohlrogge, 2016).

1.4 Surface lipid structure and biosynthesis

In plants, the cuticle represents the main interface between the plant surface and its environment (Delwiche & Cooper, 2015). The cuticle is a hydrophobic layer that consists of waxes and cutin. Waxes are a chemically diverse group of compounds that has the common characteristic of being soluble in organic solvents. Generally, waxes consist of very long chain aliphatics (at least 20 carbons in length), including alkanes, alcohols, FAs, aldehydes, and wax esters. Triterpenoids and phenylpropanoids are often part of cuticular wax extracts (Jetter *et al*, 2006). Cutin, however, is an insoluble polyester typically consisting of glycerol and long-chain hFAs, mostly 16 or 18 carbons in length, the latter with up to one or two degrees of unsaturation: i.e., 16:0, 18:0, 18:1, and 18:2 (Yeats & Rose, 2013). Additionally, cutin may also include unsubstituted FAs, unsaturated dicarboxylic acids, epoxides and phenylpropanoids. Because cutin is insoluble in organic solvents, it is challenging to investigate its native structure and biosynthesis. These polymers are generally studied by depolymerizing the cell wall residues after exhaustive solvent extractions to remove any non-membrane-bound lipids (Kolattukudy, 1981).

Monomer profiles of cutin may vary between species, and even among organs and developmental stages within a single species (Kolattukudy, 1981). While at least six variations of cuticle fine structure have been identified by transmission electron microscopy (TEM), how these translate to cutin composition and structure is unclear (Jeffree, 2006). The structure of cutin may depend on its composition as the amount and position of hydroxyl groups allow for ester linkages: terminal (ω) hFAs only contribute to single chain elongation, while mid-chain hydroxyl groups allow for branching to occur, and the presence of dicarboxylic acids allows for cross-linking between chains (Fig.4; Pollard *et al*, 2008). Different models have been proposed based on the monomer chemical composition after depolymerization. For example, Arabidopsis stem and leaf cutin is very rich in dicarboxylic acids (DCA) and contains 14% weight in glycerol, research has shown a 2:1 molar ratio of glycerol to DCA and proposes that “glycerol-DCA-glycerol” is a dominant structural motif (Yang *et al*, 2016). However, tomato fruit cutin composition is vastly different; it is composed primarily of 9(10),16-dihydroxyhexadecanoic acid (9/10,16-OH 16:0) which accounts for 81.5% (w/w) with only 1.1% (w/w) glycerol content (Holloway, 1982; Graça *et al*, 2002). Both linear and branched ester linkages have been shown to occur in tomato cutin (Graca & Lamosa, 2010).

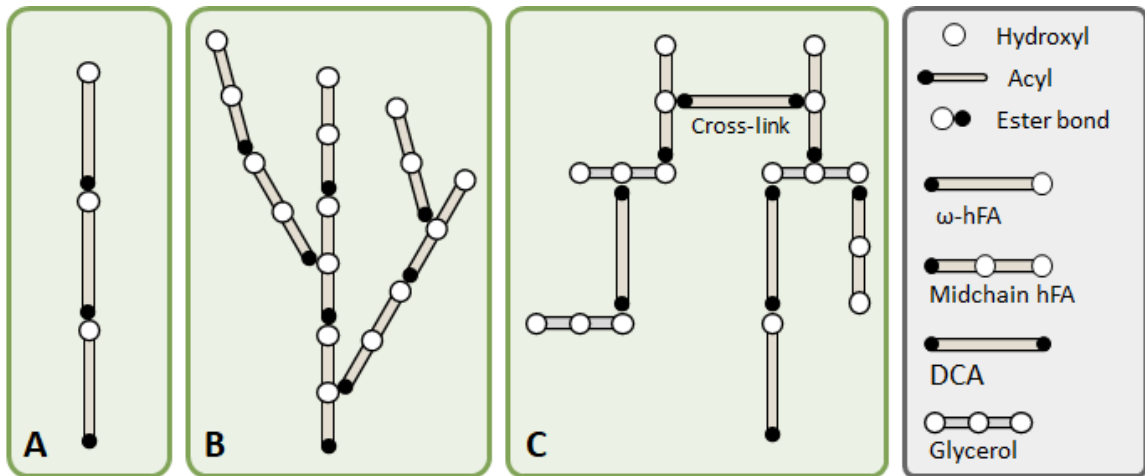


Figure 4. Possible cutin molecular structures based on monomer type. A: Linear cutin chain with ω -hFA. B: Dendritic or branching structure with midchain hydroxyl groups. C: Cross-linking of multiple chains with dicarboxylic acids (DCA).

The biosynthesis of cutin has mostly been studied in Arabidopsis, a species that paradoxically produces a cutin rich in dicarboxylic acids rather than hFAs (Bonaventure *et al*, 2004). Cutin monomers are derived from plastidial FAs synthesized identically to those described above and transported to the ER as long chain fatty acyl-CoA. Cutin long chain FA precursors are oxidized by ER-localized cytochrome P450 enzymes of the CYP86A subfamily for terminal carbon oxidation (Duan & Schuler, 2005), and CYP77A subfamily for mid-chain carbon oxidation (Li-Beisson *et al*, 2009). Then, GPAT enzymes transfer the hydroxy acyl from the acyl-CoA to G3P exclusively to the *sn*-2 position (GPAT4, GPAT6, and GPAT8; Li *et al*, 2007), forming the monohydroxyacylglycerol (*sn*-2-MAG) cutin precursor. These precursors are transported across the plasma membrane, and through polysaccharide cell walls to the site of polymerization (Fig.5).

The only known enzymes to be involved in the polymerization step of cutin are CUTIN SYNTHASE 1 (CUS1), a GDSL lipase/esterase first discovered in tomatoes (Girard *et al*, 2012; Yeats *et al*, 2012), and CUTIN SYNTHASE 2 (CUS2), identified in Arabidopsis (Hong *et al*, 2017). CUS1 was shown to polymerize 2-MAG precursors by transesterification of the terminal hydroxyl groups *in vitro*, but contrastingly prefers mid-chain hydroxyl groups *in vivo* (Yeats *et al*, 2016). Furthermore, this cutin synthase has been demonstrated with tomato primary and secondary alcohols to have enantioselectivity to favor the esterification of secondary hydroxyl groups (Bakan & Marion, 2017). In Arabidopsis, CUS2 was determined to be primarily required for cuticular ridge maintenance in sepals during cellular expansion (Hong *et al*, 2017). Furthermore, other proteins are involved in cutin synthesis, for example the protein BODYGUARD (BDG) plays a crucial role involving C18 unsaturated monomer, but its specific biochemical function is still unclear; it has been speculated that it may act as an extracellular transacylase for Arabidopsis cutin precursors (Kurdyukov *et al*, 2006; Jakobson *et al*, 2016). DEFECTIVE IN CUTICULAR RIDGES (DCR) is required for mid-chain hFA incorporation into cutin (Panikashvili *et al*, 2009; Lashbrooke *et al*, 2016), while another member of the same family of HXXXD-motif acylCoA-transferases, DEFICIENT IN CUTIN FERULATE (DCF), catalyzes the transfer of ferulic acid from CoA to an ω -hFA and incorporates ferulate in cutin (Rautengarten *et al*, 2012). Evidence suggests that the linkage of cutin to the polysaccharide cell wall occurs via a covalent linkage mechanism of ester-linked cutin and xyloglucan heteropolymers generated by CUTIN:XYLOGLUCAN TRANSACYLASE (CXT) activity (Xin & Fry, 2021).

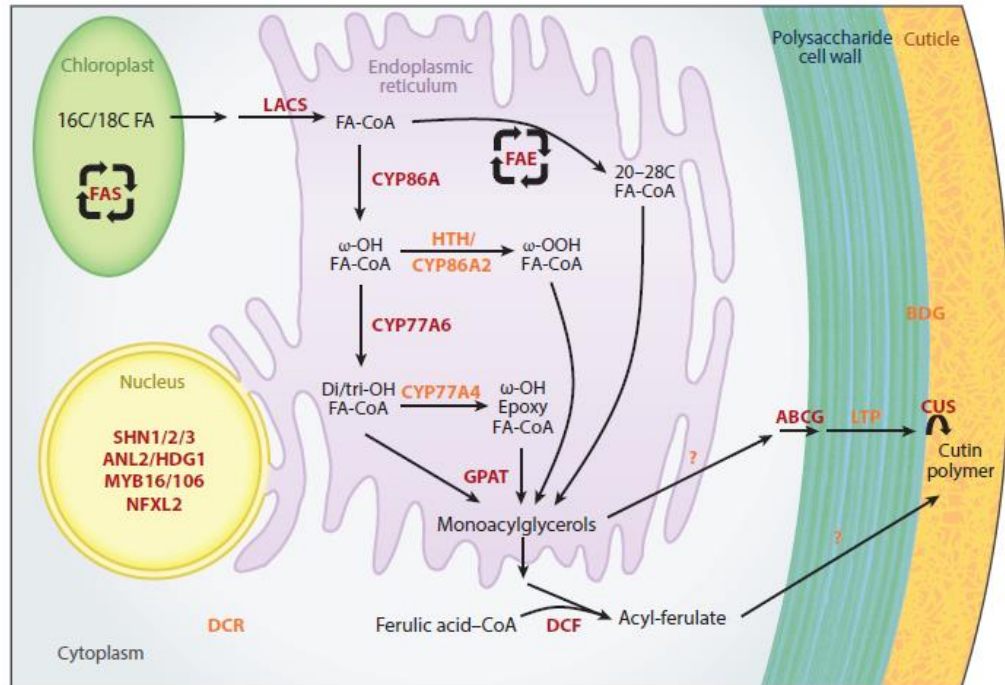


Figure 5. Biosynthesis and regulation of cutin (Fich *et al*, 2016). Proteins and complexes denoted in red have a demonstrated function, whereas those in orange have unproven or unknown function.

The focus of this research is to identify the mechanism of biosynthesis for soluble stigma lipid polyesters. So far, the only known enzyme involved in stigma exudate TAG biosynthesis is the cytochrome P450 monooxygenase, CYP86A22 (Han *et al*, 2010). This enzyme was identified as the key fatty acyl-CoA ω -hydroxylase responsible for ω -hFA biosynthesis in *Petunia hybrida* stigmas, which is a necessary substrate for estolide-containing TAG formation. RNAi suppression of CYP86A22 in petunia stigma showed essentially no estolides in the resulting DAG and TAG fractions and the enzyme was shown to prefer CoA activated acyl groups. Interestingly, CYP86A22 is an ortholog of AtCYP86A2, an enzyme required for cutin biosynthesis (Xiao *et al.*, 2004). This suggests at least one known commonality between stigma lipid biosynthesis and the cutin pathway. Alternatively, stigma TAG synthesis could involve a novel, not yet described pathway.

1.5 Secretion of lipids to plant surfaces

Once synthesized, surface lipids need to be transported from their location of biosynthesis to and through the cell membrane, and then travel through the hydrophilic and charged environment of the cell wall (Samuels *et al*, 2008). Various mechanisms for surface lipid transport have been proposed. The transport of cuticular lipids (i.e., wax and cutin precursors) from the endoplasmic reticulum (ER) to the plasma membrane likely involves one or many of the following: plasma membrane fusion sites, cytoplasmic carrier proteins, oleophilic droplets, or Golgi-mediated secretion vesicles (Pollard *et al*, 2008; Samuel *et al*, 2008; Li-Beisson *et al.*, 2013). A Golgi transport mutant was shown to influence surface wax accumulation, but it was uncertain if this mutation affected wax transport directly (McFarlane *et al*, 2014). Oil bodies in high cutin-producing epidermal cells have been shown through transmission electron microscopy (TEM) to fuse with the plasma membrane and may be involved with lipid secretion however the presence of cuticular lipids in these oil bodies have yet to be concluded (Hoffman-Benning & Kende, 1994).

The intracellular movement of TAG has been reported in certain organisms but not yet in plants. In mammary epithelial cells, the TAG-rich fat droplets in milk are secreted by a unique mechanism; microlipid droplets fuse and migrate to apical regions of the plasma membrane where they are enveloped (Heid and Keenan, 2014). This envelopment of the plasma membrane causes the release of the lipids into the surrounding extracellular space. In arbuscular mycorrhizal fungi, TAG containing lipid bodies were shown to travel through cells with the cytoplasmic stream, moving from intraradical to extraradical mycelium (Bago *et al*, 2002).

1.5.1 Movement through plasma membrane

The involvement of ATP-binding cassette (ABC) transporters is ubiquitous in all biological organisms (Neumann *et al*, 2017). These proteins use the energy released from ATP hydrolysis to overcome electrochemical and concentration gradients to transport a broad range of molecules, including but not limited to surface coating materials, defense molecules, and hormones across cell membranes. ABC transporters consist of nucleotide binding domains and transmembrane domains. In eukaryotes, only one of each domain is present forming a half-transporter that requires either homo- or heterodimerization for full functionality (Higgins, 1992). Multiple subfamilies of ABC

transporters exist however surface lipids seem to rely primarily on the G class of these proteins, which presents its nucleotide binding domains and transmembrane domains in the reverse order (Verrier *et al*, 2008).

Cuticular monomers produced within the epidermal cells need to be transported across the plasma membrane, and through polysaccharide cell walls to the site of polymerization. Although the lipid-enzyme interactions of this process is not yet fully understood (Philippe *et al*, 2022), ABC transporters are believed to mediate cutin precursor (i.e., *sn*-2-MAG) transport across the plasma membrane, such as the ABCG half-transporters ABCG11 (Bird *et al*, 2007) and ABCG13 (limited to flower cuticle; Panikashvili *et al*, 2011), as well as the ABCG full-transporter ABCG32 (Bessire *et al*, 2011; Fabre *et al*, 2016). ABCG11 was required to form a homodimer for cutin accumulation in *Arabidopsis*; heterodimers with ABCG12 (CER5) only affected wax deposition (Bird *et al*, 2007). While mutants for these transporters display apparent wax and cutin reductions, *in vitro* recreations have not proven their ability to transport specific cuticular lipids.

The transport of bayberry wax precursors is not yet understood, however some of the most highly expressed gene transcripts were related to transport (Simpson *et al*, 2016; Simpson & Ohlrogge, 2016). The most abundant ABCG transporter gene expressed is ABCG1 which functions as a homodimer. The expression increases 20-fold throughout bayberry fruit development and is expressed 3 to 5 times higher than the next highest expressed ABCG transporter. A homolog of this transporter has been reported to be involved in suberin production for potato tuber (Landgraf *et al*, 2014) and for *Arabidopsis* root, seed coat, and pollen wall (Yadav *et al*, 2014).

The mechanism of transport of stigma lipid polyesters to the surface may involve the ABC transporter gene NtWBC1 (*Nicotiana tabacum* ABC transporter of the White–Brown Complex subfamily; Otsu *et al*, 2004). The white-brown complex falls under the G subfamily for ABC transporters (Verrier *et al*, 2008). This gene was first described in a stigma cDNA library (Goldman *et al*, 1992). The gene codes for a “half-transporter” in which it should interact with another polypeptide chain, forming either a homo- or heterodimer with an unidentified ABC transporter. Based on predictive localization, it is thought to exist on the plasma membrane (Nakai & Horton, 1999) yet it contains a signaling motif potentially related to protein localization, usually attributed to ABC

transporters associated with the trans-Golgi network, such as *Drosophila* White, Scarlet, and Brown (Mackenzie et al, 2000) and ABC transporters ABCG1, ABCG5 and ABCG8 (Schmitz et al, 2001). Otsu et al (2004) showed that NtWBC1 is expressed distinctively in tobacco reproductive organs, to a greater degree in the stigma/style (1.5 times) than the stamens. It is also expressed in other floral organs, such as the sepals, petals, and ovaries, albeit at much lower levels (6.2-, 12.7-, and 17.0- times lower, respectively). Furthermore, higher expression levels coordinate with higher production of stigma exudate across developmental stages and NtWBC1 mRNA is distinctively located in the cells of the stigmatic secretory zone. Therefore, it is postulated that NtWBC1 is either involved in exudate production or in another reproductive physiological process.

1.5.2 Movement through cell wall

After surface lipids have crossed the plasma membrane, they need to travel through the cell wall. Multiple transport avenues are available such as channel, pores, diffusion, protein-mediated, or combination of these options (Kunst *et al*, 2006). Lipid transfer proteins (LTPs) may assist in transporting the hydrophobic monomers across the hydrophilic polysaccharide wall as it has been demonstrated that they accumulate on plant surfaces, have a hydrophobic binding core, and can interact with lipids, as reported with broccoli (Pyee *et al*, 1994) and tomato (Yeats *et al*, 2010). LTPG1 mutants in *Arabidopsis* reported a decrease in cuticular wax accumulation (DeBono *et al*, 2009; Lee *et al*, 2009). However, there is no confirmation verifying that LTPs actually transport cuticular lipids (Kunst *et al*, 2006). For cutin, it is suggested that the hydrophobic precursors can travel through the hydrophilic apoplast simply by passive phase-separation, as is the case for cell wall assembly, and diffuse towards the more hydrophobic cutin microenvironment (Fich *et al*, 2016; Philippe *et al*, 2022). This provides a passive mechanism of transport that avoids metabolic investments such as protein transport (Philippe *et al*, 2022).

In bayberry knobs, the most highly expressed gene transcript is a type 1 lipid transfer protein that is homologous to LTP1 in *Arabidopsis* (AT2G38540; Simpson *et al*, 2016; Simpson & Ohlrogge, 2016). Two other type 2 LTPs (LPT2) were also among the top 40 highest expressed transcripts (AT1G48750; AT3G18280). Conventional classification of LTPs divided type 1 and type 2 LTP based on their molecular sizes, where LTP1 has about 90 amino acids and LTP2, about 70 (Kalla et al. 1994). Newer

classification based on intron spacing, amino acid sequence identity and motif spacing preserves previous classification but discovers that LTP1 is limited to vascular plants, and LTP2 only in seed plants (Edstam *et al*, 2011). However, unlike bayberry's high expression of ABCG transporters and other cutin-related genes, the high expression of LTPs is not unusual, unexpected, or relatively high in comparison to their abundance in other plant tissues (Pyee *et al*, 1994; Yeats *et al*, 2010).

In tobacco, the *Nicotiana tabacum* LTP1 (NtLTP1) gene is expressed in long glandular trichomes and is involved with lipid secretion which account for up to 16% of dry leaf weight (Choi *et al*, 2012; Wang *et al*, 2001). Trichomes in tobacco are presented as glandular hairs which produce and secrete alkaloids, terpenoids, and defensive proteins (Wagner, 1991; Shepard *et al*, 2005). Overexpression of NtLTP1 demonstrated increased secretion of trichome exudate as well as epicuticular wax, whereas transgenic RNAi mutants showed a decrease in secretions but not in wax (Choi *et al*, 2012). It is suggested that the NtLTP1 protein is a non-specific lipid transfer protein and is ubiquitous for all lipid bindings from trichome glands and the leaf epidermis.

Tobacco stigmas are formed by two distinct zones: the top two-three cell layers comprise the glandular zone formed by the papillae and basal cells, and below those is the parenchymatous non-glandular zone composed of non-vacuolated cells (Fig.6A; Dumas, 1978; Cresti *et al*, 1982). An epidermal layer with a cuticle envelopes these zones. TEM of the glandular zone showed loosely arranged thin cell walls with large intracellular spaces (Fig.6B; Cresti *et al*, 1986), which is typical of secretory tissue (Fahn, 1988). Furthermore, the imaging shows that the secretion of exudate lipids is accompanied by the presence of lipid droplets in the cytoplasm and then later in the cell wall (Cresti *et al*, 1986). While it is confirmed that the exudate lipids travel between the cell walls and cuticle and in the intercellular spaces (Fig.6C), the mechanisms of which are still not understood. No surrounding membranes were observed in intracellular or extracellular lipids but Thiery staining shows that polysaccharides accumulate around the lipids prior to secretion. However, none of these polysaccharides were detected to associate with either the plasma membrane or the cell wall across development. Imaging micrographs in petunia wet stigmas demonstrate that the exudation of stigma lipids occurs after massive accumulation in the intercellular spaces in the glandular zone followed by the rupturing of the cuticle through which the exudate is exported to the surface (Fig.7; Konar & Linskens, 1966).

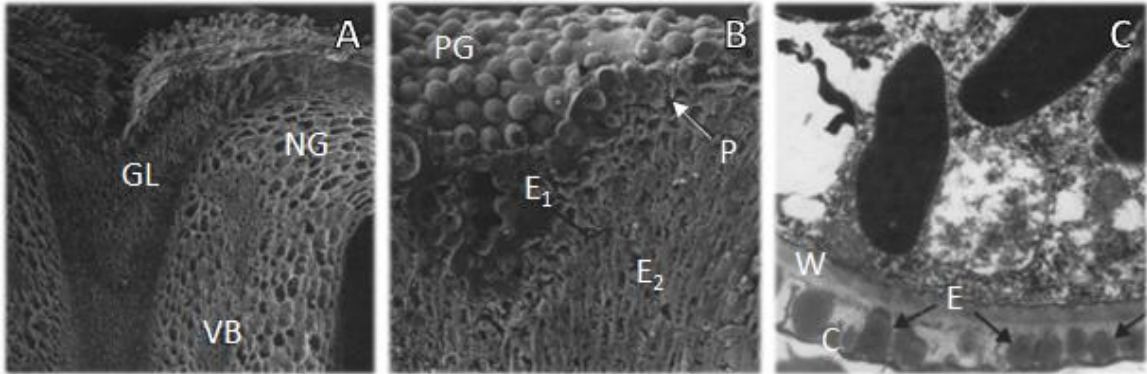


Figure 6. TEM images of tobacco stigmas (Adapted from Cresti *et al*, 1986). A: Cross section of a young stigma; glandular zone (GL) is filled with exudate, vascular bundles (VB) are visible in the non-glandular zone (NG). B: Cross section of a mature and pollinated stigma; pollen grains (PG) are adhered to the exudate present on the surface of the stigma (E_1), exudate is present in intercellular spaces (E_2) and papillae (P) are visible. C: Cross section of papillae; exudate droplets (E) are visible in the spaces between the cell wall (W) and the cuticle (C).

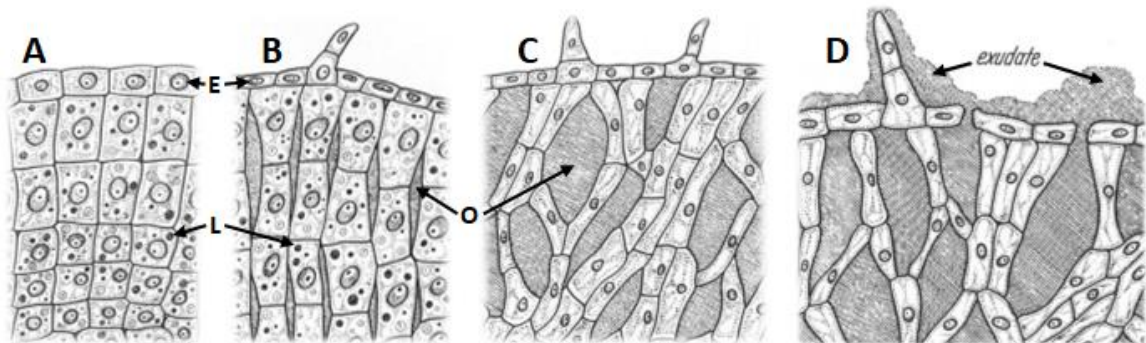


Figure 7. Secretion of exudate in petunia stigmas (Adapted from Konar & Linskens, 1966). A: Glandular cells begin producing lipids (L). B: Produced lipids accumulate in the intercellular spaces as oil bodies (O). C: Large schizogenous cavities filled with stigmatic lipids are formed. D: Epidermal layer (E) is ruptured allowing the secretion of stigma exudates.

The literature concerning stigma lipid polyesters show clear gaps in relation to their biosynthesis and transport. These polyesters share certain structural similarities with oilseeds triacylglycerols with estolides as acyl groups, bayberry fruit waxes, and cutin. However, it is unclear if stigma lipid polyesters are synthesized by any of these established pathways or by a novel pathway that may combine different steps of known lipid metabolic routes. Establishing more parallels between these systems may elucidate the unknowns and provide the groundwork for further investigations.

1.6 Objectives

The overlying objective of the work presented in this thesis was to predict the mechanism of extracellular glycerolipid biosynthesis in tobacco stigmas. The techniques used include isolating and characterizing the structures and compositions of developing wet stigma glycerolipids using a combination of thin layer and gas chromatography, and kinetic radiolabeling with [¹⁴C]-labeled substrates using a novel experimental method developed for *in planta* isotope analysis. The work is presented in two chapters: Chapter 2 focuses on the chemical characterization of the tobacco stigma lipids, and Chapter 3 hypothesizes on the metabolic processes involved in synthesizing stigma exudate lipids.

Chapter 2: Chemical Characterization of Developing Stigma Lipids

2.1 Introduction

Wet stigma species, including the model *Solanaceae* species *Petunia hybrida* and *Nicotiana tabacum*, secrete an exudate from their stigmas containing lipids, whereas dry stigmas contain an overlaying pellicle (Heslop-Harrison & Shivanna, 1977). The exudate secretion was found to consist of a variety of proteins, lipids, sugar, and pigments (e.g., chlorophylls) (Cresti *et al*, 1986). The lipid fraction of their stigma exudates has been shown to be rich in ω -hFAs (Koiwai & Matsuzaki, 1988). In tobacco, crude lipids account for 7.5% of the wet weight of fresh stigma tissue (Matsuzaki *et al*, 1983b). Some dry stigma species contain ω -hFAs as well, albeit in much lower quantities, so it is not exclusive to wet stigma exudates.

The lipid polyesters found in the exudate of wet stigmas are glycerolipids that consist of polymerized (i.e., ester bonded) hydroxyacyl monomers attached to a glycerol moiety, i.e., polyacylglycerols, or PAG(n). These can be named according to the number of acyl groups attached to the glycerol backbone and the number of hydroxyacyl monomers (estolide bonds; n) in each polyester. Tri-, di-, and monoacylglycerol polyesters are denoted as TAGs, DAGs, and MAGs. For example, a TAG(3) is a triacylglycerol with 6 acyl “monomers”, 3 of which are hydroxyacyl monomers and thus each form an estolide bond to another FA, distributed in chains across the 3 positions on the glycerol backbone (Fig.8). Two isomers of DAG exist, α,α -DAG or α,β -DAG, such that the former represents acyl chains on the *sn*-1 (stereospecific numbering-1) and *sn*-3 terminal positions of the glycerol backbone, and the later, *sn*-1 and *sn*-2, represents acyl groups esterified to the one of the terminal carbons and the central carbon of glycerol.

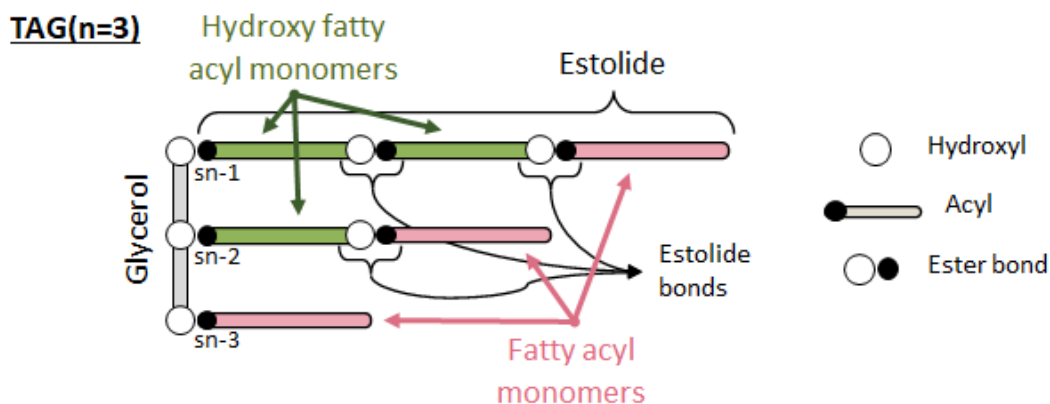


Figure 8. General structure of polyacylglycerol. Pictured is a possible TAG(3) isomer; 3 corresponds to the number of ω -hFAs or estolide bonds in the molecule. The depicted isomer is 2:1:0, meaning that 2, 1 and 0 estolide bonds are present in *sn*- positions 1, 2, and 3, respectively.

Chemical characterizations of stigma lipid TAG(n) fractions have shown the petunia stigma exudate has much higher ω -hFA content (96% ω -hFA content; Koiwai & Matsuzaki, 1988) than that of tobacco (58% ω -hFA content; Koiwai & Matsuzaki, 1988). Petunia stigmas produce soluble polyesters with up to 125 acyl groups but averaging around 49 per polyester, whereas that of tobacco stigmas averages around 5 or 6 acyl groups per polyester (Wang *et al*, 2003). This large range in PAG(n) size makes it quite difficult to analyze individual PAG species in petunia by TLC, while tobacco is much more feasible. Therefore, this research focused on using tobacco as a model system to investigate wet stigma lipid structure and biosynthesis.

Tobacco stigma lipids polyesters consist of three major fractions: TAG, DAG, and the polar lipid fraction (PL), the first two containing the lipid polyesters, and the last including known membrane lipids, namely phosphatidylcholine (PC) which is known to be involved in glycerolipid biosynthesis, as well as phosphatidylethanolamine (PE), phosphatidylinositol (PI), and monogalactosyldiacylglycerol (MGDG) being the most abundant (Matsuzaki *et al*, 1983a). The authors also identified the presence of ω -hFAs in the polar lipid fraction but none of the membrane lipids contained any hFAs. This higher polarity ω -hFA-containing lipid fraction was originally attributed to MAG estolides, but without providing evidence for such speculation. TAG(n) estolides (n=1 to 4) where

identified and isolated with estolide chains, attached to the glycerol backbone, were determined to always be terminated (“end-capped”) with a normal FA (Matsuzaki *et al*, 1983b). The presence of both α,α -DAG(n) and α,β -DAG(n) isomers was also confirmed, containing the same end-terminal normal FAs (Matsuzaki *et al*, 1986). Furthermore, free estolides, FFA(n), were mentioned as a smaller fraction of the neutral lipids found in tobacco stigma lipid fractions (Matsuzaki *et al*, 1986). FFA(n) were defined as “estolides having no glycerol”, but their structure was not confirmed.

The solubility of stigma lipid polyesters facilitates the separation and isolation of entire PAG(n) species in their natural form based on their polarity. Thin layer chromatography methods can be used to distinguish distinct PAG(n) groups, as well total acyl chain length within these groups (Matsuzaki *et al*, 1983b). MAGs, DAGs, and TAGs vary in polarity due to the presence of free hydroxyl groups on the glycerol head group. Even α,α -DAG and α,β -DAG differ in polarity due to stereochemistry, the latter being less polar (Matsuzaki *et al*, 1986). Finally, each addition of an acyl group includes an extra ester bond, changing the polarity and allowing the segregation of individual PAG(n) species. However, these separation methods make it difficult to identify and isolate PAGs containing unusual fatty acyl monomers, such as those containing mid-chain hydroxy and epoxide groups. These have not officially been reported in tobacco stigmas (Koiwai & Matsuzaki, 1988). However, another research group (Wang *et al*, 2003) identified some unusual FAs containing cutin-like mid-chain hydroxy acyl monomers and acyl monomers containing allylic alcohol functional groups, as those reported in Chinese tallow tree oilseeds (Sprecher *et al*, 1965), present with other ω -hydroxy acyl compounds in the most non-polar region of the polar lipid fraction. This lipid fraction was dubbed intermediate polarity polyesters (IPPE). These were identified as potential TAG(n) and DAG(n) polyesters yet are separate due to their increased polarity and are likely the source of the ω -hFAs that Matsuzaki *et al* (1983a) identified in the polar fraction. Confirming the presence of these monomers may help identify key proteins involved in the biosynthesis of stigma lipid polyesters. Thus, the main lipid classes characterized in this thesis work involved five major fractions: TAG(n), DAG(n), FFA(n), IPPE, and PL.

This first objective sought to characterize the soluble lipid species found in tobacco stigmas and monitor for any change in composition across developmental stages or difference in surface and internal lipids; this may give insight into the location and mechanism of PAG(n) biosynthesis, polymerization, and transport.

2.2 Materials and Methods

2.2.1 Plant material and harvesting

N. tabacum plants, grown from seeds obtained from the Molina lab at Algoma University, were raised in a growth chamber at the same university. The growth chambers were programmed with an alternating light and dark cycle. The light cycle occurred between 7:30 AM and 11:30 PM with a light intensity of 150-200 $\mu\text{E}/\text{m}^2/\text{s}^1$ and a temperature of 23°C, whereas the dark cycle was from 11:30 PM to 7:30 AM with a temperature of 20°C. The humidity of the growth was set at 55% across both cycles. Stigma harvesting was accomplished by removing the tobacco flower, opening the corolla, cleaving the stigma from the style using forceps, and then placing the stigma into a pre-washed and chloroform rinsed tube positioned in ice. The developmental stages of tobacco flowers were adapted from Matsuzaki *et al* (1983c; Fig.9).

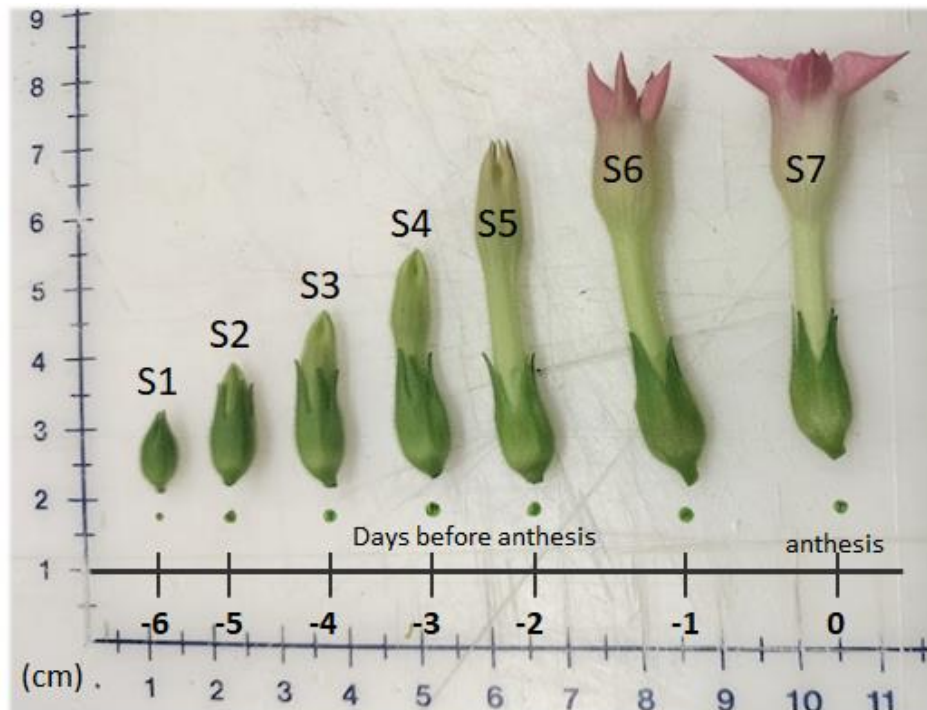


Figure 9. Tobacco flower developing stages. In S₁, the corolla remains inside the calyx and bud length is about 0.5 cm. In S₂, the calyx opens and the corolla becomes visible, bud length about 1 cm. In S₃, the corolla begins emerging from the bud, bud length about 1-2 cm. In S₄, the corolla length is greater than that of the calyx, about 2-3 cm. In S₅, the corolla is fully extended yet remains closed and pink pigmentation begins to appear at the tip of the petals, about 3.5-4.5 cm in length. In S₆, the corolla tip is more pigmented and slightly opened, the stigma is visible, and the anthers remain indehiscent. In S₇, the corolla is fully pigmented and open but not yet fully mature, pollen begins to appear on the anthers.

2.2.2 Stigma lipid extraction

For experiments requiring the distinction of surface and internal stigma lipids, the stigmas were first gently rinsed in chloroform for 10 seconds, which corresponds to the surface lipid extract. Otherwise, this first step was skipped. The stigmas were then quenched in isopropanol containing 0.05% butylated hydroxytoluene (BHT) at 85°C for 10 min. The stigma tissue was then homogenized, and the remaining lipids were extracted following the methods described by Hara & Radin (1978) using a 3:2 hexanes:isopropanol extraction solvent. Both lipid extracts were dried under nitrogen (N₂) and kept at -20°C until further analysis, where they were resuspended in chloroform.

2.2.3 Lipid fraction isolation by thin layer chromatography (TLC)

Thin layer chromatography (TLC) was performed in a 20x20x5 cm glass tank using either 5x20, 10x20, or 20x20 cm silica analytical plates (Supelco silica gel 60 F₂₅₄), or 20x20 cm silica preparative plates (Supelco silica gel 60 PF₂₅₄). A sheet of filter paper was placed in the tank prior and during plate development to allow for quicker and more uniform saturation of the solvent in the tank. Full saturation (at least 1 hour) was achieved before plates were placed in the tank. Temperature and humidity were recorded to allow for slight adjustments to the solvent conditions, since higher humidity in the laboratory increases the polarity of the solvent. For plates that required multiple developments, the plates were set to dry completely prior to the subsequent developments: analytical plates took about 5-10 min and preparative plates took about 20-25 min to dry. TLC solvent conditions, adapted from Wang (2003) are listed below (at 20°C and 30% humidity):

FAME(n): 0.4% EtOH in CHCl₃
TAG(n): 0.5% EtOH in CHCl₃ dual development
DAG(n) & FFA(n): 1.5% EtOH in CHCl₃ dual development
FFA(n): 1.5% EtOH in CHCl₃ triple development
PL: 85:15:5:2 CHCl₃:MeOH:AcH:H₂O
PL (alternate): 3.0% EtOH in CHCl₃ dual development then 91:30:7:1
acetone-toluene-water-acetic acid (Christie & Han,
2010)

TLC plates were visualized under UV (365 nm) using a non-destructive method (Christie & Han, 2010), 5% primuline (w/v) in 80:20 (v/v) acetone:water, or with a destructive method, iodine staining. The latter was used for densitometry semi-quantification (Fluorchem FC3; Santa Clara, CA USA) using AlphaView (V3.4.0) software.

2.2.4 TLC lipid recovery

Lipids could be recovered from the silica on the TLC plates through filtration system (we used a combination of glass wool and filter paper through a glass funnel) using 5:5:1 CHCl₃:MeOH:H₂O (v/v/v) solvent as first described by Gray (1967). Subsequent solvent washes and lipid purification were achieved following the Folch wash method (Folch *et al*, 1957). Recovered lipids bands from the TLC plates were identified using non-destructive primuline staining.

2.2.5 Monomer analysis

Extracted or recovered lipids were depolymerized through transmethylation by either acidic or basic protocols with methyl heptadecanoate (C17:0 FAME) and pentadecalactone (C15:0 hFAME) as internal standards. Acidic transmethylation consisted of heating for 2 h at 80°C in 5% sulfuric acid (H₂SO₄) in methanol. Basic transmethylation consisted of heating at 60°C for 2 h in 6% sodium methoxide (NaOMe) and 15% methyl acetate (MeOAc) in methanol, terminating the reaction by adding acetic acid such that pH≈4. The products recovered following the Folch wash method (Folch *et al*, 1957) were then esterified to trimethylsilyl (TMS) or acetyl derivatives for monomer identification and analysis by gas chromatography mass spectroscopy (GC-MS). TMS was preferred for identifying potential unknown compounds as the mass spectra

database library was more complete but prone to hydrolysis, whereas acetylation was much more stable and thus preferred for quantification.

2.2.6 Partial depolymerization

Mild transmethylation protocol described in Wang (2003) is used to cleave the acyl-glycerol bonds while the acyl-acyl bonds remain intact in triacylglycerol estolides. This protocol uses a low concentration and duration of the base catalyzed transmethylation reaction: 0.25% NaOMe, 15% MeOAc in methanol with diethyl ether as co-solvent (2:1 v/v). The reaction ran for 10-15 min at 25°C, where TAG(0) ran for 10 min and TAG(5), for 15 min. Reaction times were adapted through Wang (2003) and experimental trials. TLC was used to separate the resulting FAME(n) fractions and then iodine staining was performed for densitometry analysis.

MAG(n) ladder

A similar procedure was performed using the partial depolymerization method (Wang *et al*, 2003) to produce a MAG(n) ladder from TAG(n) molecules. Using the same base catalyzed reagents described above, pooled TAG(n) extracts from stages 3-5 stigmas were incubated for 2 min at room temperature. Single TLC development in 4% EtOH in CHCl₃ was used to isolate the MAG(n) fraction.

2.3 Results

2.3.1 Tobacco stigma lipids accumulate through stigma development.

To assess lipid distribution in the stigma across developmental stages, longitudinal sections of the stigmas were stained with the lipophilic dye Fluorol Yellow 088 and observed by fluorescence microscopy (Fig.10). Fluorescent lipid staining was observed in the glandular zone of the stigma where the fluorescence intensity increases proportional to the lipid accumulation at each development stage until anthesis (Fig.11-B; Appendix Fig.A1). In stage 1 stigmas, the initial lipid accumulation occurred near the stigma surface, indicating active exudate synthesis early in development, while in the later stages, the exudate accumulated both in the intercellular spaces within the glandular zone and on the surface. The surface fluorescence corresponding to the exudate lipids presented the highest intensity at all stages analyzed.

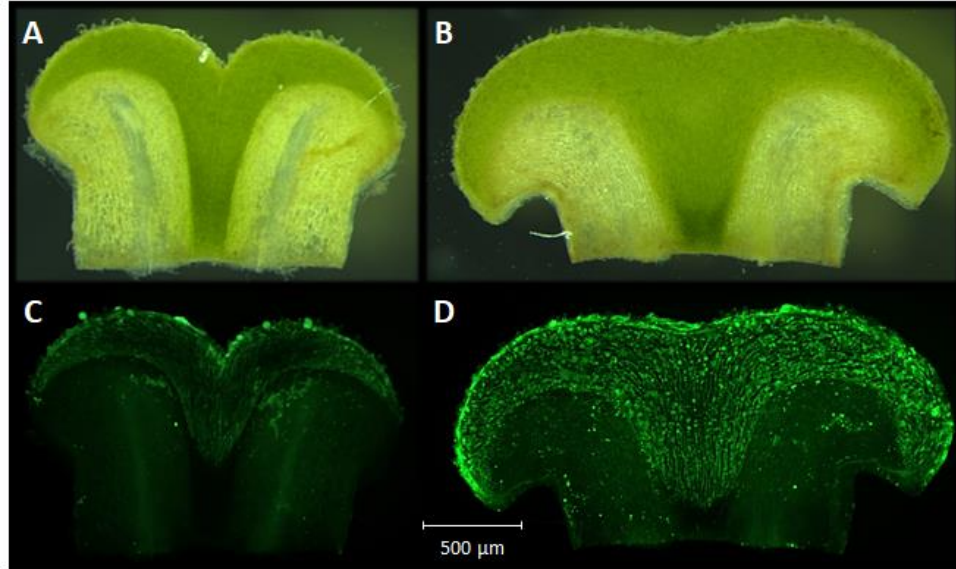


Figure 10. Free-hand longitudinal sections of *Nicotiana tabacum*. A: Stage 1 stigma stained with Fluorol Yellow 088 under dark-field. B: Stage 3 stigma stained with Fluorol Yellow 088 under dark-field. C: Stage 1 stigma stained with Fluorol Yellow 088 under fluorescence microscopy. D: Stage 3 stigma stained with Fluorol Yellow 088 under fluorescence microscopy. Pictures from Shirisha Maharjan (2022).

Solvent-soluble lipids were extracted from stigmas at each development stage by quickly dipping the tissue in chloroform (surface lipid fraction) and by homogenizing the tissue and fully isolating the remaining lipids (internal lipid fraction). The surface lipids contained mainly the lipidic exudate deposited externally, although the stigma tissues are fragile and some of the glandular (though extracellular) content may be also part of this fraction. The internal lipids, extracted from homogenized stigma tissue post surface lipid extraction, contained inter- and extracellular lipids, as well as membrane lipids. Gravimetric analysis of fresh stigmas and their extracted lipids showed that the fraction of soluble lipids to total fresh weight per stigma ranged from about 4.5% to 11.5% across the development of the tobacco flower and that the distribution of surface lipids ranged from 13% to 58% (Fig.11-A). Surface lipid concentrations of tobacco stigmas were determined to accumulate up to 3 mg/cm² (Appendix Table A1).

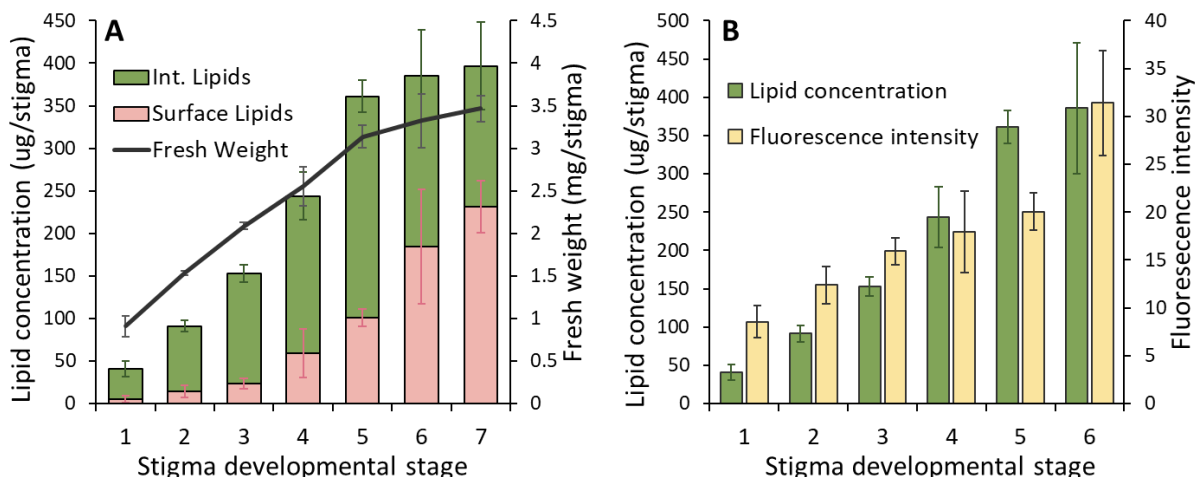


Figure 11. Average fresh weight and lipid content of developing stigmas. A: Average fresh weight and crude extractable lipids obtained per stigma. B: Extractable lipids against fluorescence intensity. Fresh weight was calculated gravimetrically from a total combined weight of pooled stigmas divided by the stigma count. Surface lipid mass obtained from chloroform dipping and internal (Int.) lipid mass was obtained from homogenized tissue from their respective stigma pool. Fluorescence intensity data obtained from Maharjan (2022) using Fluorol Yellow 088 dye and ImageJ for analysis. Lipid fluorescence was not analyzed for stage 7.

2.3.2 Distribution and structure of stigma lipid estolides throughout development show polyesters are formed prior to being exported to the surface.

Stigma lipid fractions were separated by thin-layer chromatography (TLC) using chloroform-ethanol solvent systems, following conditions previously established (Wang *et al*, 2003). One dimensional TLC developments revealed noticeable estolide bands that form a ladder TAG(n), DAG(n), and FFA(n) lipids (Fig.12). Low polarity solvents (0.5% EtOH, single or dual development) separated TAG(n) estolides, with TAG(0) to TAG(5) being distinguishable; the addition of an additional acyl group (n) increases the polarity of the molecule (Fig.12-D). With higher ethanol concentrations (1.5% dual development), the DAG(n) estolide ladders were visible for both α,β -DAG(n) and α,α -DAG(n) isomers, the former slightly more polar of the two. An extra development with the same solvent concentration allows the separation of FFA(n) estolides. For the

DAG(n) molecules (Fig.12-B) and FFA(n) (Fig.12-A), an increase in n decreases the polarity of the molecule. The fractions above, namely TAG(n), DAG(n) and FFA(n), correspond to neutral lipids. The same trend and the same estolide ladders were observed in both surface and internal lipid fractions; the former extracted by a nonpolar solvent and the latter with a polar solvent mixture.

The polar lipid (PL) fraction remained at the baseline where the samples were loaded after separating neutral lipids (Fig.12-B). This fraction was further separated into membrane lipids and an intermediate polarity polyester (IPPE) fraction using a chloroform-methanol-acetic acid-water (85-15-5-2 v/v) solvent system (Fig.12-C). The most abundant membrane lipids were phosphatidylcholine (PC), monogalactosyldiacylglycerol (MGDG), phosphatidylethanolamine (PE), and phosphatidylinositol (PI). MAG, nor any estolide-containing MAG(n), was determined to not accumulate significantly in our experimental conditions (Appendix Fig.A3), despite initial speculation by Matsuzaki (1983a). Thus, the ω -hFA fraction they found in the PL fraction is likely attributed to that of the IPPE fraction, as ω -hFA content was reported in the IPPE fractions by Wang *et al* (2003). Relative distribution of lipid classes pooled from stage 3 to 5 stigmas is shown in Fig.13. Lipids that did not belong to either of these categories were pooled together into "Other", which may include alkanes, sterols, pigments, and unidentified lipids.

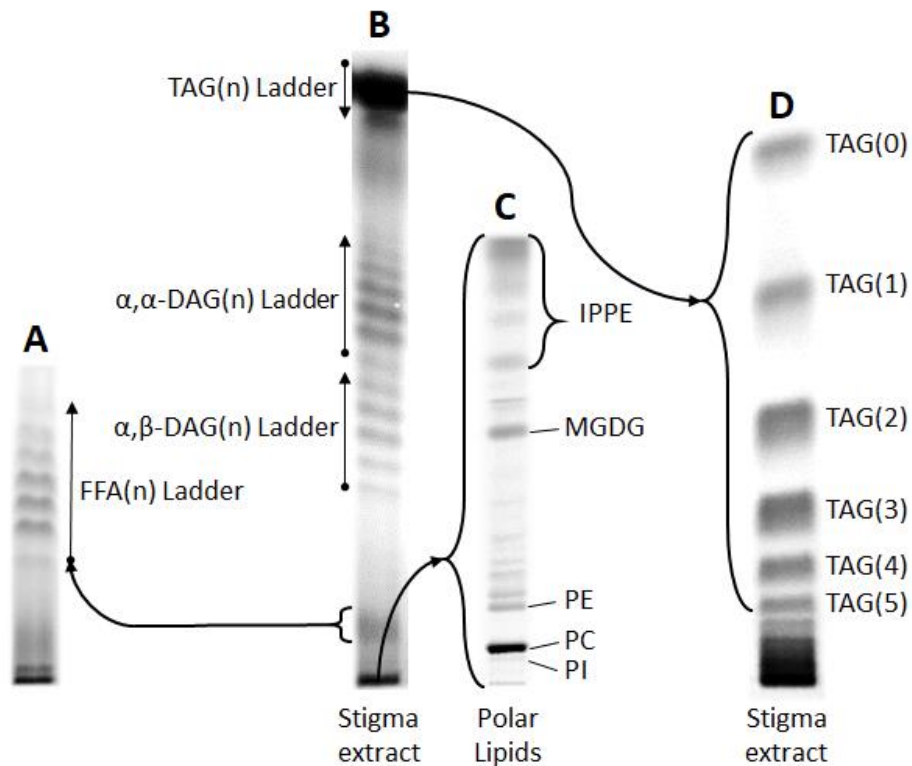


Figure 12. Soluble stigma lipid fractions and separation. The figure represents a composite of multiple TLC developments and lipids were identified by developing alongside known lipid standards (not shown). A: FFA(n) distribution. B: DAG(n) separation. C: Polar lipids and IPPE (intermediate polarity polyesters). D: Separation of TAG(n) molecules. MGDG = monogalactosyldiacylglycerol, PE = phosphatidylethanolamine, PC = phosphatidylcholine, PI = phosphatidylinositol. See Materials and Methods section for developing solvent conditions.

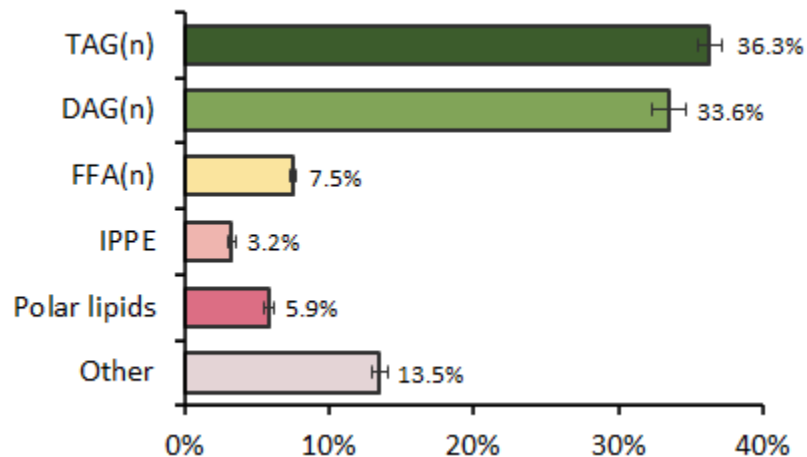


Figure 13. Soluble lipid class and distribution. Ratios determined from pooled stage 3 to 5 stigmas using iodine-stained densitometry TLC band analysis.

To better understand the mechanism of assembly of PAG(n) species, it is important to reveal the compartmentalization of their biosynthesis. For each developmental stage, the lipid monomer compositions of the exudate on the stigma surface were compared to that of the internal tissues. Surface lipids mostly represent an extracellular fraction, while the internal lipids represent both intra- and intercellular pools. Total soluble lipids extracted from the surface or from internal tissues at each development stage were depolymerized by acidic transmethylation, using 5% H₂SO₄ in methanol, derivatized with trimethylsilyl (TMS), and analyzed by GC-MS. As expected, the lowest proportion of hFAs relative to normal FAs for each developmental stage was found in stage 1 for both lipid fractions (Table 1). In the internal fraction, hFA content increased until anthesis (S7) with a maximum of 28.9% at stages 5 and 6. However in the surface lipid fraction, hFA content began to decrease after stage 3, achieving a maximum of 54.2% which is almost double that of the internal fraction. Furthermore, surface lipids demonstrated a higher proportion of 18:2 normal FA and hFA at all stages than internal lipids.

Table 1. Total soluble lipid composition of tobacco stigmas across developmental stages. Pooled surface and internal lipid extracts were depolymerized by acidic transmethylation to obtain methyl esters of their respective monomers. Quantitative analysis accomplished using GC-MS after derivatizing the monomers with TMS. 18:3 data not obtained as it co-eluted with 18:1 FAME.

Development Stage	Normal FAs (rel. mass %)							ω -hFAs (rel. mass %)					Ratio FA:hFA	
	16:0	18:0	18:1	18:2	20:0	22:0	Total	16:0	18:0	18:1	18:2	Total		
S1	Internal	6.7	2.9	58.0	19.3	0.8	0.6	88.3	0.7	0.1	6.7	4.2	11.7	7.6 : 1
	Surface	5.4	3.5	48.2	9.1	2.0	2.6	70.7	0.3	0.2	18.5	10.3	29.3	2.4 : 1
S2	Internal	3.8	2.0	58.9	15.2	0.6	0.5	81.0	0.7	0.1	11.6	6.6	19.0	4.3 : 1
	Surface	1.5	0.9	35.7	7.6	0.6	0.6	46.8	0.3	0.2	31.3	21.5	53.2	0.9 : 1
S3	Internal	3.7	2.1	65.3	12.3	0.7	0.4	84.7	0.6	0.2	10.3	4.2	15.3	5.5 : 1
	Surface	1.4	0.8	35.3	7.2	0.4	0.5	45.7	0.3	0.2	32.9	20.9	54.3	0.8 : 1
S4	Internal	5.4	4.0	56.5	6.6	0.9	0.9	74.3	2.9	0.6	17.1	5.2	25.7	2.9 : 1
	Surface	0.8	0.5	37.4	7.4	0.3	0.5	46.9	0.3	0.2	32.3	20.2	53.1	0.9 : 1
S5	Internal	3.9	3.2	55.4	7.1	0.7	0.4	70.8	2.0	0.4	20.1	6.7	29.2	2.4 : 1
	Surface	1.0	0.6	43.1	7.8	0.3	0.3	53.1	0.3	0.2	30.0	16.4	46.9	1.1 : 1
S6	Internal	5.7	4.6	53.1	5.2	1.1	0.8	70.5	3.3	0.7	20.7	4.7	29.5	2.4 : 1
	Surface	1.0	0.8	51.9	7.8	0.4	0.2	62.2	0.3	0.1	26.6	10.8	37.8	1.6 : 1
S7	Internal	8.6	6.1	53.5	6.1	1.5	1.1	76.8	2.5	0.7	17.2	2.8	23.2	3.3 : 1
	Surface	0.9	0.8	46.6	7.2	0.4	0.3	56.2	0.4	0.1	30.9	12.5	43.8	1.3 : 1

Further analysis of TAG(n), DAG(n), and FFA(n) was accomplished through TLC separation followed by iodine staining and densitometry analysis. This showed that the accumulation of estolide TAG species across developmental stages followed a near normal distribution of species with TAG(2) having the greatest value (Fig.14), such that TAG(2) > TAG (1) > TAG (0) and TAG(2) > TAG(3) > TAG(4) > TAG(5). Only trace amounts of all TAG estolides were observed in the exudate of stage 1 stigmas. Conversely, only minimal amounts of TAG(0) were observed in the extracted surface lipids in all stages. Total lipid amount in the internal fraction decreased starting at stage 6, while the surface fraction continued to accumulate throughout.

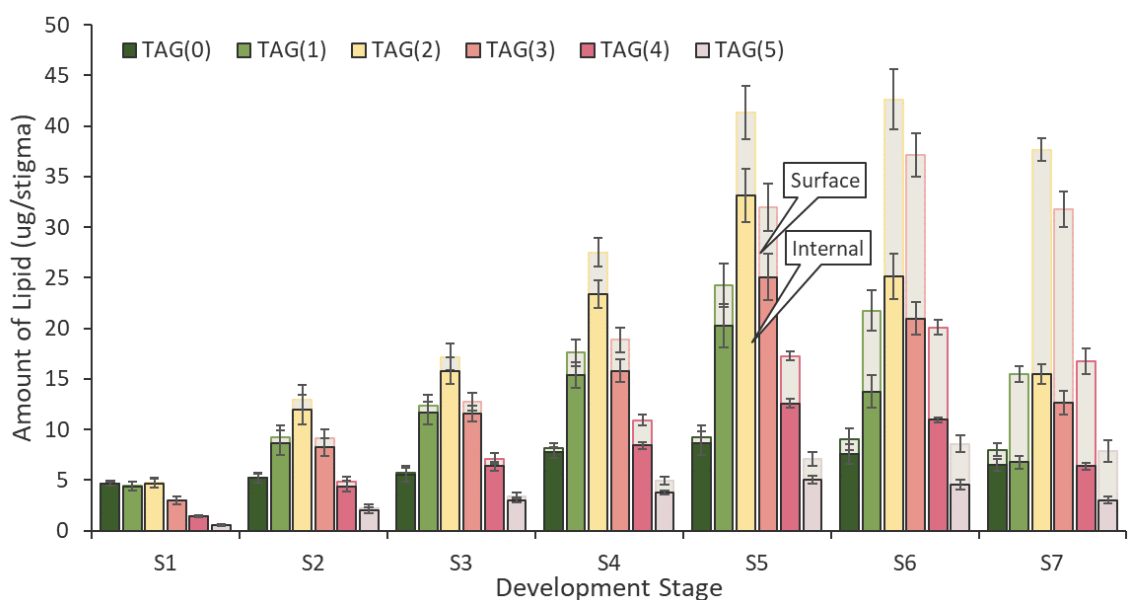


Figure 14. TAG(n) distribution across developmental stages. Data represents the average of four replicates obtained through iodine-staining densitometry from TLC plate development. Triolein was used as an internal standard. The overlapping shaded bar graphs represent the total lipid amount while the coloured bar represents the internal lipid fraction, such that the difference represents the surface lipid fraction.

The distribution of FFA estolides shows a higher relative proportion of normal FAs, FFA(0), in the early stages (1, 2, and 3) of stigma development and at anthesis (S7; Fig.15). The internal lipid estolides accumulate until S5 while the surface fraction accumulates until S7. The FFA(n) estolides, while not yet structurally demonstrated in the literature, are likely end-capped with a normal FA given their chromatographic

behavior when analyzed by TLC. However, further characterization of these molecules is needed using a reagent such as diazomethane, which converts carboxylic acids into their methyl esters and can be analyzed further by ESI-MS, GC, or further TLC quantification (Gutsche, 2004).

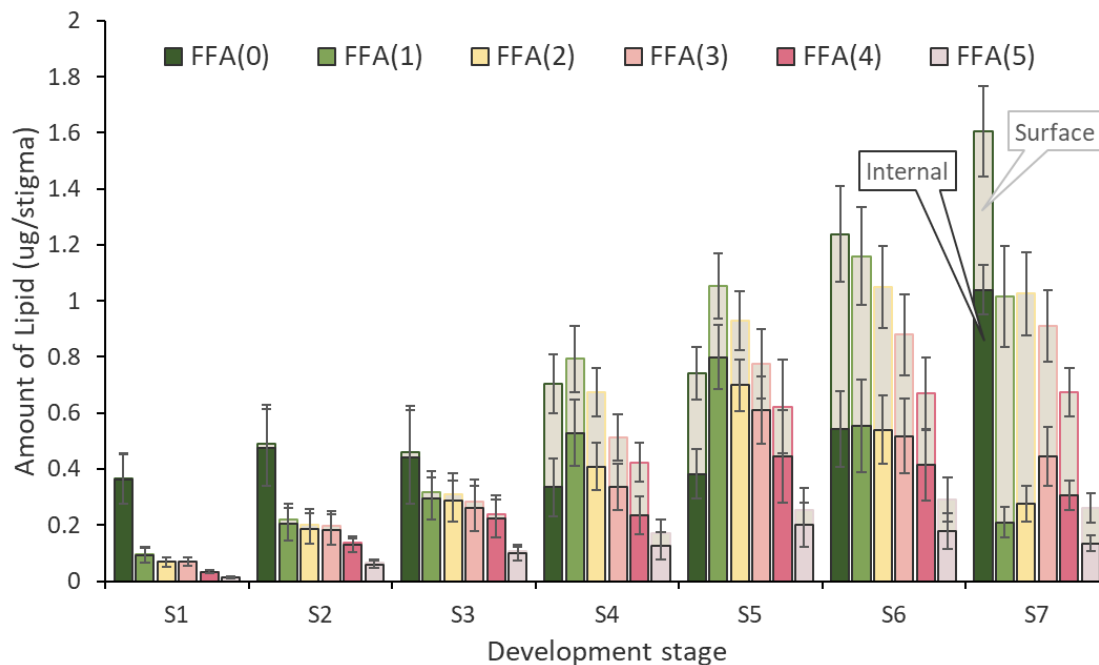


Figure 15. FFA(n) distribution across developmental stages. Data represents the average of four replicates obtained through iodine-staining densitometry from TLC plate development. Oleic acid was used as an internal standard. The overlapping shaded bar graphs represent the total lipid amount while the coloured bar represents the internal lipid fraction, such that the difference represents the surface lipid fraction.

The same trends observed in the TAG fraction were found for the DAG fraction (Fig.16). However, the internal α,β -DAG estolides did not accumulate showing the same distribution trend as TAG(n) in the more mature stages of flower development (stages 5-7), such that α,β -DAG(3) accumulated in higher amount than either α,β -DAG(1) or α,β -DAG(2). Furthermore, α,β -DAG(1) accumulated at higher level than α,β -DAG(2). Yet, the normal distribution present in the TAG(n) species was still observed in the surface exudate fraction. Stigma polyesters contained a significant portion of α,α -DAG isomers across all stages and estolide lengths. Interestingly, the proportion of α,α -DAG increased

with the degree of catenation (Fig.17). Typically, α,β -DAG is the intermediate of TAG biosynthesis in plants through both the Kennedy pathway and the MAG-derived pathway suggested for bayberry wax. The high proportion of α,α -DAG and the presence of estolides in these TAG metabolic precursors may suggest an unusual mechanism of PAG(n) assembly or may simply be a result of DAG isomerization in developing stigmas (Crossley *et al*, 1959; Mattson *et al*, 1962), or both.

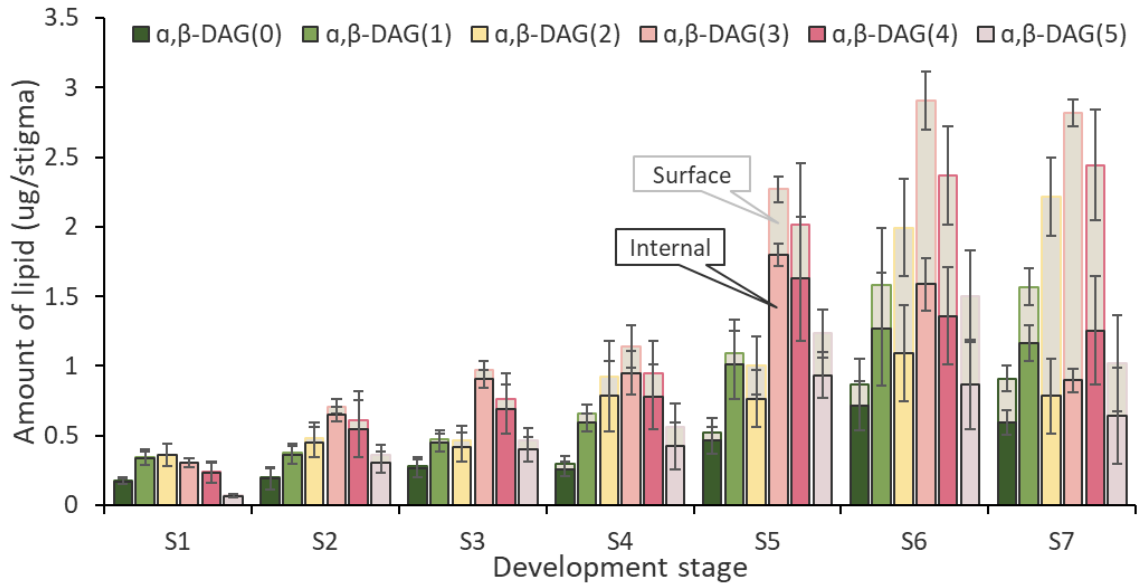


Figure 16. α,β -DAG distribution across developmental stages. Data represents the average of four replicates obtained through iodine-staining densitometry from TLC plate development. Diolein (α,β) was used as internal standard. The overlapping shaded bar graphs represent the total lipid amount while the coloured bar represents the internal lipid fraction, such that the difference represents the surface lipid fraction.

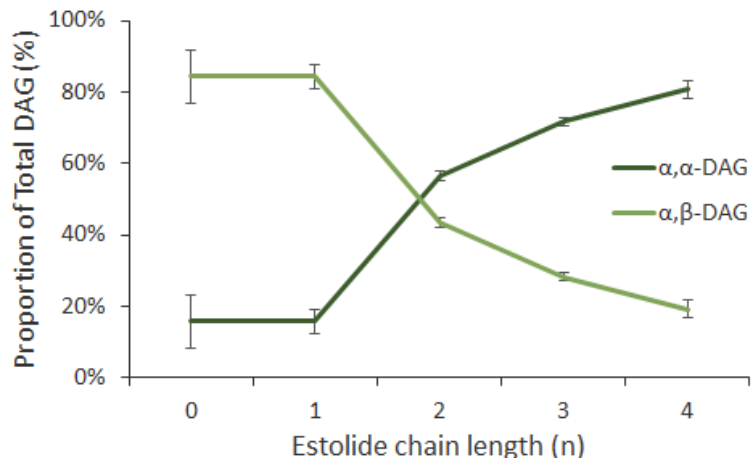


Figure 17. DAG isomer ratios relative to estolide chain length. Ratios taken from Stage 4 stigmas through iodine-staining densitometry.

2.3.3 Characterization of the TAG(n) fraction suggests that FAME(1) is the predominant estolide chain.

TAG(n) species from n=0 to n=5 were isolated by preparative TLC separation. Each TAG(n) species, separated as a discrete band on the TLC plate, was purified, depolymerized through basic transesterification using 6% NaOMe, derivatized to form acetyl esters and analyzed by GC-MS for compound identification and quantification (Molina *et al*, 2006; Jenkin & Molina, 2015). Through this process, the FA monomers are converted to fatty acid methyl esters (FAMEs) and the hydroxyl groups derivatized to acetyl esters (hFAMEs). These results showed the expected trend where the amount of hFAs increased with higher degrees of catenation (Fig.18). Trace amounts of 16:0, 18:0, 18:3, ω -h16:0, ω -h18:0, and ω -h18:3 FAs were also identified in the depolymerization products of tobacco stigma TAG(n), which accounted for a combined total of about 3%, except TAG(0) which had around 6% each of 16:0 and 18:0 normal FA content. When comparing the monomer classes, the measured ratio of hydroxy to non-hydroxy FAs of each molecular species showed an excess of normal FAs than the expected ratios for end-capped polyesters (Fig.18 inset). For example, all end-capped TAG molecules should contain 3 normal FAs, and thus TAG(4) should have a FAME:hFAME molar ratio of 3:4, while the experimental ratio was 3:3.68 (Table 2).

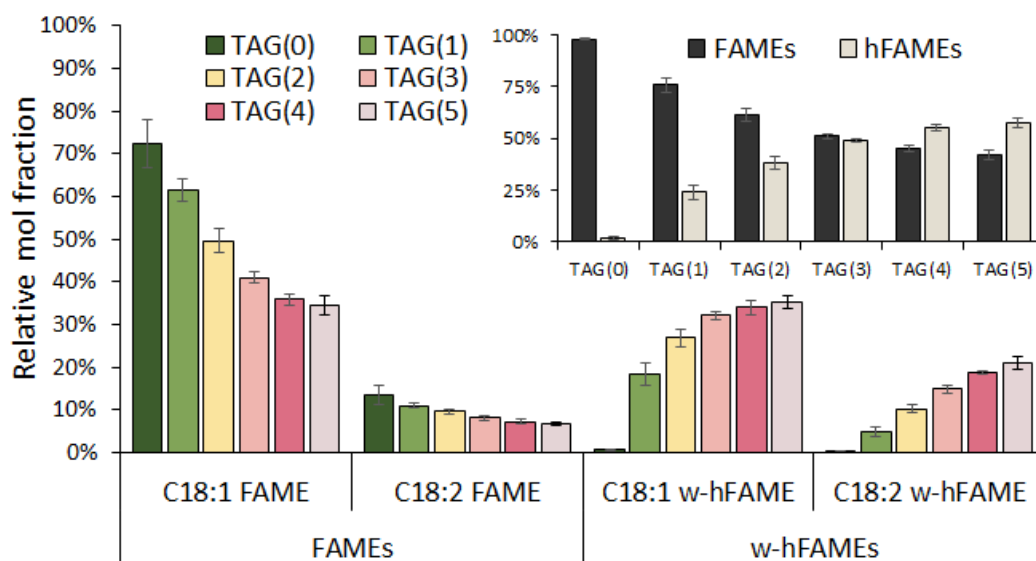


Figure 18. Composition of TAG(n) species. Pooled surface and internal lipid TAG estolide fractions were isolated by preparative TLC and extracts were depolymerized to obtain methyl esters of their respective monomers. Quantitative analysis was accomplished through GC-MS using methyl heptadecanoate (17:0) and pentadecalactone (ω -h15:0) as internal standards for normal and hydroxy FAs, respectively.

Table 2. Measured and expected molar ratios of ω -hFAs in TAG estolides. Measured ratios were calculated from GC-MS monomer data of TAG estolide depolymerization.

	TAG(n)	TAG(0)	TAG(1)	TAG(2)	TAG(3)	TAG(4)	TAG(5)
Molar ratio	Normal FA	3	3	3	3	3	3
	Expected ω -hFA	0	1	2	3	4	5
	Measured ω -hFA	0.06	0.96	1.87	2.87	3.68	4.12

For any given TAG(n) estolide molecular species (when $n > 0$), a mixture of regioisomers (estolide chains attached to any *sn* position of glycerol) may be present (Matsuzaki *et al*, 1983b). Furthermore, a given TAG(n) (when $n > 1$) may present estolides of different lengths (e.g., TAG(2) may include 2:0:0 and 1:1:0 isomers). To measure the estolide distribution of the TAG(n) fraction, TAG(n) were separated

according to their MW (i.e. chain length) and a mild depolymerization protocol was used to cleave the acyl-glycerol bond while keeping the acyl-acyl bond intact, following the method described by Wang *et al* (2003). The resulting products could then be analyzed by TLC after iodine staining where the estolides were distinguishable as discrete bands separated according to their chain length (Appendix Fig.A2). These chains are denoted as FAME(*n*), as in fatty acid methyl esters with an *n* number of hydroxy monomers. Molar ratios of chain length composition for each TAG(*n*) is presented in Table 3. For each TAG(*n*), the distribution of FAME(*n*) can be analyzed to identify the dominant isomers. However, this method only serves to analyze estolide chain compositions of the structural isomers present in each group. For example, a TAG(3) can have 3 possible acyl compositions, 3:0:0, 2:1:0, and 1:1:1. Although the regiochemical arrangement of the different acyl chains may also differ, this information cannot be inferred by this method (i.e. this method cannot differentiate 3:0:0 from 0:3:0 for example). A quantitative analysis of these chain lengths can still infer whether estolides can be found in all glycerol positions but not in which positions. Knowing the dominant isomer compositions may help us to establish potential TAG assembly and polymerization mechanisms.

Table 3. TAG(*n*) estolide composition and molar distribution. Relative abundance was obtained through iodine staining densitometry from TAG estolides after their glycerol-acyl bonds were cleaved.

TAG(<i>n</i>)	Estolide chain length composition (%)					
	FAME(0)	FAME(1)	FAME(2)	FAME(3)	FAME(4)	FAME(5)
TAG(0)	100.0	-	-	-	-	-
TAG(1)	65.4	34.6	-	-	-	-
TAG(2)	52.1	40.4	7.5	-	-	-
TAG(3)	43.7	36.4	17.8	2.1	-	-
TAG(4)	38.1	34.9	19.8	6.5	0.7	-
TAG(5)	37.6	32.5	19.5	8.3	1.4	0.7

Normalizing the relative FAME(n) distribution obtained through mild-transmethylation to relative TAG(n) abundance showed that FAME(1) was the dominant estolide. However, the lack of estolide, FAME(0), has a higher relative proportion than any estolide species (Fig.19).

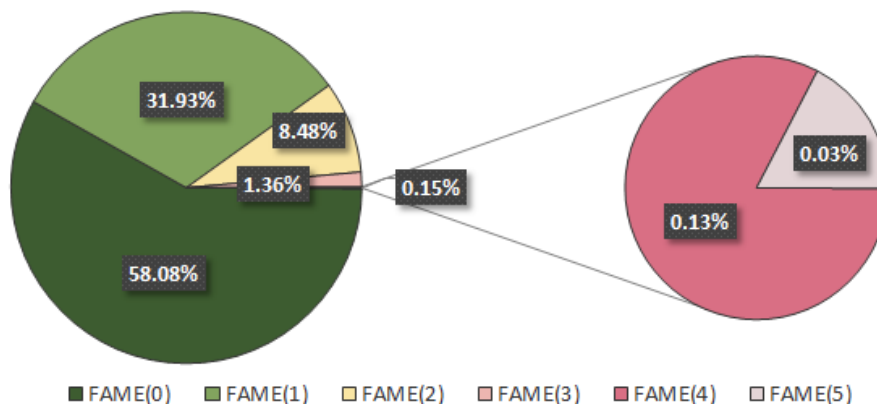


Figure 19. Overall FAME(n) composition. Molar ratios of FAME(n) distribution were normalized to the ratios of relative TAG(n) abundance.

However, using molar FAME(n) ratios for each TAG(n) molecular species to recalculate the FAME:hFAME ratio showed an even greater overestimation of normal FA content than calculated previously (Table 4). Clearly, beyond TAG(1) with increasing size the estolides had increasingly less hFA (or excess n-FA) content than anticipated. The source of the problem is unclear, but despite the use of the mild-depolymerization reaction, it remains possible that some estolide bonds are cleaved as well, albeit at a slower rate than the glycerol-acyl bonds. Furthermore, the cleavage time of estolides may also be dependent on chain length, such that an estolide with only one hFA may be cleaved faster than another with three. For TAG(2) and above there was a substantial amount of staining in the $R_f = 0.05-0.2$ region (Appendix Fig.A2). This could result from either incomplete transmethylation of the glyceryl ester linkages (giving DAG(n) and MAG(n) products), or partial clipping of the estolide chains. This last would release hydroxy-estolides and FAME, thereby removing some hFA from the analysis, and adding normal FA.

Table 4. Measured and expected molar ratios of ω -hFAs in TAG estolides. Measured ratios were calculated from molar FAME(n) ratios obtained from iodine-stained densitometry data of TAG(n) mild depolymerization.

	TAG(n)	TAG(0)	TAG(1)	TAG(2)	TAG(3)	TAG(4)	TAG(5)
Molar ratios	Normal FA	3	3	3	3	3	3
	Expected ω -hFA	0	1	2	3	4	5
	Measured ω -hFA	0	1.04	1.66	2.35	2.91	3.17

2.3.4 Estolides are attached to all three positions of glycerol to form TAG(n).

Due to the biosynthetic significance of showing that estolides can occur in any position, an alternative experiment was designed and conducted that did not rely on the quantitative approach presented above. First, the mild transmethylation approach used to release estolides from TAG(n) molecules was adapted to cleave only one glyceride ester bond and release a FAME(n) and a DAG(n) product. Then, specific DAG(n) produced from this first step was further treated with the mild-transmethylation protocol to release FAME(n). These FAME(n) molecules were then used as a diagnostic tool for the initial TAG(n) estolides. The methodology and results are depicted in Fig.20 using TAG(3) and TAG(4) as substrates. For example, TAG(3) contains one possible configuration in which an estolide is in all three positions of the glycerol backbone: 1:1:1. The partial depolymerization reaction of TAG(3) produced DAG(0) to DAG(3) however only DAG(2) can be derived from a 1:1:1-TAG(3). Thus, DAG(2) was isolated from the initial reaction and underwent further mild depolymerization. DAG(2) has two possible estolide chain length configurations, 2:0:OH or 1:1:OH, only one of which can be derived from 1:1:1-TAG(3). The mild depolymerization of DAG(2) yielded FAME(1) > FAME(2) ~ FAME(0), confirming the existence of 1:1:1-TAG(3) and presence of estolides in all three positions of glycerol. With TAG(4), it was necessary to identify its 2:1:1 estolide configuration which requires isolating DAG(2) or DAG(3) from the initial partial depolymerization and their resulting FAME(1) or FAME(1 & 2), respectively, from the final mild depolymerization.

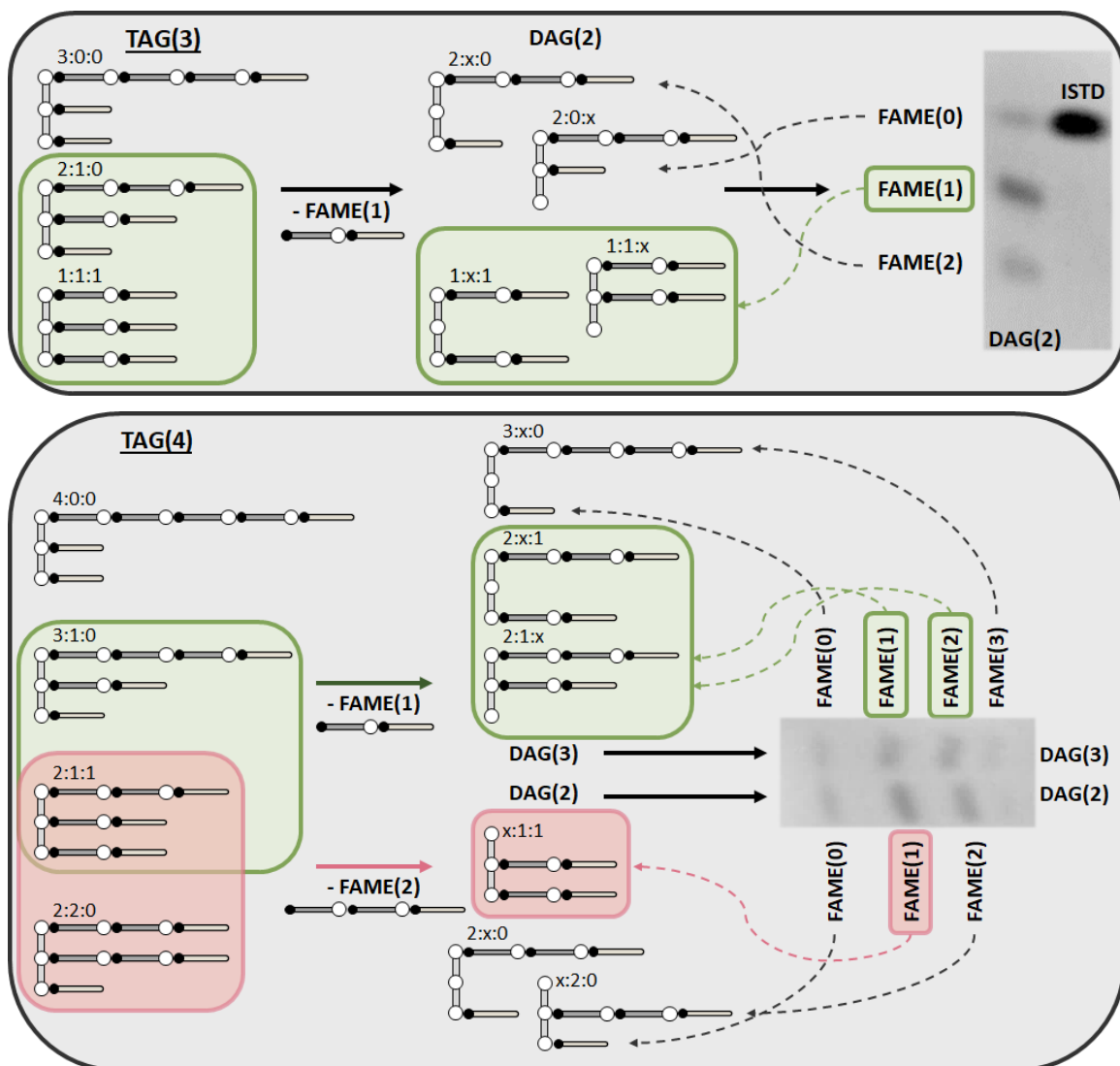


Figure 20. Flowchart for positional estolide analysis of TAG(3) and TAG(4). The “x” indicates the free hydroxyl group on the glycerol backbone in DAG(n) species. TLC analysis by Jessica Yanni (2023).

2.3.5 PC provides selected acyl groups for PAG(n) synthesis.

Phosphatidylcholine

The presence of linoleic acid (C18:2) in the stigma lipid polyesters demonstrates the involvement of the acyl editing cycle in their biosynthesis. While involved in the metabolism of membrane lipids, phosphatidylcholine (PC) is also a key element in the acyl desaturation process (Sperling *et al*, 1993; Li-Beisson *et al*, 2013) and is potentially a precursor for PC-derived DAG/TAG biosynthesis (Dahlqvist *et al*, 2000; Bates & Browse, 2011). The PC fraction from tobacco stigma was purified from TLC by first removing the polar band from neutral lipid solvent conditions, and then redeveloping that fraction in polar lipid conditions where it could be isolated from the other membrane lipids (Fig. 12-C). After transmethylation, the monomer composition of PC in stigma lipids was then analyzed by GC-FID, showing 24.9% palmitic acid (C16:0), 17.6% stearic acid (C18:0), 17.5% oleic acid (C18:1), 33.2% linoleic acid (C18:2), and 6.9% linolenic acid (C18:3) (Table 5). A notable observation is that the composition of PC differed from that of the polyester estolides as these only contain trace amounts of 16:0, 18:0 and 18:3 FAs. Therefore, these acyl monomers do not enter the PAG(n) synthesis pathway. PC data from Matsuzaki *et al* (1983a) is also presented however their data was obtained using flowers at the anthesis stage of development and also includes the style, whereas I used only developing stigmas pooled from stages 3-5 detached from the style. No hFAs were discovered in PC lipid fraction in either this work or Matsuzaki *et al* (1983a).

Table 5. Composition ratios of fatty and ω -hFAs in TAG(n) species and PC. Both TAG and PC¹ data were acquired from pooled stage 3-5 stigmas. PC² is data obtained from Matsuzaki *et al* (1983a). TAG(n) monomer data was obtained by GC-MS analysis, while PC data was acquired using the GC-FID. The “tr” denotes trace amounts and “-”, not detected. 18:3 data not obtained for TAG(n) as it co-eluted with 18:1 FAME with GC-MS analysis.

Species	FAs (% w/w)					ω -hFAs (% w/w)	
TAG(n)	C16:0	C18:0	C18:1	C18:2	C18:3	C18:1	C18:2
TAG(0)	6.0	6.1	83.4	15.1	tr	0.9	0.4
TAG(1)	1.7	1.5	64.2	11.6	tr	19.1	5.1
TAG(2)	1.3	1.0	51.5	10.0	tr	27.9	10.7
TAG(3)	1.0	0.8	42.7	8.5	tr	33.4	15.5
TAG(4)	0.9	0.7	37.4	7.6	tr	35.4	19.5
TAG(5)	0.3	0.6	35.5	6.9	tr	36.1	21.5
PC ¹	24.9	17.6	17.5	33.2	6.9	-	-
PC ²	15.0	3.9	25.6	37.6	17.9	-	-

IPPE

The IPPE, or intermediate polarity polyesters, fraction is thought to contain polyacylglycerols with unusual FAs, such as those mid chain hydroxyl groups (Matsuzaki *et al*, 1983a; Wang *et al*, 2003). A MAG(n) ladder was prepared from a TAG(n) fraction by partial depolymerization using very short incubation times developed and analyzed by TLC alongside the IPPE fraction using a chloroform-ethanol based solvent system. However, while the lipids migrated from the baseline, they smeared during development and did not produce distinct bands (Fig.21). A separate solvent system is likely required for isolating IPPE molecules. Furthermore, GC-MS analysis with acidic transmethylation and TMS derivatives failed to demonstrate any unusual fatty acyls, such as mid chain-containing diOH-FAs or allylic alcohols, as demonstrated in preliminary experiments by Wang *et al* (2003). Confirming the presence of these acyl groups may elucidate certain characterized enzymes involved in the stigma polyester synthesis and may establish further comparisons to known pathways, like cutin for example. These lipids present a significant curiosity and are expected to provide important insight upon further investigation.

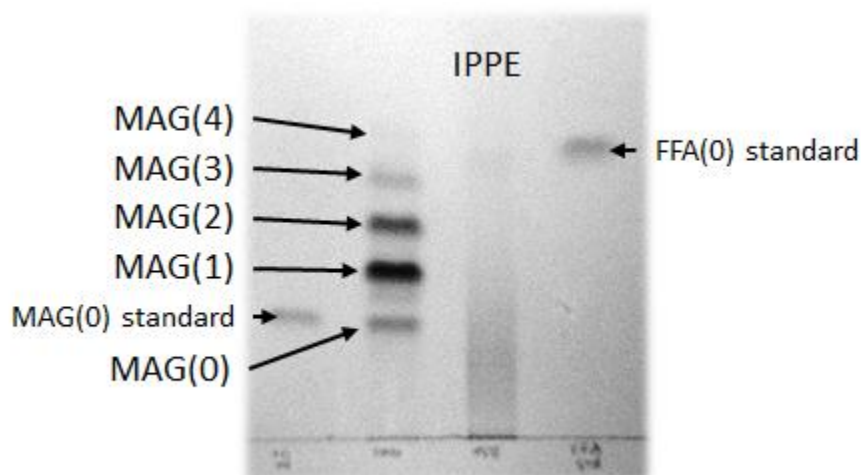


Figure 21. Attempted IPPE development with MAG(n) ladder. Dual development in solvent consisting of 3.5% EtOH in CHCl₃.

2.4 Discussion

The wet stigmas of the model *Solanaceae* species tobacco and petunia, contain a sticky exudate rich in ω -hFAs. The ester linkage between an acyl group and the hydroxyl group of an hFA forms an estolide. The glycerolipid with the most prevailing ester linkages between ω -hFAs is found in the cuticle in the form of cutin, forming its basic structure while containing additional ester linkages to glycerol and other polyhydroxyacyl monomers. Estolides containing ω -hFA are rarely found in seed oil glycerolipids but have been reported both in kamala and false white teak seed oils which consist of kamolenic acid (Rajiah *et al*, 1976; Smith *et al*, 2013). Matsuzaki *et al* (1983b) described the presence of ω -hFA estolides in the exudate of tobacco stigmas in the form of TAG(n), DAG(n) and free estolides. These estolides were demonstrated to consist of ω -hFA chains end-capped by normal FAs (Matsuzaki *et al*, 1988). A total of 51 species of *Nicotiana* along with 25 other species were investigated for their hFA content, demonstrating that petunia stigma lipids had the highest relative proportion of ω -hFA (96%) whereas tobacco contained 56% (Koiwai & Matsuzaki, 1988). The mechanism for stigma lipid polyester synthesis was the subject of this work and the lower acyl count in tobacco made it the more alluring model for observing chemical changes between lipid species.

2.4.1 Stigma polyesters are assembled in the glandular zone prior to surface export.

Gravimetric analysis of tobacco stigmas demonstrated significant accumulation of lipids within the surface exudate fraction. Bayberry fruit wax, another source of surface TAG accumulation, has the highest reported surface lipid accumulation of any plant species with up to 8.7 mg wax cm⁻². In comparison, tobacco stigma lipid yielded 3.0 mg cm⁻² (Appendix Table A1), tomato fruit cutin yields around 1 mg cm⁻² (Yeats *et al*, 2012), and Arabidopsis stems contain 32 µg wax cm⁻² and 3-8 µg cutin cm⁻² (Suh *et al*, 2005). Therefore, wet stigmas are a considerable source of easily extractable ω-hFA, a molecule with demonstrated industrial value (Isbell, 2011).

Tobacco stigma estolides were identified in three separate lipid classes across all development stages of the flowers: TAG(n), DAG(n), and FFA(n). These estolides were also present in both α,β-DAG(n) and α,α-DAG(n) isoforms. Differentiating between surface and internal lipids allowed the flux of these lipids to be tracked throughout their development, giving insight into their biosynthesis compartmentalization. The surface lipid fraction contained only extracellular lipids and mainly those deposited externally whereas the internal fraction originated from homogenized tissues post surface lipid extraction, and contained inter- and extracellular lipids, as well as membrane lipids. Monomer analysis of these fractions revealed a greater relative proportion of ω-hFA in the surface lipids across stages, indicating a greater proportion of longer estolide chains than within the stigmatic tissue. The distribution of these glycerolipid estolides revealed minimal, if any, presence of soluble polyesters in the surface exudate fraction of stage 1 stigmas. Furthermore, minimal TAG(0) was observed on the surface across all stages, suggesting that this fraction is mostly intracellular. Lastly, the accumulation of these lipids within the stigmatic tissue diminished in the later stages of development, after stage 5, while continuing to accumulate on the surface until at least stage 7. These all confirm the TEM observations by Cresti *et al* (1986) that polyester assembly is likely to occur within the stigmatic tissue and lipids within the exudate are then exported to the surface. However, whether the location of specific steps of this process (i.e. intracellular or extracellular) is still unclear.

The high accumulation of estolide-containing α,α -DAG(n) in stigma extracellular lipids make them unique compared to other triacylglycerides, including seed oil and waxes, and their mechanism of biosynthesis –as well as their analysis– must reflect such complexity. The high presence of α,α -DAG(n) brought up the questions of whether these may be precursors of TAG(n) synthesis or just an isomerization of α,β -DAG(n) to the more stable α,α -DAG(n) isoform. Isomerization between α,β - and α,α -DAGs through acyl migration has been previously described (Crossley *et al*, 1959; Mattson *et al*, 1962), reaching a natural equilibrium around 58% α,α -DAG: 42% α,β -DAG. It is possible that α,α -DAG(n) remains the more stable isoform with the addition of estolides. Thus, α,β -DAG may be the key intermediate for TAG biosynthesis in tobacco stigma lipids while α,α -DAG is simply a product of DAG isomerization. However, the distribution of α,β -DAG(1) from stage 5 and onwards presented a greater quantity than both α,β -DAG(0) and α,β -DAG(2) observed only in the internal lipids fraction (Fig.16) which may involve the possible co-eluting of an unknown internally-located compound.

The distribution of free estolides demonstrated the largest accumulation and relative proportion of free fatty acid, FFA(0), at stage 7, which defines the anthesis stage of the flower. It is likely that anthesis represents a significant metabolic change in which these polyesters begin to depolymerize, as seen in Fig.15 with the decrease in TAG(n) content. TAG degradation has been reported in the stigmas of sunflowers during the staminate stage (when stamens protrude from the flower which coincides with anthesis, S7) and are resynthesized during the pistillate (stigma protrudes and exposes papillate) stage of flower development; this activity is concurrent with lipase (β -1,3 glucanase) and acyl ester hydrolase activity (Shakya & Bhatla, 2010; Sharma & Bhatla; 2014). The same lipase is also expressed in petunia stigma (Wakelin & Leung, 2009). Since the main objective of this research is to study the assembly mechanisms of these polyesters, the anthesis stage serves as the upper limit for the labeling assays described in Chapter 3.

2.4.2 TAG(n) characterization shows an underestimation of hFA content.

Understanding the chemical composition of stigma lipid polyester will help elucidate the metabolic processes involved in their biosynthesis. TAG(n) polyesters were determined to consist mainly of 18:1 and 18:2 FAs and their respective ω -OH counterparts, consistent with the results reported by Matsuzaki *et al* (1983b). The ratios of ω -hFAs to normal FAs presented in the published work demonstrated that the polyesters, both TAG(n) and DAG(n), consisted of ester-linked ω -hFA chains that were end-capped by normal FAs (Matsuzaki *et al*, 1986). These ratios were identified through GC-MS and confirmed using IR spectroscopy. However, my data shows either an underestimation of ω -hFA content or an overestimation of normal FA abundance (Table 2) to match those ratios.

A possible explanation for the underestimation of hFA content in our analysis could be the choice of internal standard used for our GC analysis, ω -pentadecalactone (PDL). This compound is present as a cyclic FA where the head is ester bound to the tail, during transmethylation this ring is cleaved forming a C15:0 ω -hydroxy fatty acid methyl ester (ω -HFAME). PDL is used to verify the completion of the transmethylation reaction as well as to quantify the amount of hFAs in the sample post-derivatization (Bonaventure *et al*, 2004; Molina *et al*, 2006). A GC experiment by Yang *et al* (2016) tracked the degree of PDL transmethylation and found a significant loss in total PDL when unreacted PDL and its depolymerization product were added up from the chromatographic results. It is implied that PDL is forming oligomers with itself via ester bond rather than creating methyl esters, a concept known as ring-opening polymerization (ROM; Nuyken & Pask, 2013). This process has been shown to occur using enzyme catalysts (Bisht *et al*, 1997; Kumar *et al*, 2000), organic catalysts (Bouyahyi *et al*, 2012), and metallic catalysts (Zhong *et al*, 2000; Wilson *et al*, 2014). Thus, it is important to find an alternative internal standard to accurately quantify the hFA content in GC analyses. Furthermore, future experiments should use GC-FID rather than GC-MS for monomer quantification. While GC-MS should be used for compound identification, GC-FID has a much better linear dynamic range for FA analysis (Wu *et al*, 2017).

2.4.2 Iodine-stained densitometry is not suitable for quantitative analysis.

Total lipid fractions and lipid estolide ladders were quantified directly from TLC plates through iodine-stained densitometry. The relative ratios obtained between lipid classes (TAG, DAG, FFA, IPPE, PL) are comparable to previous research (Wang *et al*, 2003) which used a similar iodine-staining densitometry analysis method. However, it differs from the initial studies completed by Matsuzaki *et al* (1983a) that rely on GC quantification, which show that stigma lipids contain nearly twice the TAG(n) to the DAG(n). It is important to note that the results obtained through band intensity analysis from iodine-stained TLC plates intrinsically induce error to the calculations. Iodine-staining is a destructive analysis method which binds to and disrupts the double bonds present in a compound (Christie & Han, 2010), so there are concerns regarding uniform staining across multiple TLC plates, loss due to over exposure, overestimates of compounds with multiple double bonds, and lack of identification to those without unsaturation. Nonetheless, with consistent methodology, this analysis technique proves useful for researching intact lipid polyesters and observing trends. The majority of the experiments that rely on TLC imaging in this chapter need to be repeated in the future to include band isolation and gas chromatography (FID) monomer analysis for more accurate quantification.

2.4.3 Estolides can occur in any glycerol position.

The positional estolide analysis of TAG(n) species in tobacco stigmas demonstrated that the estolides can occur in any glycerol position (Fig.20) and may suggest that their mechanism of assembly is thus different from that of TAG oil estolides. Furthermore, DAG(n) and TAG(n) estolides have been shown to consist of ω -hFA end-capped by normal FAs. These estolides were shown to have considerable potential for a wide range of industrial applications, especially lubricants, specifically free estolides containing both hydroxy and unsaturated FAs, such as the oleic acids estolides in tobacco stigmas (Isbell *et al*, 2006; Isbell, 2011). The presence of estolides in triacylglycerols has been reported in various oilseed species, however never in all three glycerol positions. For example, Greek thistle seed oil contains a penta-acylglycerol with an estolide in the central position of glycerol (Mikolajczak & Smith, 1968); Chinese tallow tree seed oil has its estolide in the third position of glycerol (Sprecher *et al*, 1965); some

Lesquerella species, contains estolides on both outer positions of glycerol (Hayes *et al*, 1995); and false white teak seed oil contains a long (up to 14 acyl group) ω -hFA estolide in one glycerol position that is end-capped by a normal FA (Rajiah *et al*, 1976; Smith *et al*, 2013). While these estolides can potentially be observed in cutin, they are not as readily extractable due to their insolubility. Tobacco stigma lipids produce free estolides and their ability to have estolides attached to any glycerol position essentially triples the potential output of highly desirable FAs over most oilseed production. Thus, understanding the biosynthetic mechanisms for stigma polyester production can be a valuable venture for engineering large amounts of rare and advantageous FAs.

2.4.4 Phosphatidylcholine is involved in estolide acyl desaturation but not acyl hydroxylation.

Monomer analysis on the PC lipid fraction in tobacco stigma lipids demonstrated the presence of PC-modified FAs, such as 18:2 and 18:3, however no presence of hFAs were identified (Table 5). The most common method of triacylglycerol (TAG) biosynthesis is either through *de novo* DAG/TAG synthesis or phosphatidylcholine (PC)-derived DAG/TAG synthesis pathways, as commonly seen in oilseed lipids (Bates & Browse, 2012). In short, these use subsequent acylation of the glycerol backbone from positions *sn*-1 to 3, with the latter using PC as an intermediate for DAG/TAG production. The membrane lipid PC can be involved in the production of TAGs through acyl editing or as a precursor for DAG/TAG biosynthesis (Sperling *et al*, 1993; Bates *et al*, 2007; Dahlqvist *et al*, 2000). The desaturation of 18:1 to 18:2 FA, which is present in tobacco stigma lipids, requires the FAD2 enzyme to interact with PC-bound acyl groups (Okuley *et al*, 1994). Certain hydroxyl functional groups have been shown to be PC-produced, such as the production of ricinoleic acid through a FA hydroxylase (Moreau & Stumpf, 1981). However, monomer analysis from both this work and Matsuzaki *et al* (1983a) showed no presence of ω -hFA in PC composition whereas castor seed oil is shown to accumulate ricinoleic acid in PC. Therefore, if the hydroxylation of oleic and linoleic acid in tobacco stigma occurs via PC then it must be highly transient with a very high turnover rate. Furthermore, oat kernels have demonstrated the ability for estolide to form on galactolipids (Hamburg *et al*, 1998; Moreau *et al*, 2008), but the presence of estolides were not present in PC, or any other membrane lipids, as reported by Matsuzaki *et al* (1983a). PC composition was shown to vary significantly to that of the stigma glycerolipid estolides, which did not accumulate 16:0, 18:0 and 18:3 normal FA in similar

proportions. Thus, there likely exists a sort of exclusion mechanism or preferential selectivity of acyl monomers for stigma polyester production.

A parallel can be made between stigma lipids and cutin, both of which contain ω -hFAs ester bonded into estolides and to a glycerol moiety. In fact, the only enzyme of the stigma lipid pathway characterized so far, CYP86A22, is a homolog of CYP86A2/ATT1, a hydroxylase required for cutin monomer oxidation (Han *et al*, 2010; Xiao *et al*, 2004) and not associated with PC. In cutin, the production of *sn*-2-hydroxyacyl-MAG intermediates are catalyzed by specific GPAT enzymes (GPAT4, GPAT6, and GPAT8; Li *et al*, 2007) which are ultimately used for acyl transesterification expanding the cutin matrix through cutin synthase enzymes (Girard *et al*, 2012; Yeats *et al*, 2012; Hong *et al*, 2017). A similar process may be used in the formation of stigma estolides, and further research should investigate the presence of hydroxy-MAG components in stigma lipids. MAG(0) or MAG estolides capped with normal FAs, however, did not accumulate and if involved, must be a highly transient stage that is a limiting step in the biosynthesis process and thus gets utilized almost immediately. The lack of MAG differentiates stigma lipids to bayberry fruit wax, whose synthesis relies on MAG:MAG transacylation and subsequent MAG:DAG transacylation (Simpson & Ohlrogge, 2016). Since neither of the known glycerolipid metabolic pathways can fully describe the synthesis of stigma lipid polyesters, it is possible that a novel mechanism is involved. To gain further insight on the possible mechanism of biosynthesis of tobacco stigma PAG(n), I developed an *in planta* radiolabeling assay (Chapter 3).

2.5 Conclusions

Stigma lipid polyesters accumulated throughout development in the form of TAG(n), DAG(n), and FFA(n). These are composed primarily of oleic, linoleic acid, 18-hydroxyoleic acid, and 18-hydroxylinoleic acid that form estolides through the ester bonding of these acyl groups. The estolides consist of ω -hFAs end-capped by normal FAs. Polyester distribution between surface and internal lipid extracts and across the development stages of the stigmas suggests that these are produced within the glandular zone of stigmatic tissue and then are exported to the stigma surface. However, whether this process occurs intracellularly or extracellularly is still to be determined. Distinctions between estolide chain length and DAG(n) isomer accumulation suggest that α,α -DAG(n) may be product of α,β -DAG(n) isomerization but whether either is used as substrate for TAG(n) synthesis is also yet to be determined. Estolide positional analysis on TAG(n) species demonstrated that estolides were able to occur in any position along the glycerol backbone. Composition of phosphatidylcholine suggests it is not involved in acyl hydroxylation or estolide formation but only acyl desaturation for DAG(n)/TAG(n) biosynthesis. No significant data was obtained during the analyses of the IPPE fraction and alternate extraction and identification methods have been developed for a repeat analysis. Inherent measurement errors were discovered in this work through iodine-stained densitometry quantification and an underreporting of hFAs in GC-MS quantification. Affected results need to be reanalyzed under appropriate conditions.

Appendix A

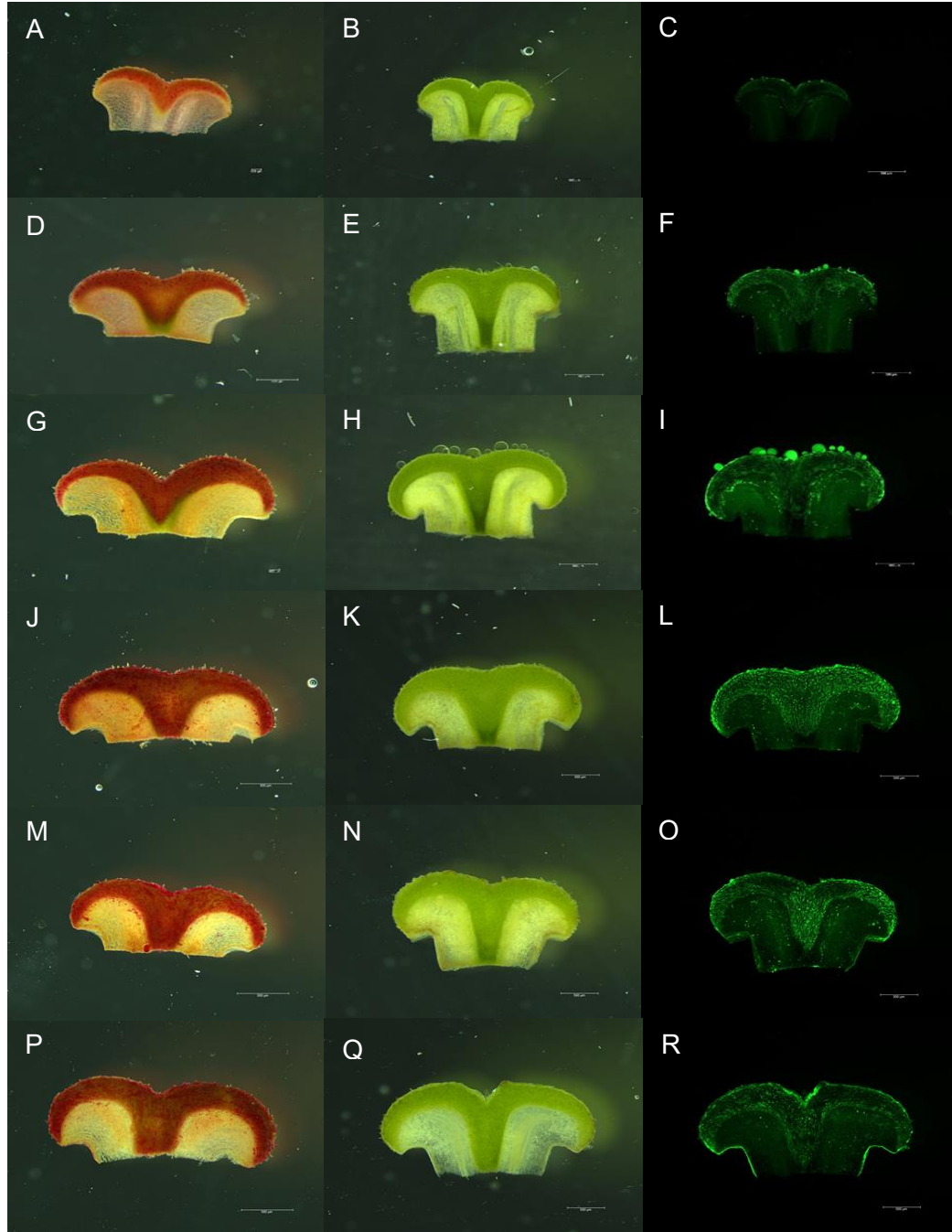


Figure A1. Free-hand longitudinal sections of *Nicotiana tabacum* (Maharjan, 2022); (A, B, C) = S1; (D, E, F) = S2; (G, H, I) = S3; (J, K, L) = S4; (M, N, O) = S5; (P, Q, R) = S6; (A, D, G, J, M, and P) stained with Sudan Red under dark-field microscopy; (B, E, H, K, and Q) stained with Fluorol Yellow 088 under dark-field and (C, F, I, L, O, and R) under fluorescence microscopy. Scale bars = 500 μm .

Table A1. Stigma lipid concentration across developmental stages. Stigma mass obtained gravimetrically from pooled samples of surface lipid extracts averaged across 4 replicates. Stigma diameter measured from microscopy imaging. Surface area is approximated as hemi-spherical and calculated accordingly.

Stage	1	2	3	4	5	6	7
Stigma diameter (mm)	1.10	1.80	2.30	2.08	2.04	2.17	2.20
Surface area (mm ²)	1.90	5.09	8.31	6.82	6.57	7.37	7.60
Surface lipid mass (ug)	5.1	14.3	23.3	59.0	100.7	184.3	231.0
Concentration (ug/cm ²)	267.8	281.4	280.8	865.2	1532.2	2501.5	3039.0

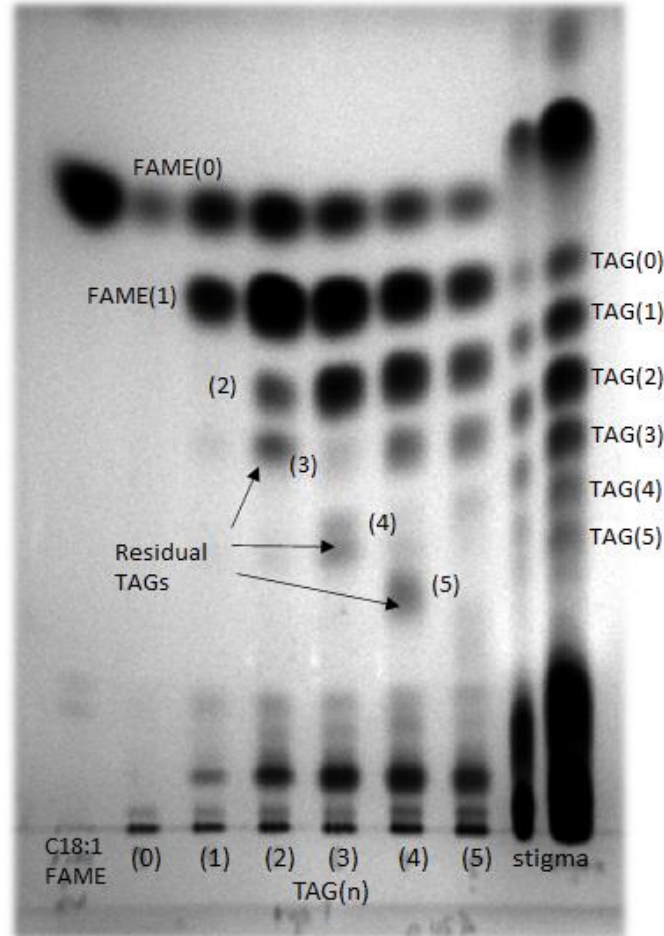


Figure A2. Iodine-stained TLC showing the mild-depolymerization of TAG(n). Estolides are cleaved from glycerol backbone and released as FAME(n).

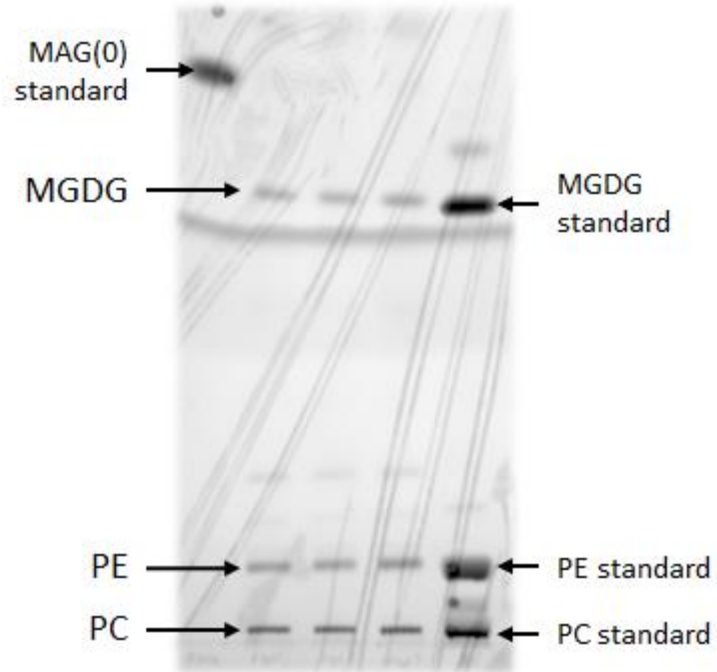


Figure A3. Iodine-stained polar lipids with MAG(0) standard. Triplicate stigma samples developed twice in 3.0% EtOH in CHCl₃ then once in 91:30:7:1 acetone-toluene-water-acetic acid.

Chapter 3: In vivo [¹⁴C]-Tracing of Wet Stigma Lipid Metabolism

3.1 Introduction

All aerial plant surfaces are protected by a cuticle layer composed of waxes and cutin. These lipids interact with the external environment and have protective functions against biotic and abiotic factors, provide a physical barrier against pathogens and prevent drought stress through the control of water exchange (Delwiche & Cooper, 2015). Cutin is an insoluble glycerolipid polyester rich in glycerol and hFAs, among other acyl monomers, with varying composition and structure depending on the plant species and organ type (Kolattukudy, 1981). Certain angiosperms plants contain another type of surface glycerolipid polyesters found in the exudate of their wet stigmas that is soluble in organic solvents. In tobacco, these stigma polyesters were found to contain estolides of ω -hFA end-capped by normal FA bound to a glycerol backbone in the form of diacylglycerol (DAG) and triacylglycerol (TAG) (Matsuzaki *et al*, 1983b; Koiwai & Matsuzaki, 1988). Unlike oilseed TAG, stigma TAG accumulates on the surface, a phenomenon seen in the wax of bayberry fruit, which is composed almost entirely of TAG and DAG (Simpson & Ohlrogge, 2016). Bayberry wax has the highest reported surface lipid accumulation of any plant species with up to 8.7 mg wax cm⁻² and tobacco stigma lipid accumulate up to 3.0 mg cm⁻² (Appendix Table A1). Therefore, wet stigmas are a considerable source of easily extractable ω -hFA, a molecule with recognized industrial applications, such as lubricants or petroleum alternatives (Isbell, 2011). Understanding the mechanisms of stigma lipid polyester biosynthesis will expedite the engineering ability of large-scale production of highly desirable acyl components.

Radioactive isotopes have been extremely useful to understand plant lipid metabolism as they can serve as “tracers” to observe fluxes in metabolic pathways (Allen *et al*, 2015). Isotopes are variants of a chemical element with a different number of neutrons but the same number of protons. They can be stable or radioactive, depending on their half-life: for example, carbon-13 is stable, whereas carbon-14 is radioactive with a half-life of 5730 years. Stable isotopes can be applied to model metabolic pathways by detecting variation in the position and the degree of isotope labeling in developing metabolites using NMR and mass spectrometry, respectively. Alternatively,

radioisotopes provide a signal that can be traced through metabolic pathways, allowing real-time monitoring of metabolite production and turnover through a given process.

Various avenues for DAG and TAG biosynthesis have been described for oilseed production (Chapman & Ohlrogge, 2012; Bates & Browse, 2012). The simplest pathway for DAG to TAG synthesis directly uses the products of FA synthesis for *de novo* DAG/TAG synthesis; where subsequent acylation of glycerol-3-phosphate (G3P) occurs to form lysophosphatidic acid (LPA), then phosphatidic acid (PA) which is dephosphorylated to DAG, and then a final acylation producing TAG (Weiss & Kennedy, 1956; Weiss *et al*, 1960). Additionally, this pathway can invoke the acyl editing cycle to incorporate modified FAs into the glycerolipid production. Acyl groups esterified to the membrane lipid phosphatidylcholine (PC) can be modified through desaturase or hydroxylases, and then released back into the acyl-CoA pool where they can be incorporated into DAG/TAG synthesis (Bates *et al*, 2007). Alternatively, PC, that is synthesized through *de novo* DAG, can be used as a substrate for both DAG and TAG synthesis. Interconversion between DAG and PC creates a secondary pool of PC-derived DAG which may contain modified acyl groups and can be used for TAG production (Slack *et al*, 1983; 1985; Vogel & Browse, 1996; Lu *et al*, 2009). Lastly, PC can be used as the source for the final acyl transfer to DAG to produce TAG (Dahlqvist *et al*, 2000).

Different plant species may have different modified acyl flux pathways for TAG biosynthesis; labeling data suggest some may rely mainly on *de novo* DAG, such as avocado mesocarp (*Persea americana*) (Griffiths *et al*, 1988), *Coriandrum sativum* (Cahoon & Ohlrogge, 1994), *Cuphea lanceolata* (Bafor *et al*, 1990), and *Theobroma cacao* (Griffiths & Harwood, 1991), while others rely on PC-derived DAG, such as *Arabidopsis thaliana* (Bates & Browse, 2011) or soybeans (*Glycine max*) (Bates *et al*, 2009). Or a combination of both methods may be used as suggested in castor (*Ricinus communis*) (Bafor *et al*, 1991).

Particular labeling substrates can be used to study metabolism depending on tissue and reaction of interest, such as water and glycerol. The elemental isotopes of carbon, namely [¹⁴C], have proven to be advantageous metabolic tracers as they are relatively safe, easy to detect, and have a very little natural occurrence (Allen *et al*, 2015). For FA biosynthesis and lipid metabolism, labeled acetate is typically used as it can be taken up into the acetyl-CoA pools incorporating almost entirely into the acyl

group of glycerolipids. Furthermore, oilseed studies generally use glycerol labeling in conjunction with acetate (Pollard *et al*, 2015). Like acetate, exogenous glycerol is taken up into the glycerol 3-phosphate (G3P) pools and used in glycerolipid biosynthesis, but instead is mostly incorporated into the glycerol backbone of these lipids. Typically, about 5-10% of glycerol label is incorporated into the acyl moieties as G3P can be used as a precursor for plastidic acetyl-CoA synthesis (Slack *et al*, 1977; Bates *et al*, 2009). This percentage has been shown to increase with higher exogenous glycerol concentrations (Pollard *et al*, 2015). This combination of substrate labeling between acetate and glycerol has been previously used to accurately define and model the metabolic fluxes for differing TAG biosynthesis mechanisms, i.e. the Kennedy pathway (Bates & Browse, 2011) and the cutin-like *sn*-2-MAG pathway (Simpson & Ohlrogge, 2016).

Radioactive (or stable isotope) labeling assays can be used to determine the relative fluxes through these potential metabolic pathways by tracing the kinetics of a labeled substrate through precursors, intermediates, and final products. First used by Smirnov (1960), [¹⁴C]-acetate became the standard substrate for FA labeling in plants due to its low cost and that it labels acyl group and not head groups. While [³H]- or [¹⁴C]-glycerol labels the head groups and is useful for monitoring lipid classes. Typically, they are partnered together for glycerolipid analysis (Slack *et al*, 1978). In the Kennedy pathway, exogenous glycerol can only be incorporated into TAG through *de novo* DAG or PC-derived DAG, whereas acetate can be incorporated through *de novo* DAG synthesis, acyl editing through PC, or DGAT (Fig.22). Glycerol labeling is thus effective for identifying the relative fluxes of TAG synthesis from either DAG pool, acetate for determining the relative rates of *de novo* DAG synthesis and acyl editing.

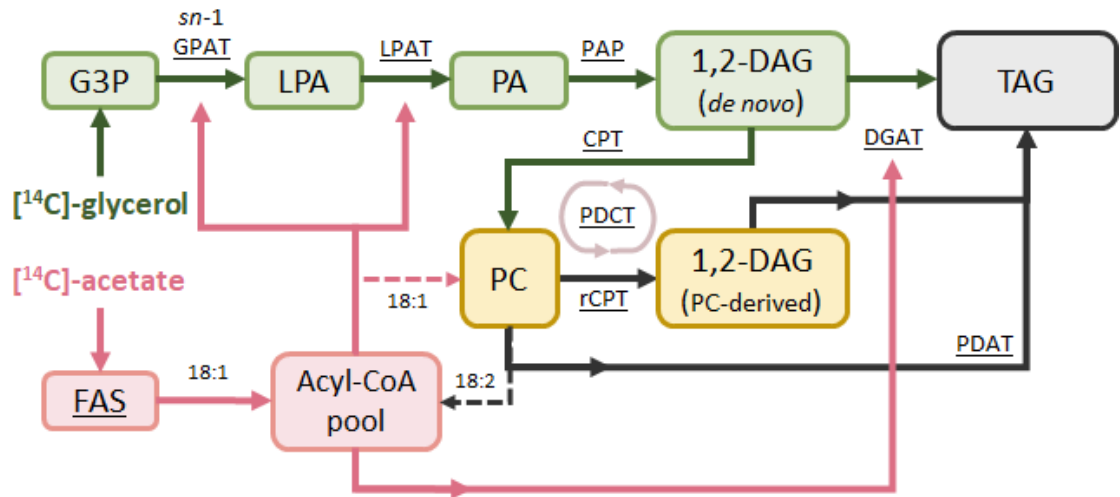


Figure 22. Combined *de novo* DAG and PC-derived DAG/TAG synthesis pathways and initial [¹⁴C] labeling flux. (Adapted from Bates & Browse, 2012). Green arrows show initial labeling flux from exogenous glycerol, pink arrows show that of acetate, and black, those that will not have any label initially but will accumulate over time. Substrate abbreviations: G3P = glycerol-3-phosphate; LPA = lysophosphatidic acid; PA = phosphatidic acid; DAG = diacylglycerol; TAG = triacylglycerol; PC = phosphatidylcholine; CoA = coenzyme-A. Enzymatic reaction abbreviations, underlined: FAS = fatty acid synthesis; GPAT = G3P-acyltransferase; LPAT; LPA-acyltransferase; PAP; PA-phosphatase; DGAT = DAG-acyltransferase; CPT = cholinephosphotransferase; rCPT = reverse CPT (can also be phospholipase C or D); PDCT = PC:DAG-CPT; PDAT = phospholipid:DAG acyltransferase.

The labeling kinetics of PC, DAG, and TAG during lipid assembly varies between substrates and according to the mechanism of acyl incorporation and presence of acyl modification steps (Fig.23). Generally, the *de novo* DAG synthesis pathway can be depicted when DAG is labeled prior to both PC and TAG when using [¹⁴C]-acetate as substrate (Allen *et al*, 2015). However, when acyl editing is involved, PC is labeled faster than both DAG and TAG. The presence of a second PC-derived DAG pool required for TAG production may result in more convoluted [¹⁴C]-glycerol labeling patterns, as they are dependent on the size of the pools and the net and reversible fluxes between them. Thus, these labeling patterns may vary drastically from what is expected of standard precursor-product relationships.

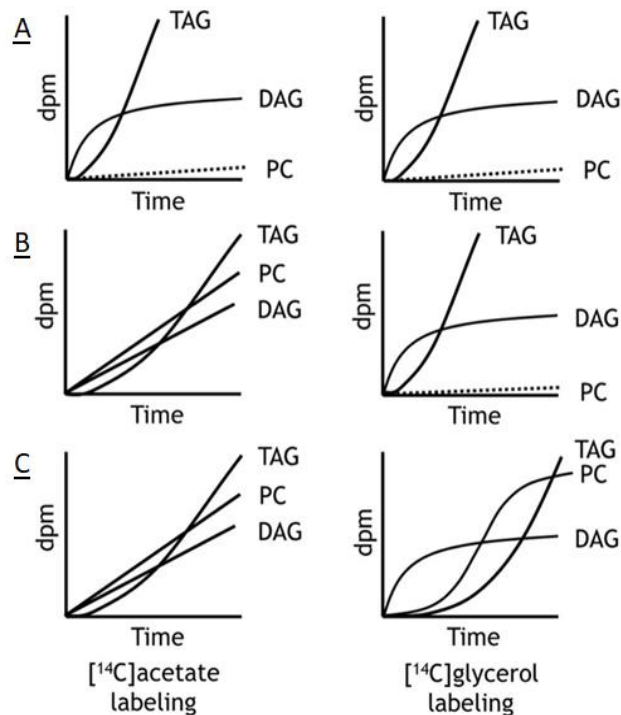


Figure 23. Expected precursor-product relationships for TAG synthesis in the Kennedy pathway and its variants (Adapted from Allen *et al*, 2015). (A) Standard Kennedy pathway using *de novo* DAG intermediates without acyl editing. (B) *De novo* DAG pathway with PC-involved acyl editing into the acyl-CoA pool. (C) Acyl editing with multiple DAG pools and PC-derived DAG/TAG synthesis.

TAG biosynthesis from PC-derived DAG has been identified in soybean embryo oil, which contains over 60% of PC-modified FAs. This study was performed by Bates *et al.* (2009) who utilized [^{14}C]-glycerol labeling with very short time points to observe the initial products of glycerolipid biosynthesis. The initial labeled DAG, synthesized *de novo*, contained more 18:1 FAs and less modified FAs than the bulk DAG pool. The acyl composition of bulk DAG was much more comparable to that of bulk PC. Furthermore, initial labeling rates indicated that over 90% of *de novo* DAG was used for PC rather than TAG synthesis. However, to achieve the desired ratio of end products, approximately a 20:1 TAG:membrane lipid ratio in soybean embryos, about 95% of DAG synthesized should be used to produce TAG. Through [^{14}C]-acetate labeling, PC was found to be labeled much faster than either *de novo* DAG or TAG. Moreover, stereochemical analysis on initial labeling showed that DAG had about equal labeling on the *sn*-1 and *sn*-2 positions whereas TAG was mostly labeled on the *sn*-3 position. The

sn-1 and *sn*-2 positions of bulk TAG were also more similar in composition to bulk DAG and bulk PC rather than *de novo* DAG. This indicates that the prevailing pathway for TAG synthesis is through PC-derived DAG. Similar results were acquired in Arabidopsis seeds as well (Bates and Browse, 2011).

TAG synthesis that uses *de novo* DAG as the major pathway is seen in plants that contain mainly plastid-derived FAs in its TAG content. Avocado fruit mesocarp contains TAG rich in 18:1 content and little PC-modified FAs (Griffiths *et al*, 1988). Substrate incorporation of [¹⁴C]-glycerol saw labeled Kennedy pathway intermediates with very little PC labeling. Similar results were found in cocoa cotyledons (Griffiths & Harwood, 1991) where the TAG content consists mainly of 16:0, 18:0, and 18:1 FAs. Furthermore, *Cuphea lanceolata* contains over 80% of TAG FAs as 10:0, an unusual FA produced in the plastid, and less than 1% in PC; [¹⁴C]-glycerol shows very little PC synthesis during TAG accumulation and suggest enzymatic acyl selectivity of 10:0-DAG for TAG production and 16:0/18:0-DAG for membrane lipids (Bafor *et al*, 1990). Nonetheless, *Cuphea l.* TAG does contain about 16% PC-derived FA which are likely introduced to the acyl-CoA pool through acyl editing then used in *de novo* DAG/TAG synthesis. In coriander, [¹⁴C]-glycerol labeling shows the same *de novo* DAG/TAG synthesis pathway and accumulates 75% of 18:1Δ6 FA (which is not PC-modified) and about 13% PC-modified FA in its TAG content. However, [¹⁴C]-acetate labeling shows 18:1Δ6 FA entering PC (through the acyl editing cycle) prior to being used for *de novo* DAG/TAG synthesis, indicating the acyl editing cycle may still be a major flux even in species which do not contain high amounts of PC-modified FAs.

Castor TAG accumulates ricinoleic acid, a 12-OH FA derived from 18:1, which is modified in the *sn*-2 position of PC by a variant of the FAD2 enzyme, castor FA hydroxylase (Moreau & Stumpf, 1981). This accounts for around 90% of the total FAs in castor TAG, and over 70% of these TAG contain them in all three positions (Lin *et al*, 2003), however only about 5% accumulates in PC (Stahl *et al*, 1995). Ricinoleic acid must then be removed from the *sn*-2 position of PC to the acyl-CoA pool where it can be redistributed to all three positions in TAG. However, di-hFA-DAG has been shown to be the preferred substrate for TAG synthesis over mono-hFA-DAG whereas PC was shown not to have any selectivity preference (Vogel & Browse, 1996). Thus, it remains a possibility that mono-hFA-(*de novo*)-DAG gets converted to PC and undergoes a second hydroxylation, leading to a di-hFA-(PC-derived)-DAG which can then be used for TAG synthesis. Using [¹⁴C]-G3P and ricinoleic acid-CoA as substrates in microsomes, PC

was found to synthesize at about $\frac{1}{3}$ the rate of TAG synthesis, which suggest that both *de novo* and PC-derived may be involved in TAG synthesis (Bafor *et al*, 1991).

The TAG found in bayberry (*Myrica pensylvanica*) wax is suggested to follow a *sn*-2-MAG derived synthesis pathway resulting from transacylation between glycerolipid species (Simpson & Ohlrogge, 2016). In the early stages of bayberry wax development, TAG was the most abundant surface glycerolipid. However, by mature stages, DAG was almost twice as abundant as TAG and MAG would accumulate to about 4%. In contrast, oilseed lipids contain over 95% of glycerolipid content as TAG and without any detected MAG accumulation (Slack *et al*, 1980). The bayberry DAG and MAG accumulation was shown not to be derived from TAG degradation but from new synthesis (Simpson & Ohlrogge, 2016). MAG was identified as predominantly the *sn*-2 over *sn*-1/3 (7:1) isoform. Both [¹⁴C]-acetate and [¹⁴C]-glycerol labeling studies were performed on bayberry glycerolipids. For glycerol, MAG initially possessed the majority (85%) of the [¹⁴C] label until it achieved a steady state. Then DAG, initially lagging behind MAG, became the most labeled until the end of the trial. Finally, TAG was labeled with a steady increase throughout the trial after a significant lag time after MAG and DAG. However, considering that only saturated FA species were detected in MAG, DAG, and TAG (16:0 < 75%; 14:0 > 25%; 18:0 > 1%), PC expressed less than 5% of the total radioactivity.

Unlike oilseed labeling, initial labeling kinetics in bayberry fruit wax using labeled acetate were quite similar to that of glycerol, initially depicting MAG with the greatest proportion of label, then the subsequent emergence of DAG, and finally TAG given their respective lag phases (Simpson & Ohlrogge, 2016). Again, PC was never more abundant than MAG in the initial stages and expressed less than 10% of the total radioactivity. In the Kennedy pathway, for plants that accumulate primarily saturated or monounsaturated FAs, the lag phase in DAG and TAG acyl incorporation is not observed. These FAs, present in the acyl-CoA pool post synthesis, have an equal chance of reacting with G3P, LPA, and DAG and therefore labeled DAG and TAG would initially be produced at similar rates (Allen *et al*, 2015).

Regiospecific analysis of labeled bayberry DAG across all time points showed a near equal amount of radioactivity distribution on its *sn*-2 and *sn*-1/3 positions, suggesting that the DAG was synthesized by the transacylation of one *sn*-2 MAG to the

sn-1/3 position of another (Simpson & Ohlrogge, 2016). Furthermore, a similar analysis performed on labeled bayberry TAG shows that the third and final acylation, which must occur on either *sn*-1 or -3 positions, had more than four times the relative label distribution compared to the *sn*-2 position. This suggests that the final acylation derives from a pool more heavily labeled than the DAG pool, and that another MAG is utilized rather than DAG for the final transacylation. Furthermore, the authors (Simpson & Ohlrogge, 2016) confirmed the incorporation of exogenous *sn*-2 MAG into DAG and TAG.

Tobacco stigma lipids show key chemical distinctions from both oilseed and bayberry wax glycerolipids that would imply an alternative metabolic pathway. First is the presence of estolides in TAG(n), two DAG(n) isomers, and as free estolides, FFA(n). Then, the high proportion of α,α -DAG(n) which is not a known intermediate for TAG biosynthesis. In addition, because these lipids accumulate on the surface and because the only enzyme known to be required for estolide synthesis in petunia, PhCYP86A22, is a homolog of the Arabidopsis hydroxylase CYP86A2/ATT1 that synthesizes cutin hFAs (Han et al., 2010; Xiao et al, 2004), it could be hypothesized that stigma lipids are synthesized following a similar mechanism as that used for cutin. However, stigma glycerolipids also have similarities with seed TAGs in terms of their extractability in organic solvents and high proportion of unsaturated acyl groups. Hence, a conventional TAG biosynthesis pathway for the synthesis of stigma lipid polyesters cannot be ruled out.

We conducted an *in planta* acyl labeling assay to gain insight into the mechanism of acyl polymerization and whether this occurs prior to or after glycerolipid assembly. In addition, flux analysis from backbone labeling can identify whether α,α -DAG, α,β -DAG, either DAG(n) isomer, or PC are used as intermediates for TAG or TAG(n) biosynthesis. The work described in this chapter sought to uncover new information regarding the mechanism of synthesis of estolide-containing glycerolipids found in stigma lipids through a novel pulse-chase *in planta* radiolabeling methodology. Both [¹⁴C]-acetate and [¹⁴C]-glycerol labeling assays were performed as well as a monomer analysis of the labeled lipids.

3.2 Materials and Methods

3.2.1 Development of *in planta* isotope labeling assay

Stable isotope labeling trials were performed using an incubation buffer which consisted of 25 mM NaMES buffer, pH 5.7, containing 25 mM sucrose, 400 mM sorbitol and 25% strength Murashige and Skoog salts (Wang *et al*, 2003) mixed into autoclaved deionized water along with the appropriate substrate. Stable isotope assays used a concentration gradient of 0, 1, 2, 3, and 5 mM with [¹³C]-glycerol aliquots. The buffer was injected directly onto stage 3 tobacco stigmas *in planta* by piercing through the corolla with a syringe (Appendix Fig.B1). After 48 hours, stigmas were homogenized and lipids were extracted using a 3:2 hexanes:isopropanol solvent, as described in Hara & Radin (1978). Lipid fractions were isolated and purified by TLC through methods described in Chapter 2. Lipids were then depolymerized in 1% NaOMe, following the methods described in Yang *et al* (2016) to preserve the glycerol content. The resulting monomers were derivatized through acetylation and analyzed on a GC-MS using full scan and single ion mode (SIM) for the ions 115, 116, 118, and 119 as reported by Yang *et al* (2016).

3.2.2 Radiolabeling assay

Radioisotope assays were performed by injecting the same incubation buffer into Stage 3 stigmas using the appropriate radiolabeled substrate. At a [¹⁴C]-acetate concentration of 2 mM, one 5 µL injection amounts to about 0.52 µCi per stigma, for glycerol, 3 mM = 1.94 µCi per stigma. Subsequently, for the [¹⁴C]-acetate time course, samples were harvested after 5, 15, 30, 60, 120, 240, 480, and 720 min, and for stigmas incubated with [¹⁴C]-glycerol, samples were harvested at 10, 45, 90, 180, 480, 720, 1440, and 2880 min after inoculation. Stigmas were harvested one at a time and gently immersed in chloroform for 10 seconds to extract the surface lipids, and then placed into boiling (85°C) isopropanol containing 0.05% BHT to quench for 15 min. The internal lipids were recovered by homogenizing the stigma tissue and extracting with a 3:2 hexanes:isopropanol solvent (Hara & Radin, 1978).

3.2.3 Radiolabeling analysis

Lipid recovery and analysis methods were adapted from Kotapati & Bates (2021). Both surface lipids and the rest of solvent-extractable lipids for each time point were

separated using analytical TLC plates (Supelco Silica Gel 60; solvent conditions described in Chapter 2) to isolate each lipid fraction: TAG(n), DAG(n), FFA(n) and PL. The plates were then enveloped in plastic wrap and exposed to a phosphor screen for 20 hours which was later analyzed through a phosphorimager (GE Amersham Typhoon; Uppsala, Sweden) at a 50 μm resolution. The plates were then iodine-stained for densitometry analysis and entire lipid fractions were purified from the silica (Chapter 2) in order to quantify the amount of radioactivity through scintillation counting (Triathler Hidex; Turku, Finland). This was accomplished using 5 mL of Ultima Gold scintillation cocktail (Perkin Elmer) with a 10 min exposure time and an internal standardization method using 2000 DPM of [^{14}C]-toluene as the internal standard by measure sample CPM before and after the addition of the standard to obtain the efficiency of the counter for each sample. Analysis used scintillation counting to quantify radioactivity and the phosphorimager to obtain the relative distribution of the label within each lipid fraction.

3.2.4 Radiolabeled monomer analysis

Lipid fraction isolated through TLC (pooled internal and surface lipids; non-iodine-stained) were depolymerized through acidic transmethylation, which involves cooking in 5% H_2SO_4 in methanol for 2 hours at 80°C , which was then extracted and separated using reverse phase (RP) TLC plates (Supelco Silica Gel 60 RP-18 F_{254s}). The developing solvent was acetonitrile:methanol:water (65:35:0.1, v/v/v). Combined phosphorimaging and scintillation counting was used for analysis.

3.3 Results

3.3.1 Development of an isotope labeling assay *in planta*.

Previous research on stigma polyesters (Wang *et al*, 2003) determined that hFAs in all polyester classes are labeled when developing tobacco stigmas excised from the plant are incubated *in vivo* with [^{14}C]-acetate. Furthermore, these experiments established that the maximum incorporation rate of exogenous acetate occurred between stages 2 and 5 of stigma development, and the maximum lipid deposition rate between stages 4 and 5. The most efficient acetate incorporation rate per stigma occurred at a maximum of 20 stigmas using 2mM acetate. Incorporation rates remained linear for 5 hours and assay in light had much better activity than in darkness. Note that

these preliminary experiments removed the stigmas and placed them in an incubation buffer for the duration of the time course.

As we do not possess a nuclear substances and radiation devices license, as regulated by the Canadian Nuclear Safety Commission (CNSC) in accordance with the Nuclear Safety and Control Act (NSCA) (CNSC, 2022), we were restricted to a maximum of 270 μCi of radioactive materials, including waste, on hand at any given moment. Thus, our labeling assay was designed to minimize the amount of [^{14}C]-substrate used in an eight-point time course experiment (about 65 μCi was employed in total for this experiment). This was feasible by developing an *in planta* assay, rather than incubating detached stigmas in a buffer. This approach has the additional advantage of minimizing any wound response, which is known to trigger a number of mechanisms and produce confounding metabolites that complicates the interpretation of the results, for example the wounding of petunia stigmas was demonstrated to accumulate kaempferol, a flavonoid which also accumulates during pollination (Vogt *et al*, 1994).

The *in planta* method for incorporating exogenous substrate I developed involves injecting the incubation buffer containing the substrate of interest directly onto the surface of the stigma with a syringe, piercing the corolla in the process. To minimize the amount of ^{14}C used and with the goal of assessing the incorporation of a labeled substrate using this method, we employed [^{13}C]-glycerol to assess whether the substrate would effectively reach the internal stigmatic tissue when applied on the surface. The detection of stable isotopes requires the use of gas chromatography mass spectroscopy (GC-MS) to measure the ion pair differences between native and the exogenous isotope substrates (Yang *et al*, 2016). In the case for [^{13}C]-glycerol labeling, for GC analysis the glycerolipids must first be transesterified to break the glycerides and release glycerol, which is then derivatized with acetate to form triacetin. Triacetin has a molecular weight of 218, but triacetin containing the [^{13}C]-glycerol backbone has a molecular weight of 221. The difference between ion pairs 115 and 116, seen only in [^{12}C]-triacetin, and 118 and 119, from the [^{13}C]-glycerol-derived triacetin, was determined to be the most accurate in quantifying [^{13}C]-glycerol incorporation (Yang *et al*, 2016).

The stable isotope labeling assay was performed with incremental substrate concentrations with a 48 hour incubation period (Fig.24). A volume of 5 μL of incubation buffer per stigma containing the desired [^{13}C]-glycerol concentration was applied. This revealed that 3 mM of [^{13}C]-glycerol provided the highest incorporation of label, while

increasing the concentration to 5 mM contributed to insignificant increased label incorporation. These trials showed that after 48 hours, up to 8% of the total glycerol was [¹³C]-labeled and from this we determined that it would be feasible to run a time course experiment using [¹⁴C]-glycerol substrate using the non-invasive *in planta* approach described.

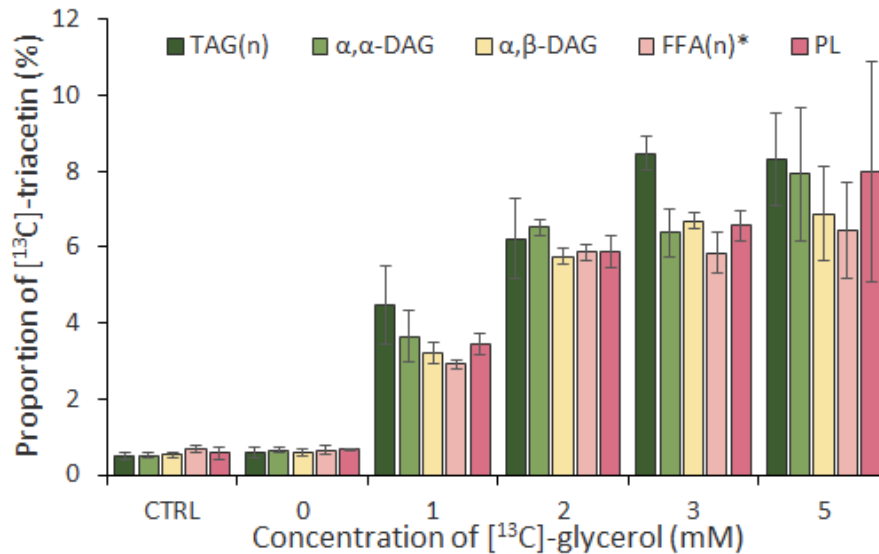


Figure 24. Incorporation of [¹³C]-glycerol in stigma lipid fractions. Data is pooled from triplicate sets of 10 stigmas incubated for 48 hours and as an average of the detected ion pair ratios between 115/118 and 116/119. The control (CTRL) was not injected with the incubation buffer whereas the 0 mM lacked the labeled substrate. *The accumulation of glycerol in the FFA(n) fraction is likely due to poor TLC separation as this fraction also contains elements of the IPPE fraction which was not analyzed in this assay.

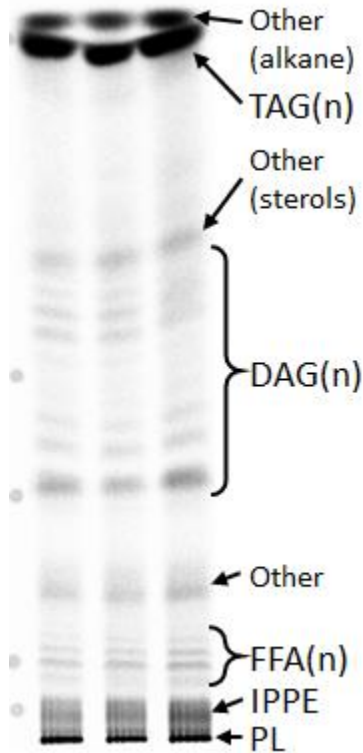
The [¹⁴C]-acetate radiolabeling assay was performed using the concentration established in the preliminary assay (2 mM; Wang *et al*, 2003) across a 12-hour incubation period. After completing the [¹⁴C]-acetate assay, I decided to extend the time course experiment for [¹⁴C]-glycerol to 48 hours such that the assay would exhibit a pulse-chase experiment, and that stigmas would remain in the pre-anthesis development stages. Concurrently, I decided to use 3 mM of [¹⁴C]-glycerol to ensure sufficient label was present for the duration of the assay. Note that saturating concentrations for exogenous glycerol to supply the majority of G3P for glycerolipid synthesis in *Camelina* oilseeds was determined to be 0.5 mM (Pollard *et al*, 2015), but this same concentration only provides 3% of backbone labeling in soybeans (Bates *et al*, 2009).

3.3.2 Radiolabeled substrate was incorporated into all lipid fractions demonstrating a lag phase until surface accumulation.

Two radiolabeling assays were performed using the novel method described above. The first assay used 2 mM [¹⁴C]-acetate over a time course of 12 hours divided into eight time points, and the second used 3 mM of [¹⁴C]-glycerol over 48 hours divided into eight time points. While [¹⁴C]-acetate labels newly synthesized FAs, [¹⁴C]-glycerol is metabolized to glycerol-3-phosphate (G3P) and can also label acyl chains via the glycolysis pathway (Slack et al., 1977). Surface and internal lipids were extracted from the inoculated stigmas at their respective time points and total lipid fractions were separated by TLC following the methods described in Chapter 2. Label distribution was quantified using phosphorimaging and liquid scintillation counting (Fig.25).

All described lipid fractions showed incorporation of both exogenous substrates across the time course experiments. Initial relative label distribution varied from that obtained in steady-state conditions (Table 6) showing a significant relative decrease in polar lipid label to a significant relative increase in TAG(n) label for both substrates. As expected, acetate labeling showed a much higher label in the “Other” fraction of lipids than glycerol since this fraction includes aliphatics and sterols. The label in the polar lipid fraction consists primarily of phosphatidylcholine; initially PC accounts for the entirety of the label but by steady state it accounts for above 70% (acetate and glycerol) of the total PL radioactivity. Other polar lipids include, from acetate labeling, 13% from PE, 8% from MGDG and <1% from PI, and from glycerol labeling, 6% from PE, 13% MGDG, and 1% PI at steady state conditions.

Table 6. Percent label distribution across stigma lipid fractions. Data obtained as averages from initial (~5-10 min) and steady-state (s.s.) conditions (~2-8 hours) across the labeling assay time course.



[¹⁴ C]-substrate		Acetate		Glycerol	
		initial	s.s.	initial	s.s.
Lipid fraction label distribution (%)	Time point				
	TAG(n)	10	42	11	55.5
	DAG(n)	13.5	12	15	21
	FFA(n)	2.5	3	0.5	2
	IPPE	4	6	17	6
	PL	55	15	54.5	10
	Other	15	22	2	5.5

Figure 25. Phosphorimager display of radiolabeled stigma lipids. TLC plate shows [¹⁴C]-acetate labeling after 12 hours separated in a dual development of 1.4% EtOH.

Maximum combined radioactivity for all recovered lipids (pre-TLC separation) in the [¹⁴C]-acetate assay occurred at 12 hours (further time points were not available and thus label may have continued to accumulate) with only 21% of the injected buffer total radioactivity recovered. For [¹⁴C]-glycerol, maximum combined radioactivity occurred at 24 hours with 30% of the total injected label recovered. This indicates that not all of the label was incorporated into the stigma lipids, indicating that part of the substrate was transported to other tissue, or that the substrate was incorporated into molecules that partitioned into the aqueous phase during the lipid extraction step. The incorporation of ¹⁴C into TAG(n), DAG(n), FFA(n), and PC lipid fractions across the time course of both assays are displayed in Fig.26.

Initial acetate labeling (Fig.26-A inset) showed that initially DAG(n) had the highest amount of label but was overtaken by TAG(n) after two hours (Fig.26-A). PC labeling achieved steady state at around two hours for the rest of the assay while TAG(n) and DAG(n) continued to accumulate until 8 hours, and FFA(n) to 12 hours. This may have indicated TAG(n) and DAG(n) degradation to form free estolides, but a prolonged time course would be required to confirm this hypothesis.

Initial glycerol labeling showed that PC had the highest rate of ^{14}C incorporation followed by nearly equal rates of DAG(n) and TAG(n) accumulation up until 1.5 hours (Fig.26-B inset). After 3 hours, PC and TAG(n) were accumulated in nearly equal amounts while DAG(n) slowed its rate of accumulation and accumulated roughly half of the radioactivity of PC and TAG(n) (Fig.26-B). By 8 hours, TAG(n) achieved over 50% of the relative label distribution as PC labeling began to decrease. FFA(n) showed the lowest ^{14}C accumulation of the measured species and was consistently about 25% of the value of DAG(n) throughout the assay. Maximum label accumulation in TAG(n), DAG(n), and FFA(n) were achieved at around 24 hours.

In the glycerol labeling assay, PC achieved its maximum labeling at around three hours, which may indicate that supply of labeled glycerol was depleted below the maximum exogenous substrate uptake concentrations and must be supplied with native glycerol to maintain optimal PC synthesis rates. The decrease in PC labeling at this time was likely due to high turnover and may be indicative of PC being used as a substrate in DAG(n)/TAG(n) synthesis pathways.

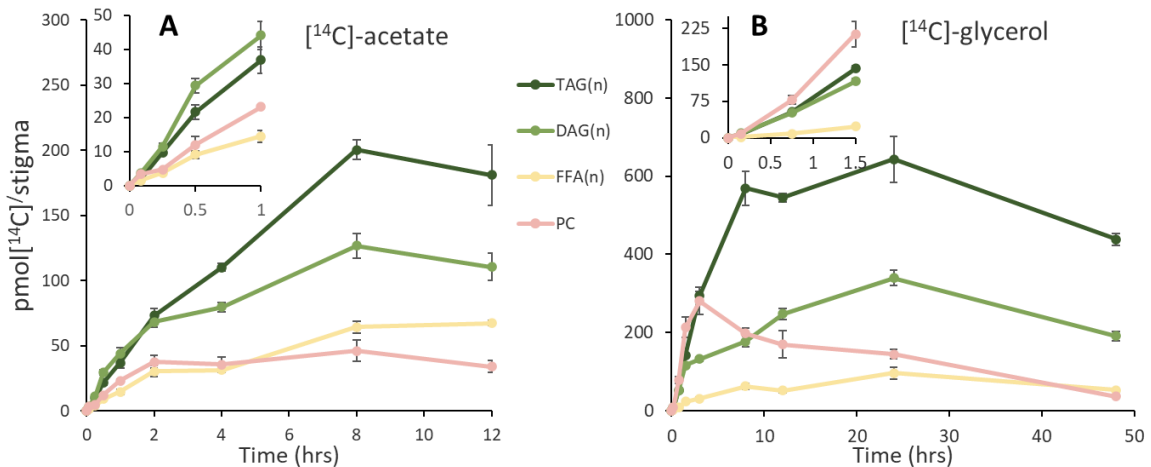


Figure 26. Time course of radiolabeled substrate accumulation in tobacco stigmas. A: 12-hour time course with 2 mM [¹⁴C]-acetate; inset shows an expanded view of the initial kinetics of incorporation. B: 48-hour time course with 3 mM [¹⁴C]-glycerol; inset shows an expanded view of the initial kinetics of incorporation. Data is averaged from triplicates and combined internal and surface results.

Radiolabeled products largely accumulated in the internal stigmatic tissue prior to being exported to the stigma surface (Fig.27). Labeled polar lipids were not present in the surface lipid fraction. The [¹⁴C]-acetate assay depicted a pulse labeling experiment where the total incorporated substrate was consumed around 8 hours (Fig.27-A). A slow release of lipids to the surface was observed but this accounted for a maximum of 6.4% of the total label at 12 hours. The kinetics of [¹⁴C]-glycerol incorporation shown in Fig.27-B can be interpreted as a pulse-chase labeling experiment, with maximum label incorporation rates up to 8 hours, then diminished uptake rates due to lower substrate concentrations up to 24 hours, then the chase phase until 48 hours where the available exogenous substrate has been fully incorporated. A significant lag phase in label accumulation was observed between the internal and surface lipid fractions such that only trace amounts of radioactivity were detected prior to 8 hours. The label accumulation in the surface lipid fraction only achieved about 10% of the peak internal label after 48 hours. However, a 44% decrease in total label accumulation was observed between 24 and 48 hours and presumably a result of polyester degradation or transport to other tissue as the stigma prepares for pollen reception (see Chapter 2 where polyester distribution begins to change prior to anthesis: Fig.14;15;16). Note that free

(and potentially labeled) glycerol from polyester disassembly would be removed into the aqueous phase which was not quantified in these analyses.

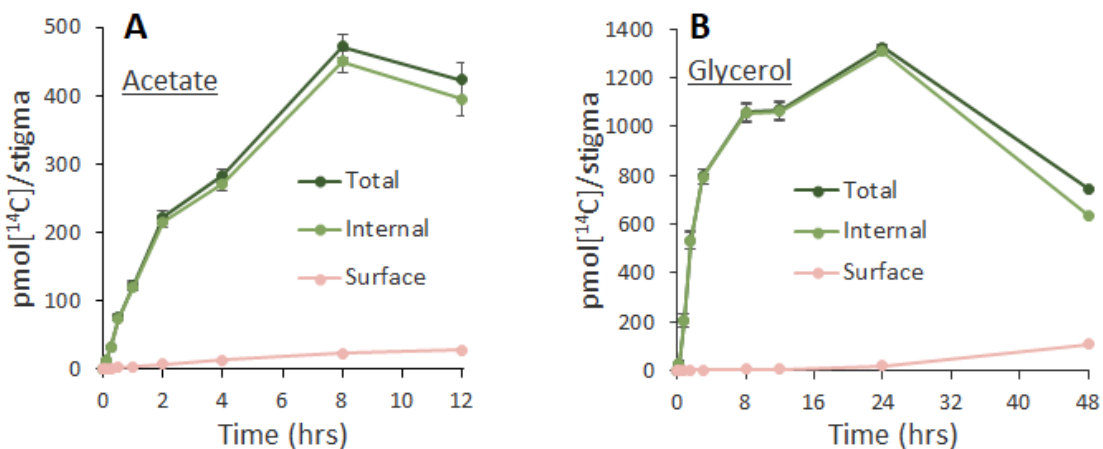


Figure 27. Total label distribution between internal and surface stigma lipids. A: [¹⁴C]-acetate assay. B: [¹⁴C]-glycerol assay. Data combined from all lipid fractions.

3.3.3 A portion of radiolabeled glycerol was incorporated into acyl groups.

Transmethylation of the different stigma lipids isolated after [¹⁴C]-glycerol inoculation was performed to quantify the label present in acyl groups. Not all exogenous glycerol is used strictly for G3P biosynthesis and subsequent incorporation in the glycerol backbone of glycerolipids. A fraction of the substrate may undergo degradation to acetyl-CoA where it can be incorporated into acyl lipids via the FAS pathway (Slack *et al*, 1977). A distinct lag phase was observed as no label was detected in the initial (0.15 hours) time point (Fig.28). ¹⁴C did accumulate marginally in the acyl groups of PC (~0.5%), but neutral glycerolipids presented different proportion of [¹⁴C]-labeled acyl groups 12 hours after exogenous glycerol was introduced: 15.1% in FFA(n), 12.8% in DAG(n), and 40.4% in TAG(n). This suggests a high PC turnover rate of the whole molecule, not just acyl groups, such that it may be used as a substrate for DAG(n)/TAG(n) synthesis and that glycerol concentrations were in excess of saturating conditions resulting in significant glycolysis and high levels of acyl labeling in estolides.

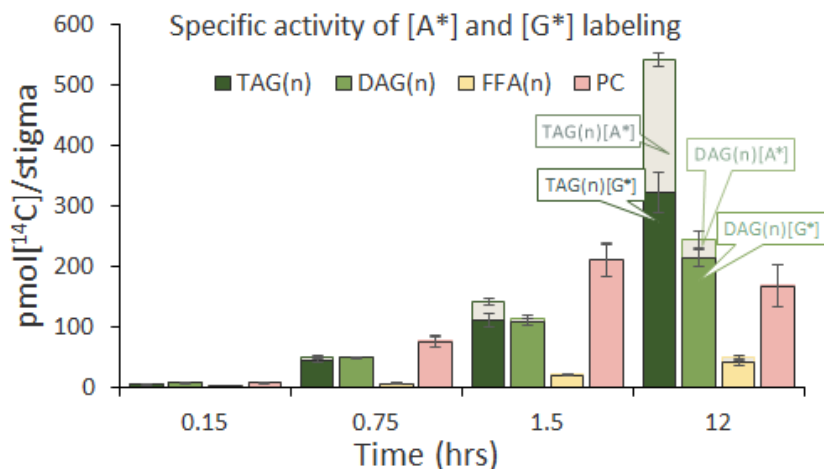


Figure 28. Acyl group and glycerol backbone labeling from [¹⁴C]-glycerol incorporation. The faded portion of the bar graphs represent the total label concentration, where [A*] denotes portion of the label found in the acyl groups and the coloured portion, [G*] denotes the portion of the label found in the glycerol backbone. Data was obtained from analyzing labeled acyl depolymerization products from [¹⁴C]-glycerol labeled lipid fractions.

3.3.4 Estolide formation showed precursor-product relationship.

Following the TLC separation methods for TAG(n) (0.5% EtOH), DAG(n) (1.5% EtOH), and polar lipids (91:30:7:1) described in Chapter 2, distinct bands of TAG(n), DAG(n), and FFA(n) were separated to form an estolide ladder. Relative label distribution was quantified directly on each plate by phosphorimaging and, after scraping the bands on the silica and eluting the lipids with solvent, the total radioactivity for each lipid fraction was quantified by liquid scintillation counting.

[¹⁴C]-Acetate labeling

As detailed above, a labeling assay using [¹⁴C]-acetate as the exogenous substrate was performed using a concentration of 2 mM with 8 samples taken over a 12-hour time course experiment. Exogenous acetate was incorporated into the acyl groups of the analyzed glycerolipids. Here, surface and internal lipids were combined due to minimal labeling recovered in the surface lipid fraction. The accumulation of labeled substrates was observed in all TAG(n) species (Fig.29). TAG(0), TAG(1), and TAG(2) showed near instantaneous substrate accumulation while TAG(3), TAG(4), and TAG(5)

showed increasing lag times (Table 7). The initial rates of label incorporation were shown to be inversely proportional to the estolide count, such that TAG(0) > TAG(1) > TAG(2) > TAG(3) > TAG(4) > TAG(5). TAG(0) presented the highest relative proportion of label accumulation across the duration of the assay.

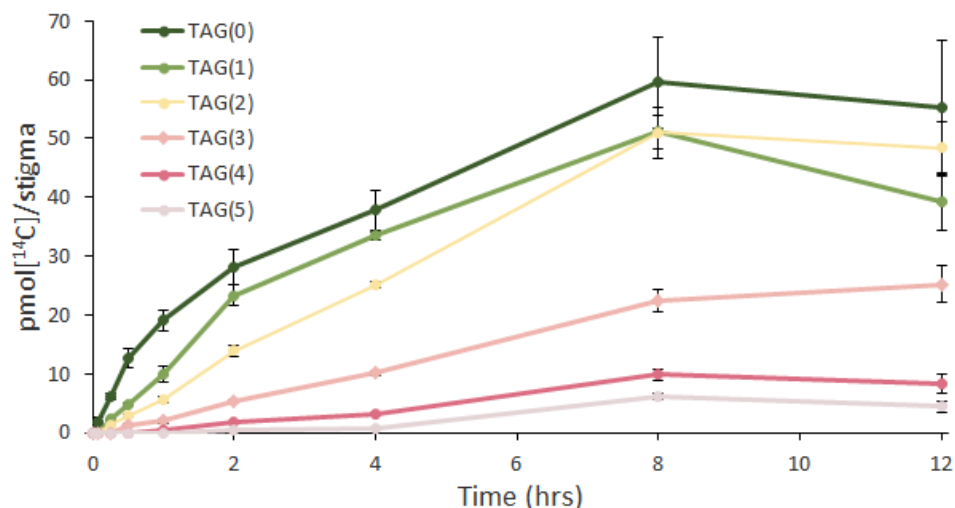


Figure 29. Time course of TAG(n) [¹⁴C]-acetate labeling. Data is combined from internal and surface lipids and was normalized to pmol of radioactive carbon incorporated to a per stigma basis.

In [¹⁴C]-acetate labeling, the initial rate of free estolide appearance followed the same trend observed in TAG(n) such that FFA(0) > FFA(1) > FFA(2) > FFA(3) > FFA(4) (Fig.30) (Table 7). However, only FFA(0) showed no lag time while that of FFA(n) estolides was demonstrated to be inversely proportional to the estolide count. Initially, FFA(0) had the highest relative label distribution but by about 30 min it reached a steady state. Shortly after 1 hour, FFA(1) became the most abundantly labeled of the free estolides for the duration of the assay, accumulating to about three times the amount of FFA(0). After 8 hours, the estolides with two estolide bonds and longer continued to increase.

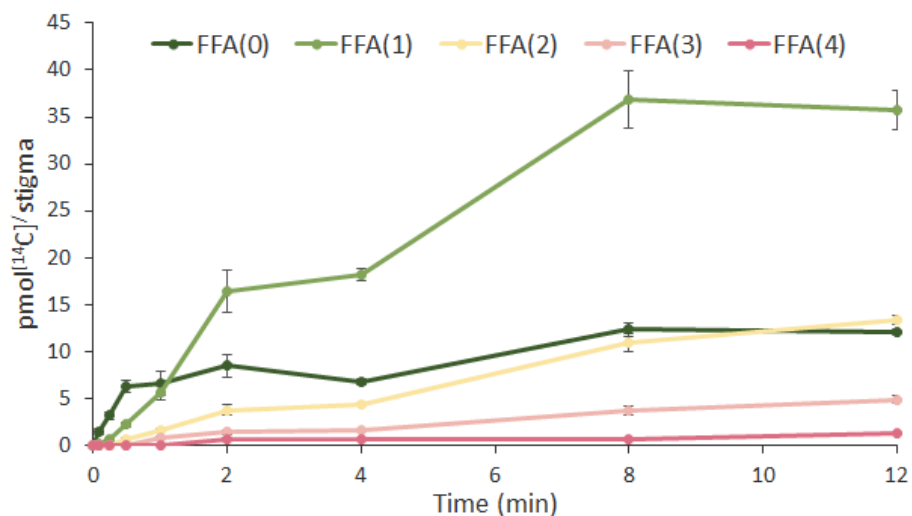


Figure 30. Time course of FFA(n) [^{14}C]-acetate labeling. Data is combined from internal and surface lipids and was normalized to pmol of radioactive carbon incorporated on a per stigma basis.

The labeling trends in the DAG(n) fraction however did not follow the same accumulation kinetics as the other estolide fractions. Similar to the FFA(n) lipid fraction, quick substrate accumulation was observed for DAG(0) which accounts for the highest relative label accumulation until about 1.5 hours when it is surpassed by DAG(1), instead by almost tenfold by the end of the assay (Fig.31). The equilibrium attained by DAG(0) occurred at less than half its maximum accumulation value and was achieved around 4 hours. Intriguingly, DAG(3), and to a lesser extent DAG(4), accumulated a significant fraction of the labeled substrate in the first hour of the assay (Fig.31-inset). Interestingly, the α,β -DAG(n) isomer accounted for up to 95% of DAG(1) throughout the duration of the trial as well as the entirety of DAG(3) in the first hour (Fig.32). DAG(0) in the first hour and DAG(2-4) after two hours shared near equal proportions of each DAG isomer. The initial rates of appearance for α,β -DAG(n) and α,α -DAG(n) isomers did not show the same trends observed in TAG(n) and FFA(n), however the combined DAG(n) fraction did demonstrate lag times that were inversely proportional to estolide count (Table 7).

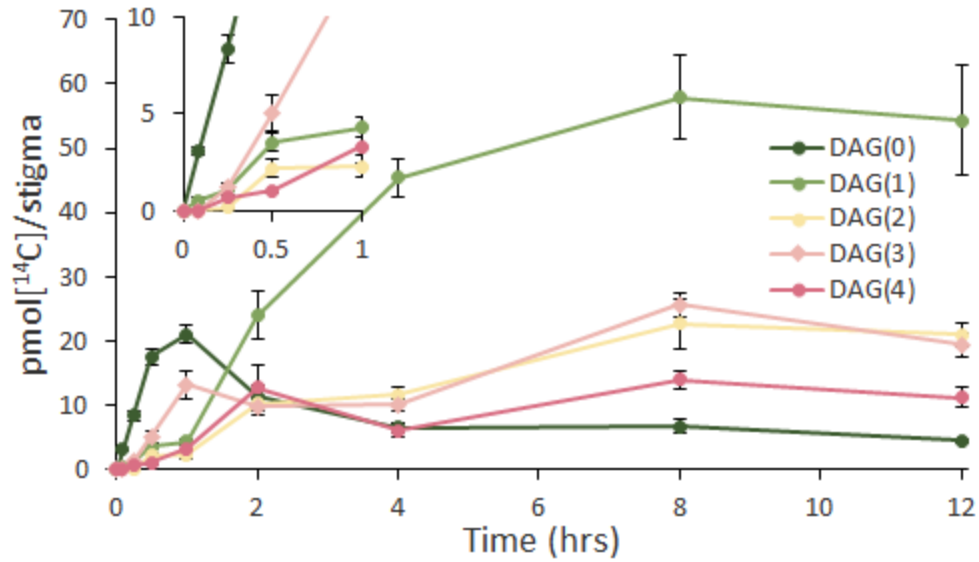


Figure 31. Time course of DAG(n) [^{14}C]-acetate labeling. Data is combined from internal and surface lipids, combined α,β -DAG(n) and α,α -DAG(n) isomers, and was normalized to pmol of radioactive carbon incorporated to a per-stigma basis. Inset: expanded view of the initial kinetics of incorporation.

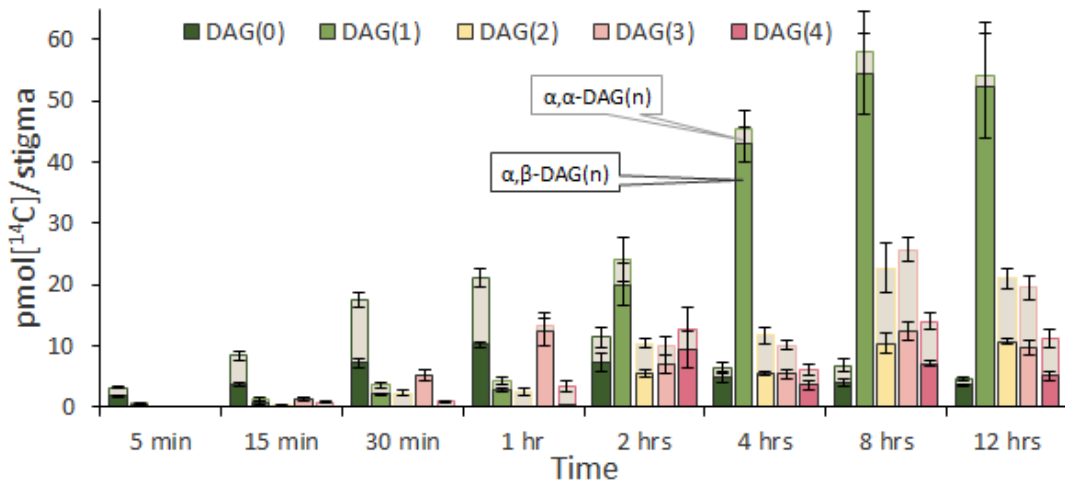


Figure 32. DAG(n) [^{14}C]-acetate labeling distribution between α,β -DAG(n) and α,α -DAG(n) isomers. Combined internal and surface lipid fractions.

Table 7. [¹⁴C]-acetate reaction kinetics and lag times. Only internal fraction data was used for all lipid fractions. Data was obtained from linear regression of the first three time points after the initial appearance of the lipid species. Negative values obtained for lag times were set as zero. DAG isomer data is combined.

Neutral lipids		Estolide count (<i>n</i>)	0	1	2	3	4	5
TAG(<i>n</i>)	Rate (pmol[¹⁴ C] hr ⁻¹ stigma ⁻¹)		42.53	17.98	10.34	5.82	1.78	0.511
	Lag time (min)		0	0	0	5.26	11.16	44.90
α,β-DAG(<i>n</i>)	Rate (pmol[¹⁴ C] hr ⁻¹ stigma ⁻¹)		12.94	4.39	1.36	14.37	0.61	-
	Lag time (min)		0	2.63	1.04	9.47	24.46	-
α,α-DAG(<i>n</i>)	Rate (pmol[¹⁴ C] hr ⁻¹ stigma ⁻¹)		21.91	3.05	2.60	1.33	3.42	-
	Lag time (min)		1.69	2.98	8.12	16.41	6.56	-
DAG(<i>n</i>)	Rate (pmol[¹⁴ C] hr ⁻¹ stigma ⁻¹)		34.85	7.45	2.58	15.57	6.28	-
	Lag time (min)		0	2.77	7.98	10.4	13.72	-
FFA(<i>n</i>)	Rate (pmol[¹⁴ C] hr ⁻¹ stigma ⁻¹)		11.18	4.44	2.05	0.39	0.08	-
	Lag time (min)		0	5.13	12.16	30.56	131.5	-

[¹⁴C]-Glycerol labeling

A labeling assay using [¹⁴C]-glycerol as the exogenous substrate was performed using a concentration of 3 mM with 8 samples taken over a 48-hour time course experiment. Exogenous glycerol is incorporated into the glycerol backbone of the analyzed glycerolipids. The initial labeling of TAG occurred in the internal non-estolide species (Fig.33-A) [i.e. TAG(0)] with initial rates of TAG(0) > TAG(1) > TAG(2) > TAG(3) > TAG(4) > TAG(5) (Table 8). Due to the longer time course performed in the glycerol assay, the decline in TAG(0) and TAG(1) is clearer than that observed in the acetate labeling time course, suggesting that these molecules are precursors for higher order TAG(*n*). Contrastingly, the labeled surface lipid fraction (Fig.33-B) relative TAG(*n*) composition was comparable to that of the internal lipid fraction, such that at 48 hours the internal lipid fraction contained 20% TAG(1), 39% TAG(2), 22% TAG(3), and 7% TAG(4), whereas the surface lipids contain 25% TAG(1), 40% TAG(2), 22% TAG(3), and 8% TAG(4). In addition to initial label incorporation rates, labeling kinetics of internal TAG(*n*) showed distinct lag phases between species respective to estolide bond count

(Table 8). Taken together, these results suggest that TAG remodeling occurs, and that such remodeling takes place in the stigmatic tissue prior to reaching the stigma surface.

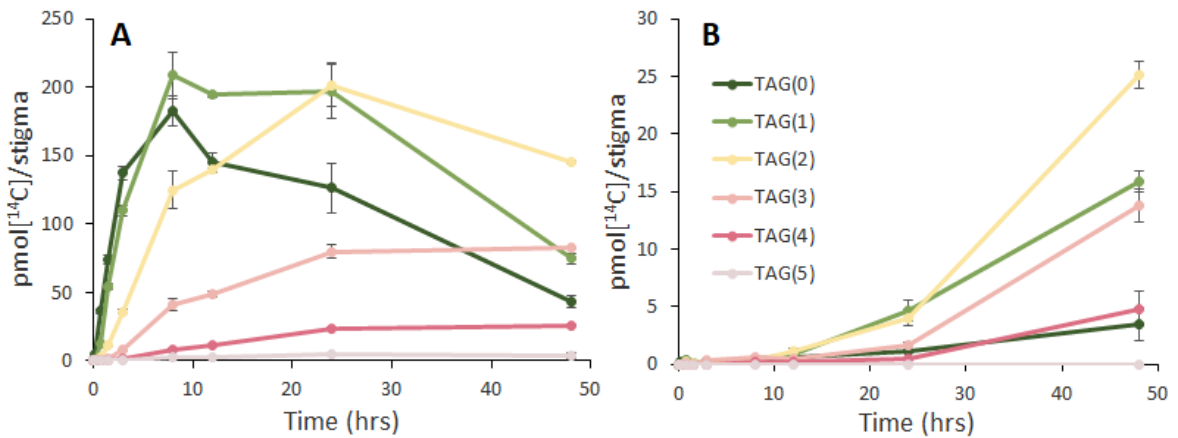


Figure 33. Time course $[^{14}\text{C}]$ -glycerol labeling of TAG(n). A: Internal lipid fraction. B: Surface lipid fraction.

Radiolabeling trends achieved with FFA(n) using $[^{14}\text{C}]$ -glycerol were analogous to those with $[^{14}\text{C}]$ -acetate, such that both lag times and the initial rate of appearance were inversely proportional to estolide count (Table 8). Furthermore, FFA(0) accumulated the highest relative proportion for the first hour of the trial (Fig.34-inset). However, the equilibrium attained by FFA(0) at 3 hours was below its maximum accumulation, akin to DAG(0) labeling in the acetate experiment (Fig.34). A sharp decrease in FFA(1) labeling was observed at 12 hours along with a decrease in FFA(0); these observations may be reflective of decreasing exogenous substrate concentrations. In this scenario, the increased accumulation of FFA(1) at 24 hours might have resulted from glycerolipid estolide degradation.

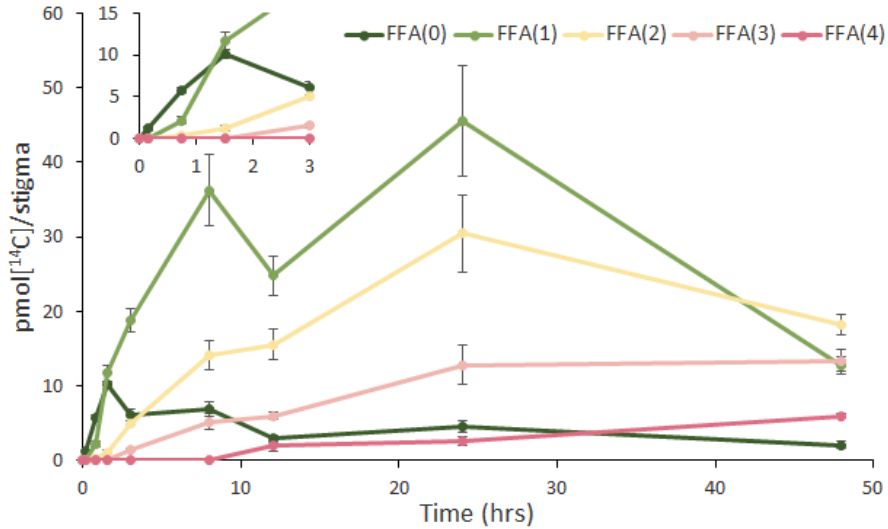


Figure 34. Time course $[^{14}\text{C}]$ -glycerol labeling of FFA(n). Includes combined data for internal and surface lipids. Inset shows an expanded view of the initial kinetics of incorporation. Inset shows an expanded view of the initial kinetics of incorporation.

The label accumulation in the DAG(n) species followed a trend comparable to that of both FFA(n) and TAG(n) labeling (Fig.35). Initial labeling (Fig.35-inset) had the fastest accumulation kinetics for DAG(0), with the labeling kinetics being inversely proportional to n , such that initial rates were DAG(0) > DAG(1) > DAG(2) > DAG(3) > DAG(4) > DAG(5) (Table 8). DAG(0) labeling achieved steady state conditions in 3 hours at a value lower than its maximum accumulation. Decrease in label accumulation was eventually observed for DAG(0) and DAG(1) across the $[^{14}\text{C}]$ -glycerol time course.

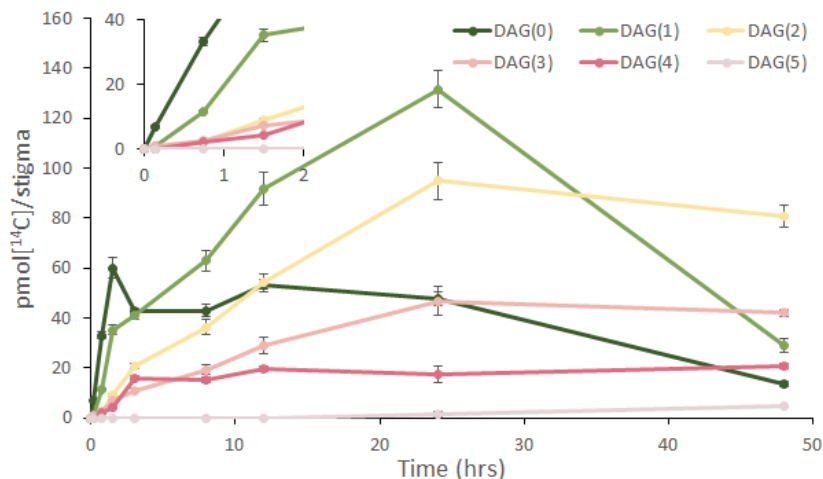


Figure 35. Time course [^{14}C]-glycerol labeling of DAG(n). Includes combined internal and surface lipids as well combined α,β -DAG(n) and α,α -DAG(n) data. Inset shows an expanded view of the initial kinetics of incorporation.

Since [^{14}C]-glycerol is used to track the flux through lipid species, it can be used to track the ratio of label accumulation between α,β -DAG(n) and α,α -DAG(n) over the time course of the labeling assay (Fig.36). At the first point (10 min), α,β -DAG(0) accounted for 77% of the total DAG(0) and similar ratios existed for DAG(1) and DAG(2). However, up to 1.5 hours only the α,β -DAG isomer was labeled for DAG(3) and DAG(4). By the end (48hrs), less than 50% for all DAG(n) was labeled in the α,β -DAG isoform. These observations suggest that the α,α -DAG(n) regioisomers are likely products of α,β -DAG(n) isomerization.

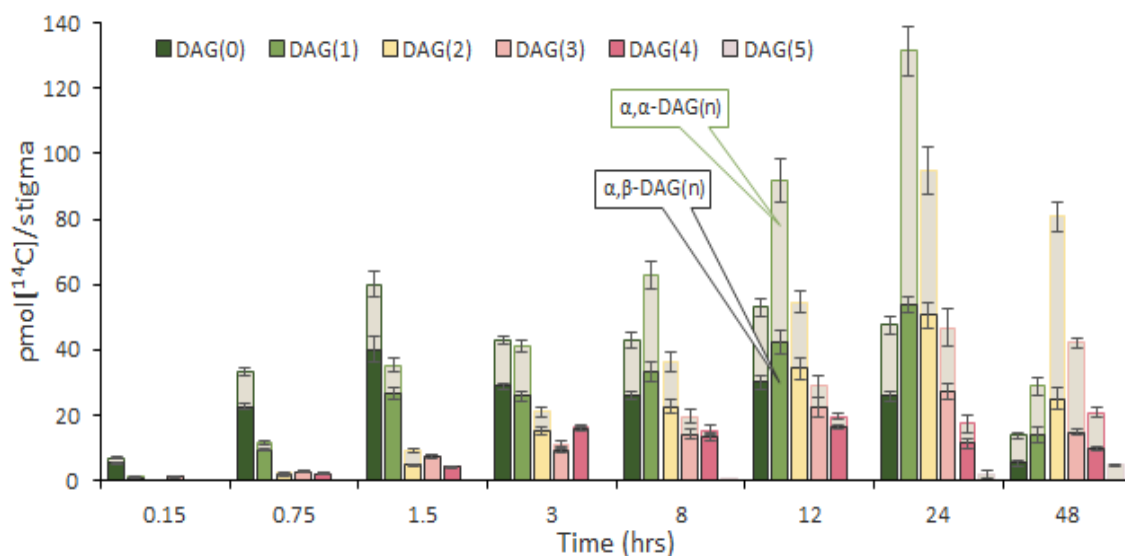


Figure 36. Proportion of α,β -DAG(n) relative to total DAG(n) fraction. Data obtained from $[^{14}\text{C}]$ -glycerol labeling and combined internal and surface lipid fractions. The overlapping shaded bar graphs represent the α,α -DAG(n) isomer fraction while the coloured bar represents the α,β -DAG(n) isomer fraction.

Table 8. $[^{14}\text{C}]$ -glycerol reaction kinetics and lag times. Only internal fraction data was used for all lipid fractions. Data was obtained from linear regression of the first three time points after the initial appearance of the lipid species. Negative values obtained for lag times were set as zero. DAG isomer data is combined.

Neutral lipids		Estolide count (<i>n</i>)	0	1	2	3	4	5
TAG(n)	Rate (pmol $[^{14}\text{C}]$ hr $^{-1}$ stigma $^{-1}$)		50.93	40.16	15.28	3.21	1.18	0.32
	Lag time (min)		2.51	14.41	40.54	48.25	68.23	141.9
α,β -DAG(n)	Rate (pmol $[^{14}\text{C}]$ hr $^{-1}$ stigma $^{-1}$)		25.75	19.09	6.05	4.60	6.19	-
	Lag time (min)		0	10.03	35.05	1.71	3.50	-
α,α -DAG(n)	Rate (pmol $[^{14}\text{C}]$ hr $^{-1}$ stigma $^{-1}$)		13.58	6.49	2.17	0.62	0.26	-
	Lag time (min)		1.22	1.30	4.31	31.54	43.87	-
DAG(n)	Rate (pmol $[^{14}\text{C}]$ hr $^{-1}$ stigma $^{-1}$)		39.33	25.57	8.22	4.60	6.44	-
	Lag time (min)		0	10.80	26.93	1.71	3.61	-
FFA(n)	Rate (pmol $[^{14}\text{C}]$ hr $^{-1}$ stigma $^{-1}$)		6.64	6.95	2.10	0.78	0.14	-
	Lag time (min)		0	11.98	44.80	80.70	226.7	-

3.3.5 Oleic acid was the first labeled acyl lipid.

Stigma estolides consist primarily of oleic (18:1) and linoleic (18:2) acids along with their ω -hydroxyl derivatives, as described in Chapter 2. TAG(n), DAG(n), and FFA(n) lipid fractions were isolated from TLC plates and transmethylated in order to analyze the label incorporation into their respective acyl monomers. Appendix Fig.B3 shows the C18 reversed-phase TLC analysis of the transmethylation product from total lipids, where the labeled lipids co-migrated with the unlabeled FAME standards. The label was incorporated into all major acyl groups: 18:1 FAME, 18:2 FAME, 18:1 hFAME, and 18:2 hFAME. TAG(n) and DAG(n) analysis showed that 18:1 FAME was the first labeled acyl group (Fig.37) and that hFAMES were not labeled until 1.5 hrs. DAG(n) showed a higher $[^{14}\text{C}]$ -hFAME/ $[^{14}\text{C}]$ -FAME ratio than TAG(n), while FFA(n) presented the highest ratio of $[^{14}\text{C}]$ -hFAME/ $[^{14}\text{C}]$ -FAME.

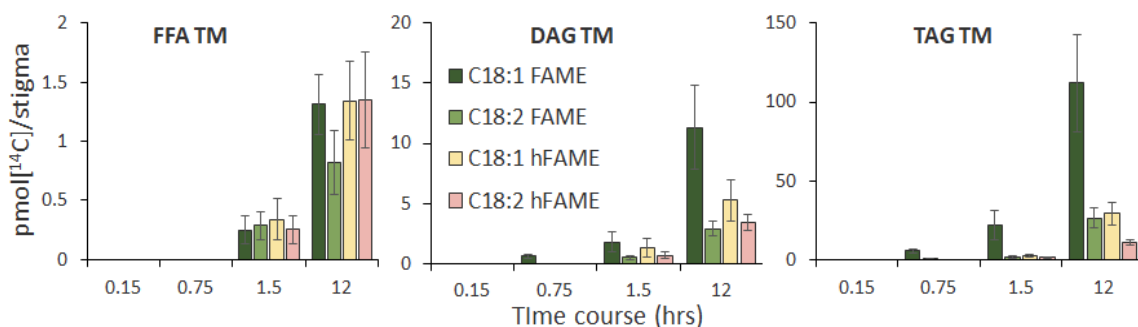


Figure 37. Labeled acyl distribution in estolide containing species. Data was obtained from acyl group labeling from $[^{14}\text{C}]$ -glycerol assay. Labeled FFA(n), DAG(n), and TAG(n) fraction were depolymerized by transmethylation and developed on reverse-phase (RP) TLC plates.

After a 12 hour incubation period, labeling has achieved a steady-state incorporation and injected stigmas were approximately at stage 3 in their development. Based on obtained estolide distributions within each unlabeled lipid fraction (Chapter 2), hFAME/FAME acyl ratios can be anticipated. For example, TAG(n) distribution in stage 3 stigmas illustrates that 43% of all TAG(n) acyl groups were ω -hFA (and 36% at stage 1). In comparison, after 12 hours, labeled TAG(n) distribution showed that only 29% of labeled TAG(n) acyl groups were ω -hFA, however, the monomer distribution in TAG(n) at 12 hours showed only 23% of the label accumulated in ω -hFAME (Table 9). If there were equal probability of label uptake between the acyl groups these values would be

equal. Thus, TAG(n) monomers showed only 75% of the theoretical potential content of ω -hFA; in DAG(n) and FFA(n), these values were 89% and 91%, respectively.

Table 9. Labeled and total ω -hydroxy fatty acyl content. Ratios obtained from lipid estolide length distributions and expected stoichiometry between normal and hydroxy FAs.

Source	Lipid distribution ratios from:	FFA(n)	DAG(n)	TAG(n)
Labeled	Labeled ω -hFA monomers at 12 hrs (%)	56	38	23
	ω -hFA in labeled lipids at 12 hrs (%)	61	42	29
Total	ω -hFA in stage 1 stigmas lipids (%)	49	56	36
	ω -hFA in stage 3 stigmas lipids (%)	66	61	43

3.3.6 Labeling kinetics of non-estolide species showed similarities to expected Kennedy pathway kinetics with acyl editing and multiple DAG pools.

Since the initial label was mostly found in the non-estolide species, comparing these to known metabolic pathway kinetics may reveal similarities between TAG synthesis in stigma lipids and the Kennedy pathway (and alternatives). Acetate labeling showed nearly simultaneous substrate incorporation into each major lipid fraction with a minor lag phase in α,α -DAG (Table 10). In contrast, glycerol labeling depicted α,β -DAG and FFA having quick label incorporation with α,α -DAG, TAG, and PC having lag phases each minutes apart. After the lag phase, PC had a much greater substrate incorporation rate than any other lipid fraction, having more than double that of the TAG fraction which is the second greatest. In comparing the two DAG isoforms at the first time point (10 min), α,β -DAG consisted of 57% of the total DAG(0) acetate-label, but up to 77% of the total glycerol label.

Table 10. Initial substrate incorporation rates and lag times for non-estolide species. Data was obtained from linear regression of the first two or three time points after the initial appearance of the lipid species. Negative values obtained for lag times were set as zero.

[¹⁴ C]-	Neutral lipid fraction	TAG	α,β-DAG	α,α-DAG	FFA	PC
Acetate	Lag time (min)	0	0	1.69	0	0
	Initial rate (pmol[¹⁴ C] hr ⁻¹ stigma ⁻¹)	26.09	12.94	21.91	11.77	21.43
Glycerol	Lag time (min)	2.18	0	0.98	0	4.86
	Initial rate (pmol[¹⁴ C] hr ⁻¹ stigma ⁻¹)	50.88	25.71	13.57	6.62	116.05

Across the full time course, using each substrate, DAG(0) attained a maximum accumulation then dropped down to a lower steady state (Fig.38). PC label accumulated linearly until its maximum where, when [¹⁴C]-acetate was supplied (Fig.38-A), achieved a near steady state, but when [¹⁴C]-glycerol was the substrate (Fig.38-B), diminished until the end of the time course. TAG seemed to follow a similar trend to that of PC but peaked at a later time point.

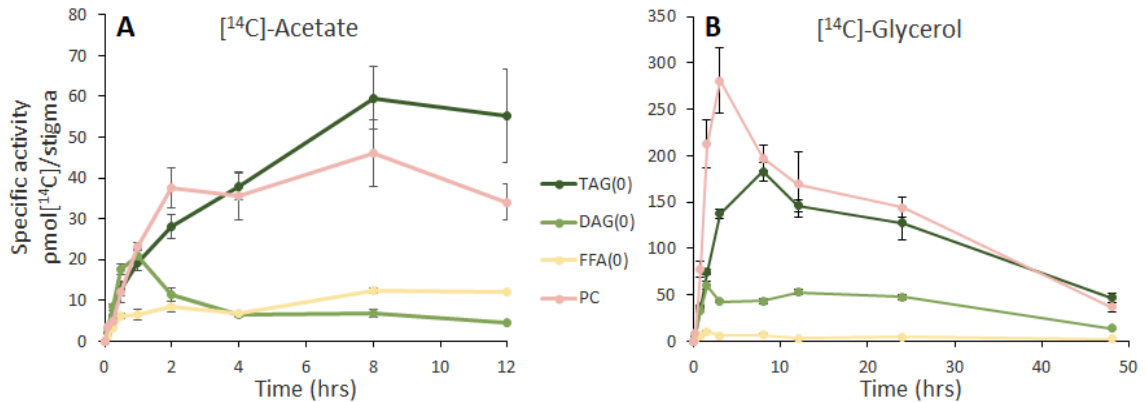


Figure 38. Time course of non-estolide lipid labeling. A: Acetate. B: Glycerol. Data is combined from internal and surface lipid fractions, DAG(0) data includes α,β-DAG(0) and α,α-DAG(0) species.

3.4 Discussion

3.4.1 Novel *in planta* substrate incubation is an effective method for analyzing stigma lipids.

Our method for tobacco stigma lipid labeling sought to not only avoid eliciting any wound response but also minimizing the release of intracellular lipases, since these may result in premature degradation of lipid estolides and compositional changes.

Furthermore, the method attempted to minimize the amount of label required for the analysis. Metabolic analysis using exogenous substrates generally involves *in vivo* or *in vitro* assays. In oilseed labeling, *in vivo* assays involved cultured embryos incubated in a medium containing the desired substrate (e.g., stable or radioisotopes) (Bates *et al*, 2009; Pollard *et al*, 2015). Other protocols have been applied to study leaf lipid metabolism where leaves are removed from the plant, cut into strips, and then placed into an incubation buffer (Roughan *et al*, 1980; Bates *et al*, 2007). Bayberry fruits were incubated whole or excised into knobs for *in vivo* radiolabel analysis (Simpson & Ohlrogge, 2016). Moreover, preliminary radiolabeling experiments to assess tobacco stigma lipid metabolism used excised stigmas that were incubated in a buffer containing the radioactive substrate (Wang *et al*, 2003). *In vivo* studies with intact tissue are preferred over those that involve cutting plant organs, which likely develop stress responses to mechanical wounding that elicit a potential metabolic change.

Our preliminary stable isotope assay using [¹³C]-glycerol demonstrated no changes in monomer quantity or composition between controls (untreated stigmas and those injected with the buffer having no substrate) and inoculated stigmas with varying concentrations after 48 hours. Furthermore, it proved to have sufficient substrate uptake for a constrained radioisotope assay. This method likely provided a less uniform exposure of the stigma to the buffer than excised tissue incubation methods, however it resulted in a pulse-chase experiment once the label was depleted. Further improvements to this method can be made, for example by quantifying the amount of residual label ([¹⁴C]-acetate and -glycerol) in the aqueous phase after solvent partition at each time point to determine the amount of label exported to other tissues of the plant. This would help determine more precise exogenous substrate uptake rates with respect to substrate concentration. Lastly, increased sample size would allow more accurate results in lipid fractions that do not accumulate as much material, such as the stigma

surface lipids or certain phospholipids which, due to lack of material, were not present in sufficient quantities to perform monomer analysis.

3.4.2 Labeling data suggests DAG(0) and TAG(0) synthesis utilizes a combined de novo DAG/TAG and PC-derived DAG/TAG pathways.

The method developed provides supply of substrate in a pulse labeling experiment. This allows individual pools of precursors, intermediates, and products to become labeled in the order they are metabolized. Assuming that there are no diffusion or substrate uptake issues, the initial metabolites should be labeled quickly without much lag time (Allen *et al*, 2015). This incorporation will occur in a linear manner until a steady state is achieved and then it will flatten out. The product of this metabolite will exhibit a lag time proportional to the time it takes for the precursor pool to fill; more significant lag times are expected if the products are distant from the source of the label. The kinetics of this product begin with a sigmoidal curve to linear labeling approaching up to a maximum value. If the products are not turned over, they will continue to accumulate labeling. Samples obtained from time points during the pulse labeling allows us to study the accumulation of labeling through the intermediates along the metabolic pathway.

My radiolabeling results showed that the initial label, when [¹⁴C]-glycerol was supplied, occurs on the species containing no estolides (i.e. FFA(0), DAG(0), and TAG(0)). When [¹⁴C]-acetate was supplied, FFA(0), DAG(0), and TAG(0-2) accumulated within the first time point. This implies that the *n* (0) molecules are likely synthesized prior to any estolide formation. By focusing on these components, we can make some correlations between labeling trends of known biosynthesis pathways. Bayberry wax TAG labeling showed distinct lag phases between MAG, DAG, and TAG accumulation in both [¹⁴C]-acetate and [¹⁴C]-glycerol, indicating that acyl groups were not incorporated directly to the glycerol backbone forming DAG and TAG molecules, as observed in labeling experiments with oilseeds, but rather required a MAG intermediate to make these acyl transfers (Simpson & Ohlrogge, 2016). The simplest form of the Kennedy pathway uses consecutive acylation of FAs to form *de novo* DAG to TAG. In avocado mesocarp, for example, labeling for glycerol showed a linear precursor-product relationship between the two glycerolipids while labeling with acetate resulted in simultaneous labeling of TAG and DAG, with this latter having the higher initial

accumulation rate (Fig.23; Griffiths *et al*, 1988). The addition of an acyl editing cycle involves the membrane lipid phosphatidylcholine (PC), which through acetate labeling, initially accumulates with DAG and TAG at similar rates. However, PC labeling is minimal for glycerol, as observed in *Cuphea lanceolata* (Bafor *et al*, 1990). DAG can also be synthesized from PC, creating a second pool that is used for TAG synthesis; in this case, acetate labeling shows initial accumulation in DAG, TAG, and PC while glycerol shows a linear precursor-product relationship from DAG to PC and a lag phase for TAG accumulation (Bates *et al*, 2009). And finally, a combination of *de novo* and PC-derived DAG-TAG synthesis exhibits a more complex labeling pattern for glycerol, as suggested for castor oil (Bafor *et al*, 1991). In stigma lipids, in both labeling assays α,α -DAG(0) had presented a lag phase while α,β -DAG(0) did not, the latter being the isomer used in the Kennedy pathway. It is possible that α,α -DAG(n) is simply a product of α,β -DAG(0) isomerization; however this remains to be studied.

When considering stigma lipids without estolides ($n = 0$), initial [^{14}C]-acetate labeling showed PC then DAG with the highest initial rates, although both TAG and FFA also initially accumulated labeling (Table 10). DAG accumulation reached a maximum around one hour then achieved an equilibrium just below half of its maximum value where it reaches a balance between its synthesis and as a precursor for both TAG(0) and DAG(1) metabolism (Fig.38). The maximum accumulation in PC occurred around 2 hours where it varied little until the end of the time course, while TAG(0) peaked around 8 hours. The high label of PC was expected given the presence of the 18:2 acyl groups in the stigma glycerolipids. The fact that TAG(0) accumulated the labeled substrate from the beginning of the time course shows its ability to incorporate FAs directly from the acyl-CoA pool. This labeling pattern is consistent with that of the Kennedy pathway with acyl editing cycle (Allen *et al*, 2015) but different from that described in bayberry wax (Simpson & Ohlrogge, 2016).

[^{14}C]-glycerol labeling in non-estolide stigma lipids ($n = 0$) demonstrated that the initial label accumulated on DAG(0) and FFA(0) only with lag times for TAG(0) and PC accumulation (Table 10). Since the TAG(0) lag time was shorter than that of PC, this suggests that TAG(0) synthesis through *de novo* synthesis likely occurs. The significant accumulation of glycerol labeling in PC suggests high levels of DAG-PC interconversion and thus the presence of a secondary PC-derived DAG pool. The maximum accumulation of PC occurred around three hours after inoculation followed by a rapid

reduction while that of TAG occurred around eight hours (Fig.26-B). However, the rate of TAG accumulation slows concurrently with the PC decline. This may indicate that a significant flux of DAG used in TAG biosynthesis occurs via PC, such as through DGAT from a PC-derived DAG pool (Weiss & Kennedy, 1956) or direct acyltransferase involving PDAT (Dahlqvist *et al*, 2000). Therefore, it seems possible that precursors of stigma lipid polyesters are initiated through an alternative Kennedy pathway that involves the acyl editing cycle and combined *de novo*/PC-derived DAG/TAG biosynthesis (Fig.23).

In order to better understand the fluxes of TAG biosynthesis, further investigation into the composition DAG(0) and TAG(0) will be required. Across the labeling time course, the acyl composition of the glycerolipids will reflect the acyl pool from which they are synthesized, such that *de novo* DAG will only obtain PC-modified FAs (e.g. 18:2) through editing cycle whereas the bulk DAG pool may differ as it includes PC-derived DAG as well. Comparing the compositions of *de novo* DAG and bulk DAG and bulk PC will aid in determining the flux proportions for TAG biosynthesis and which DAG pool serves as the preferred precursor. Furthermore, positional acyl analysis on TAG(0) will give insight into the difference in composition between the acyl-CoA pool and the bulk DAG. TAG positions *sn*-1 and *sn*-2 derive from DAG, while *sn*-3 from the acyl-CoA pool. Selective lipases can mediate the hydrolysis of specific acyl group positions from the TAG glycerol backbone. For example, a porcine pancreatic lipase can be used for positional distribution analysis of seed oils by hydrolyzing the *sn*-1 and -3 positions, leaving an *sn*-2 MAG product, as described in experiments conducted with *Mimusops elengi* and *Parkinsonia aculeata* seed oils (Sharma *et al*, 2009). The ratios of 18:1 and 18:2 can be analyzed between the hydrolyzed acyls and the residual MAG as a means to compare bulk DAG and acyl-CoA pool compositions. Unfortunately, pancreatic lipase does not seem to function for TAG(n) estolides which could have provided important regiochemical information (Appendix Fig.B4).

3.4.3 Potential impurities in α,β -DAG(n) and FFA(n) fractions.

In Chapter 2, a distinct distribution of α,β -DAG(n) was observed only in the internal lipid fraction such that concentrations of α,β -DAG(1) > α,β -DAG(2) > α,β -DAG(0) (Fig.16). In the [^{14}C]-acetate experiment, labeled α,β -DAG(1) accumulated significantly, more than twice the next highest substrate. However, with [^{14}C]-glycerol labeling, α,β -DAG(1) still had the most substrate accumulation but the distribution between species was less staggering. Thus, whichever compound may be co-eluting with α,β -DAG(1) also incorporates acetate. Future investigations should analyze this fraction to identify potential co-eluting molecules.

The free estolides fraction was found to accumulate radioactivity derived from [^{14}C]-glycerol, resulting in over 2% of the total label across all lipid fractions in 12 hours. In comparison, the same FFA(n) only amounted to 3% in 12 hours from the [^{14}C]-acetate labeling assay. Acyl labeling from glycerol has been shown to occur in other systems such as pea leaves (Bates *et al*, 2007), soybean embryos (Bates *et al*, 2009), and *Camelina sativa* embryos (Pollard *et al*, 2015), generating 5-10% of the total label from glycerol but may increase with higher concentrations of glycerol (Pollard *et al*, 2015). This process is thought to initiate through the reverse G3P dehydrogenase (GPDH) reaction after the exogenous glycerol is converted to G3P (Slack *et al*, 1977) or through a glycerol kinase (Eastmond, 2004). This forms dihydroxyacetone phosphate (DHAP) which can be metabolized to phosphoenolpyruvate (PEP), then to pyruvate through pyruvate kinase, and subsequently acetyl-CoA through pyruvate dehydrogenase where it can be assimilated into the FAS pathway. This process is thus expected to have a noticeable lag phase before glycerol uptake corresponds to acyl labeling. As shown in both Fig.28 and Fig.37, acyl labeling in FFA(n) through [^{14}C]-glycerol intake does not occur until 1.5 hours yet a non-negligible specific activity of [^{14}C] is observed prior to this. It is possible that another glycerol-containing lipid co-migrates with the FFA(n) fraction in TLC analysis and should be identified through alternative TLC solvent conditions and GC-MS analysis. Nonetheless, the acyl labeling through exogenous glycerol shows that nascent FA synthesis present in the stigma glycerolipids is not dependent on the supply of labeled acetate substrate (Bates *et al*, 2009).

3.4.4 Estolide polymerization may occur in a stepwise manner.

Both [^{14}C]-acetate and -glycerol labeling assays performed in tobacco stigma lipids demonstrated a rate of initial label accumulation inversely proportional to their estolide count, such that $n = (1) > (2) > (3) > (4)$ for both FFA(n) and TAG(n) species (Table 7; 8). The lag phases followed the same trend, however acetate-labeled TAG(n) showed near instant substrate incorporation for TAGs (0-2). DAG(n) kinetics were not as straightforward as initial rates between species did not follow the same trend as seen in TAG(n) and FFA(n) fractions. For example, for [^{14}C]-glycerol labeling, α,α -DAG(1) and α,α -DAG(2) demonstrated short lag times with longer lag times for α,α -DAG(3) and α,α -DAG(4) (Table 8), whereas α,β -DAG(3) and α,β -DAG(4) had shorter lag times compared to α,β -DAG(1) and α,β -DAG(2). This may have resulted from co-eluting impurities or unusual estolide synthesis mechanics. The stepwise kinetics observed for FFA(n) and TAG(n) fractions may demonstrate precursor-product relationships between estolide chain lengths, such that $n(0)$ is a metabolic precursor for $n(1)$, which instead is a precursor for $n(2)$, etc. However, either insufficient labeling was provided for each lipid fraction to achieve steady state conditions beyond $n(0)$ or these estolides simply continue to accumulate at a rate higher than their products until metabolic changes in the stigma lead to polyester degradation (for example anthesis, Fig.14;15;16). Fortunately, the pulse-chase labeling demonstrated in the [^{14}C]-glycerol assay illustrated a decrease in label accumulation of $n(0)$ and $n(1)$ [and slightly $n(2)$] lipids species, for FFA(n), DAG(n), and TAG(n), while $n(3)$ and $n(4)$ continued their linear accumulation (Fig.33;34;35). This information helped confirm that the remodeling of these lipid species occurs.

As demonstrated previously, the non-estolide species are the first to accumulate labeled substrates in all lipid fractions. According to these results, it is unlikely that free estolides are synthesized first and then acylated to the glycerol backbone to make TAG(n) and DAG(n) molecules and a stepwise polymerization process possibly occurs in the glycerolipid molecules. In fact, combining all the lipid fractions with the same estolide number, such that for $n = 0$ includes combined FFA(0), DAG(0), and TAG(0) fraction for all n species, shows this increment occurs simultaneously for all estolide fractions (Appendix Fig.B2). However, it is possible that the estolides polymerized in TAG(n) or DAG(n) molecules are removed by lipases, such that FFA(n) estolides would still observe the same precursor-product relationships. Evidence of lipase activity is

provided by the lag times observed for [^{14}C]-acetate (and to a lesser extent [^{14}C]-glycerol) labeled TAG(n) and FFA(n) fractions (Table 7) such that label accumulation in FFA(n) occurs at significantly lower initial rates with significantly longer lag times than TAG(n) species with the same estolide count. This trend is only observed in the internal lipid fraction; surface lipid distribution accumulates a reflection of the internal lipid composition and does not seem to follow precursor-product relationships between estolide lengths. Thus, this polymerization process may be intra- or extracellular but occurs in the glandular tissue before the exudate is exported and deposited on the stigma surface, yet the mechanism remains unclear.

The estolides found in stigmas consist of ester-bonded ω -hFAs chains end-capped by a normal FAs (Matsuzaki *et al*, 1983b) and it has been shown that these estolides can occur in any *sn* position along the glycerol backbone (Fig.20). Therefore, for a TAG(n) remodeling to occur, producing TAG(n+1), two separate methods are hypothesized. The first involves an ω -hFA (or ω -hFA-CoA) to be inserted in-between the normal FA and the glycerol backbone or between an existing estolide and the glycerol backbone (Fig.39). This TAG(n) remodeling process would require a lipase to remove an estolide, terminal hydroxylation of a free acyl(-CoA) monomer, the esterification of the newly formed ω -hFA to the carboxyl section of the estolide, and acyl/estolide transferase back to the glycerol backbone of the TAG(n) molecule. The presence of TAG(n) lipase activity may describe the disorderly labeling kinetics of between α,β -DAG(n) and α,α -DAG(n) isomers (Table 7; 8) as different estolide lengths may have preferred lipase positions along the glycerol backbone or isomerization occurs for better stability based on chain length distribution. Thus, it may be possible that the lipase can only function on the *sn*-1/3 glycerol positions and DAG(n) isomerization prior to the re-acylation is what allows the presence of estolides in any glycerol position.

Furthermore, FA hydroxylation is considered to be an intracellular function as shown by the cytochrome P450 enzymes in cutin and suberin synthesis (Duan & Schuler, 2005; Li-Beisson *et al*, 2009) and CYP86A22 for petunia stigma lipids (Han *et al*, 2010). Oilseed hFA are also produced intracellularly, such that castor bean ricinoleic acid production occurs on PC (Moreau & Stumpf, 1981), and the unusual C24 di-hFAs found in Chinese violet cress seed oils, dubbed wuhanic acid (7,18-OH 24:2 $\Delta^{15,21}$) and nebraskanic acid (7,18-OH 24:1 Δ^{15}), were found to be hydroxylated through a FAD2-type hydroxylase and a FATTY ACID ELONGASE 1 (FAE1)-encoded 3-KETOACYL-COA SYNTHASE (KCS) enzymes for their 18-OH and 7-OH whose processes are PC-

bonded and ER-localized, respectively (Li *et al*, 2018). Therefore, stigma lipid TAG(n) production must also be intracellular or either a mechanism for free estolide transport through the plasma membrane exists both ways or a mechanism of ω -hFA export to the site of polymerization occurs, such as *sn*-2-hMAG transport observed in cutin synthesis.

The second hypothesized TAG(n) remodeling pathway involves existing glycerol-bonded (or estolide-bonded) normal FA to be converted to an ω -hFA and then end-capped by a new normal FA (-CoA). This process involves subsequent hydroxylation of ester-bonded FAs and annealing to a new FA (Fig.40). The presence of incremental label accumulation in the lipid species would suggest that the activity of this method is non-specific to FFA(n), DAG(n), or TAG(n), and such this process would be required to function in all glycerol backbone positions. This process would likely be intracellular due to the hydroxylation process occurring directly on the glycerolipids/estolides. A full time course of pulse-chase acyl monomer labeling could be used to confirm whether existing glycerolipid- or estolide-bonded normal FA are converted to ω -hFA over time. Nonetheless, CYP86A22 is the only confirmed enzyme involved in stigma lipid biosynthesis with demonstrated fatty acyl-CoA hydroxylase activity in petunia stigma lipids (Han *et al*, 2010) but whether this enzyme can operate on glycerol- or estolide-bonded FAs is unclear.

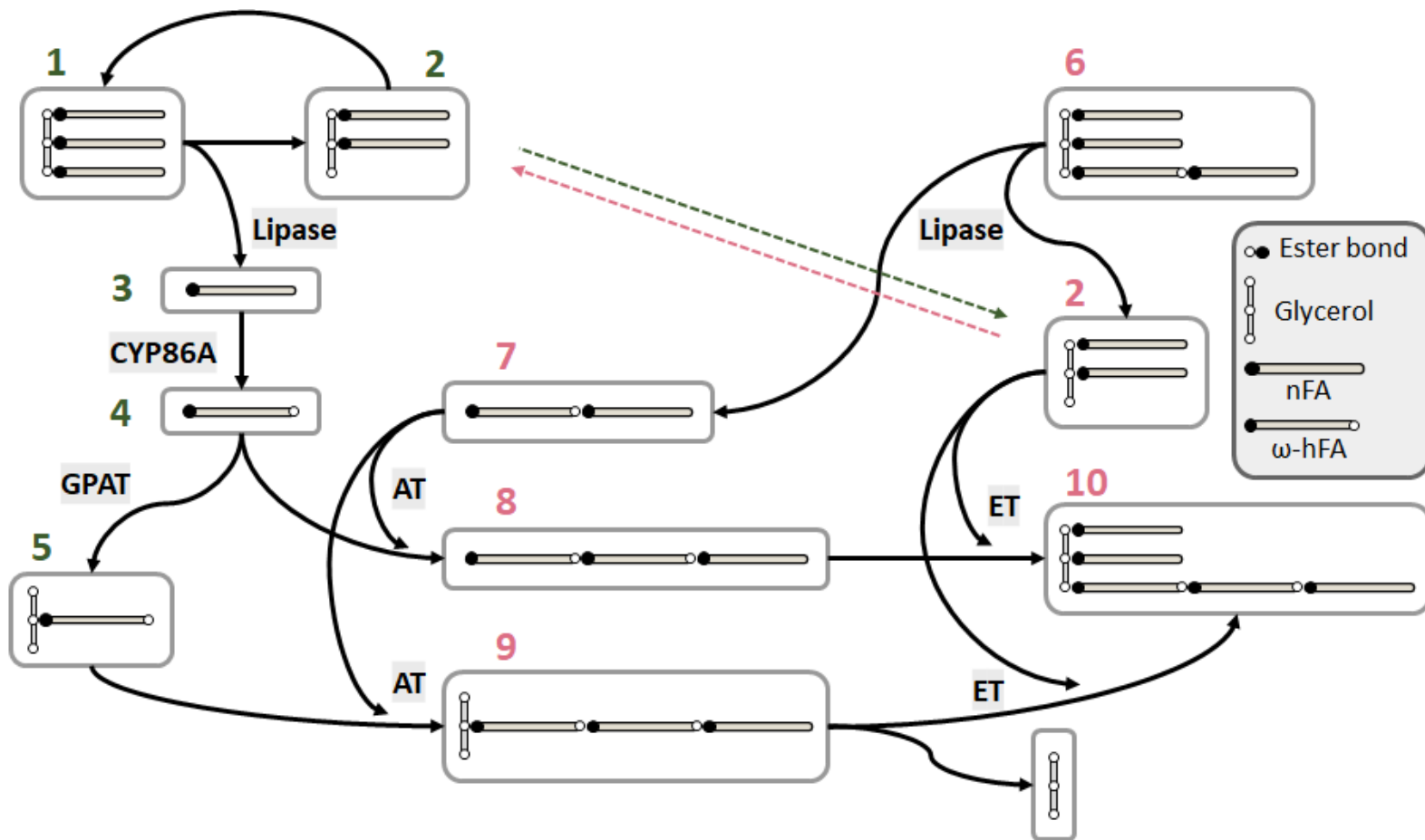


Figure 39. Proposed lipase-mediated mechanism for TAG(n) assembly. Molecules 1-5 (green) represent likely intracellular components of the process, while the compartmentalization of 6-10 (pink) is unknown. Compounds 8 and 9 are synthesized through unspecified acyltransferases (AT) and compound through an estolide transferase (ET). The fluxes through 8 and 9 may or may not co-exist. Stereochemistry simplified for representation as estolides have been demonstrated to occur in any position.

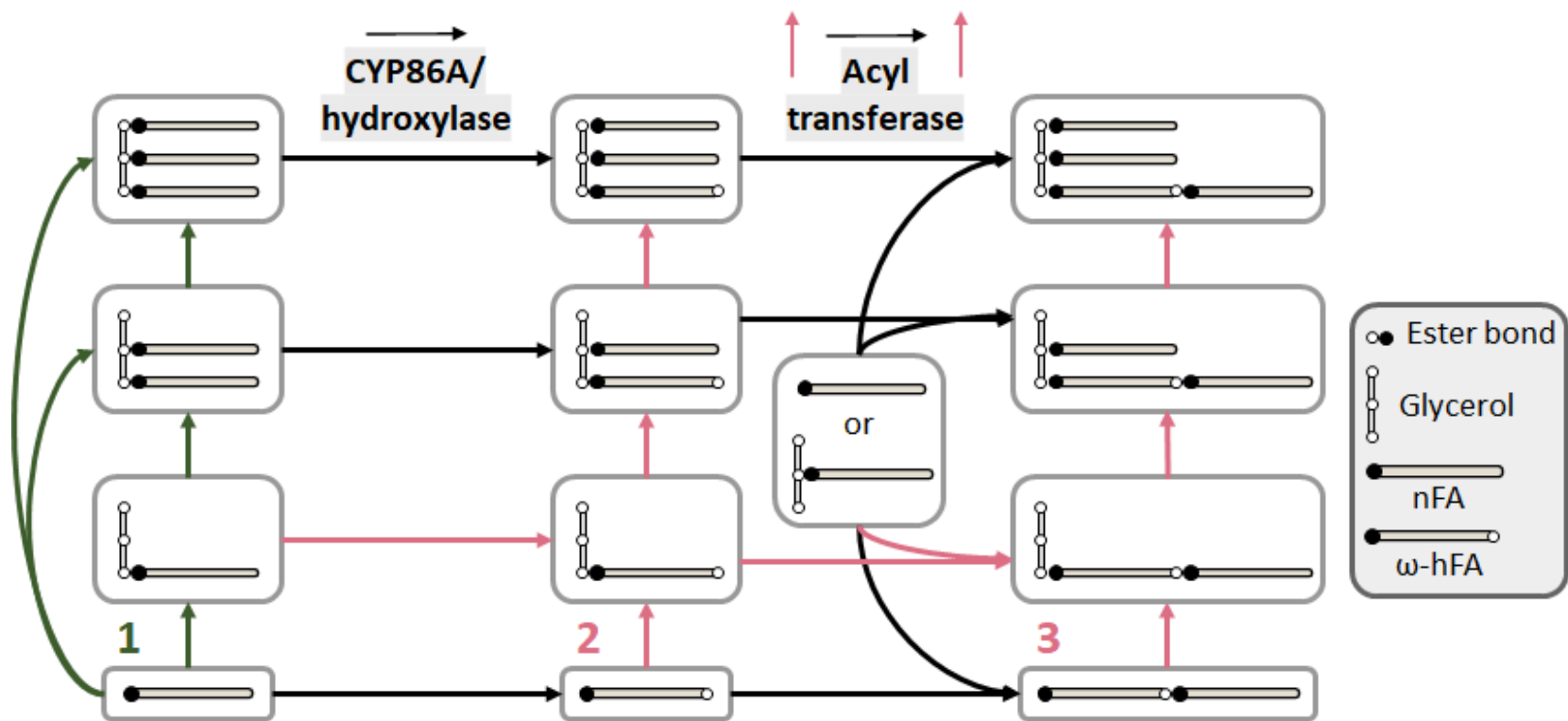


Figure 40. Proposed acyl-remodeling mechanism for TAG(n) assembly. Process 1 (green) represents DAG(0)/TAG(0) synthesis pathways. Processes 2 and 3 (pink) represent glycerol:acyltransferase activity with ω-hFA and estolides, respectively, and are unknown whether they can occur. Stereochemistry simplified for representation as estolides have been demonstrated to occur in any position.

3.5 Conclusions

Our novel method of *in planta* substrate labeling was shown to be an effective tool for studying tobacco stigma lipid polyesters *in vivo*. Both [¹⁴C]-acetate and [¹⁴C]-glycerol labeling showed that the initial rate of estolide appearance is (0) > (1) > (2) > (3) > (4) for all FFA(n) and TAG(n) fractions, while [¹⁴C]-glycerol pulse-chase labeling demonstrated a stepwise precursor-product relationship within these lipid fractions. This suggests that estolide polymerization occurs independently of initial DAG(0) and TAG(0) biosynthesis and that these molecules are used as precursors for DAG(n) and TAG(n), respectively. The labeling kinetics of the non-estolide glycerolipids and the membrane lipid phosphatidylcholine suggest a mechanism akin to the Kennedy pathway using the acyl editing cycle and combined *de novo* and PC/derived DAG/TAG synthesis. Two possible mechanisms for estolides incorporation and polymerization after initial synthesis have been hypothesized. Further research into monomer composition and regiochemical analysis may reveal new information about the estolide polymerization mechanism and the metabolic fluxes of the glycerolipid intermediates.

Appendix B

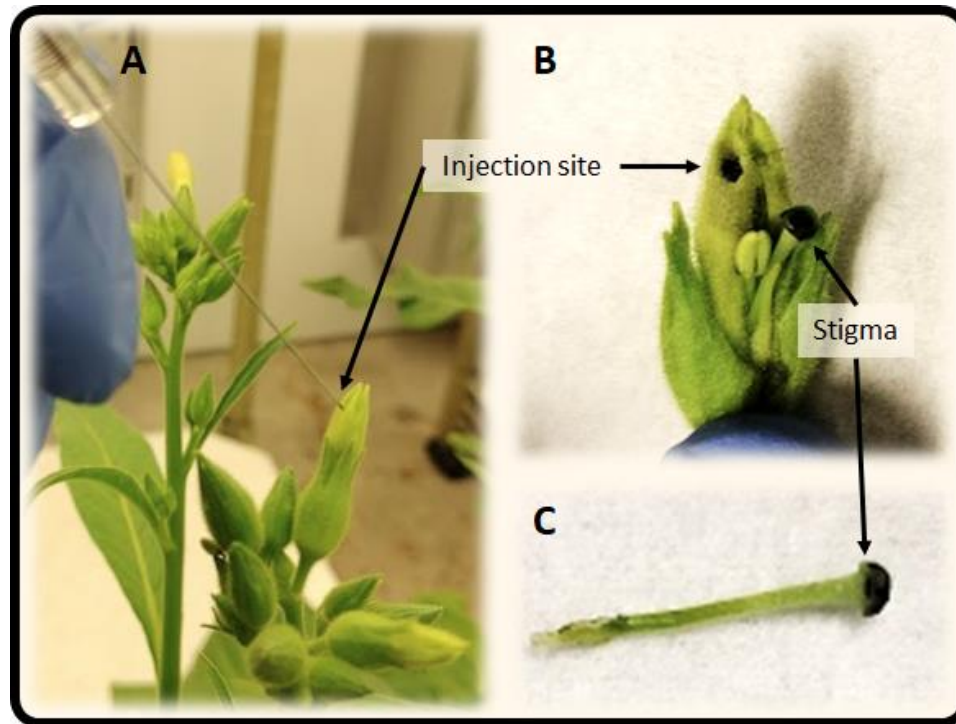


Figure B1. Stable isotope labeling *in planta* methodology. A: injection site of incubation buffer through the flower corolla. B: test injection with 0.05% toluidine blue dye to show the distribution of the injected buffer. C: remove stigma and style. Only stigmas were used in the assay. Stage 3 was determined to be ideal for injection as any earlier proved difficult to saturate the stigma and it allowed for 48 hours of incubation time without reaching anthesis.

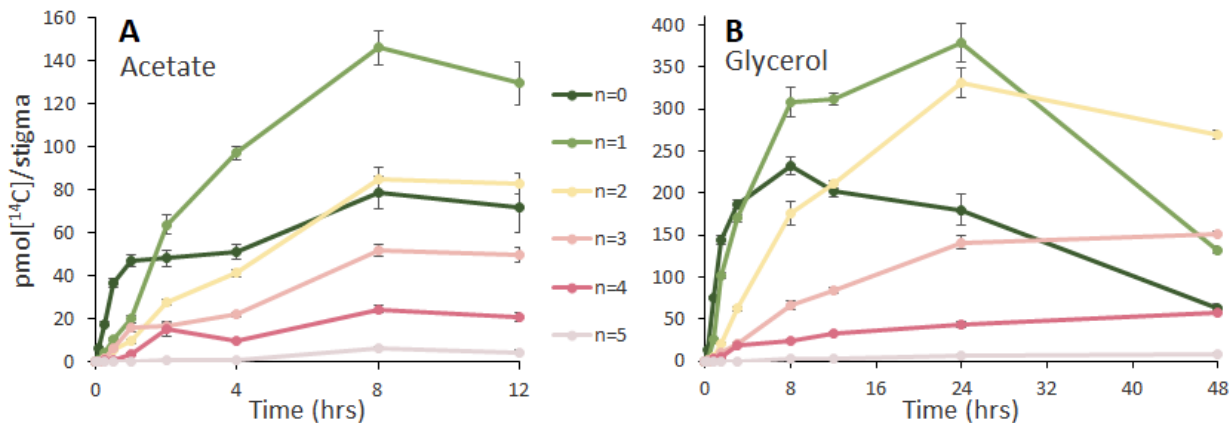


Figure B2. Labeling of combined estolide fractions. A: acetate, B: glycerol. Combined surface and internal data for all TAG(n), DAG(n), and FFA(n) lipid fractions, such that TAG(n), DAG(n), and FFA(n) fractions with the same ω -hFA count (n) are combined.

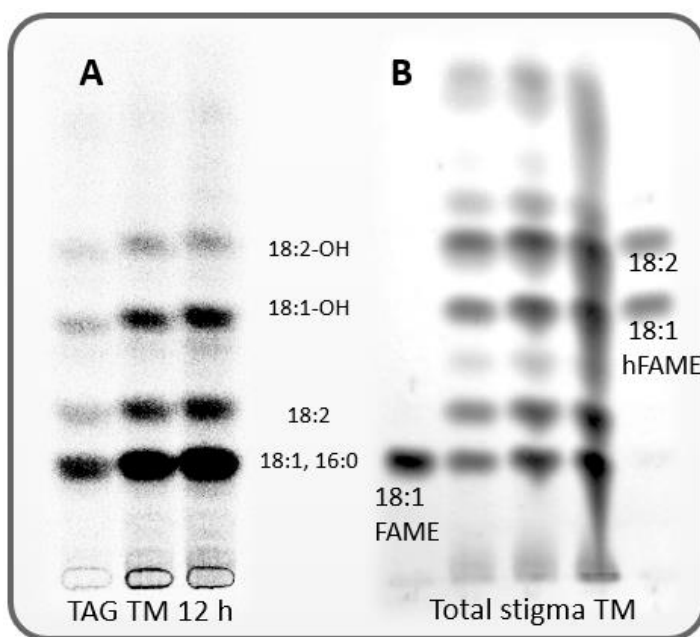


Figure B3. Reverse phase TLC of transmethylation products from stigma lipids. A: Phosphorimager screening of $[^{14}\text{C}]$ -glycerol labeled TAG transmethylation products 12 hours after incubation. B: Iodine stained transmethylation products of total stigma lipid fraction pooled from stages 3-5. Transmethylation was achieved using 5% sulfuric acid in methanol and solvent conditions were 65:35:0.1 Acetonitrile:methanol:water.

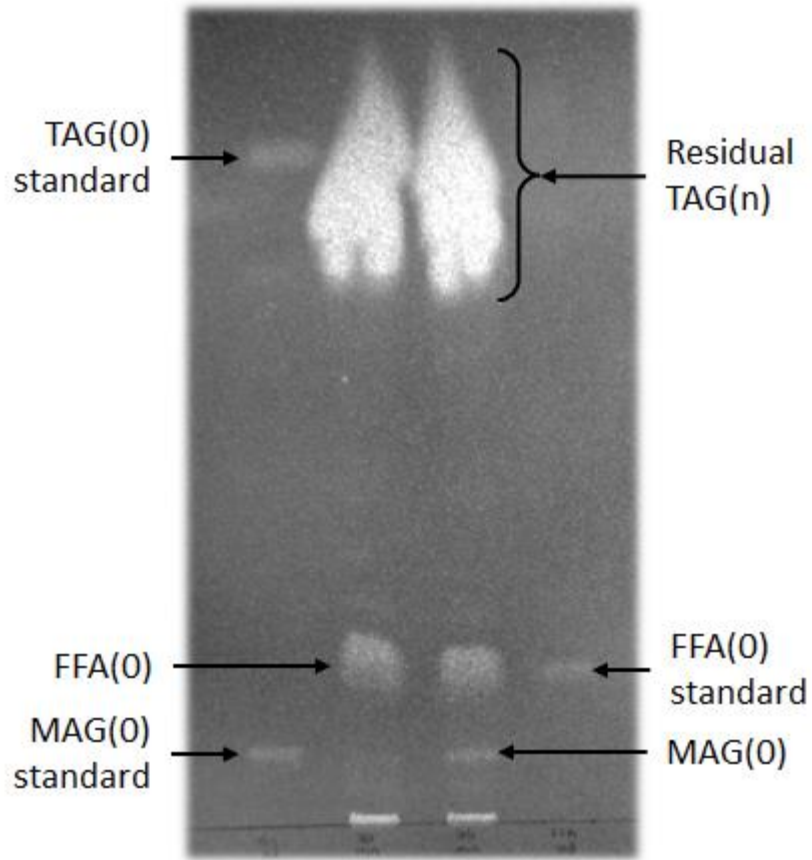


Figure B4. Pancreatic lipase use on TAG(n) estolides. Experimental conditions obtained from Christie & Han (2010). Tobacco TAG(n) extracts obtained from 10 stigmas were incubated with the pancreatic lipase buffer for 30 and 60 minutes. The lipase cleaves the *sn*-1 and 3 positions on the glycerol backbone, leaving *sn*-2 MAG. The presence of only FFA(0) and MAG(0) indicated that only TAG(0) was affected by the lipase.

Chapter 4: Conclusions and Future Research Goals

4.1 Research questions

Plant surface glycerolipids represent a vast group of structurally and functionally distinct molecules. These provide an interface for aerial tissue to interact with the external environment and provide protection against a multitude of biotic and abiotic factors. A major component of the cuticle, cutin, is a highly investigated polyester which generally contains significant amounts of glycerol and ω -hFAs, among other hydroxyl and carboxyl functional group-carrying acyls, esterified on plant surface tissues (Kolattukudy, 1981; Pollard et al, 2008; Yeats & Rose, 2013). A less ubiquitous surface glycerolipid polyester is found in the exudate of wet stigmas which retain the structure of polyacylglycerols, namely in the form of multi-acyl diacylglycerol and triacylglycerol. Massive surface accumulation of DAG and TAG wax is observed in the waxes of bayberry fruit (Simpson & Ohlrogge, 2016) however, stigma polyesters uniquely contain polymerized ω -hFAs forming estolide on the glycerol backbone (Matsuzaki *et al*, 1983b; Koiwai & Matsuzaki, 1988). Very little is known about the metabolic pathways involved in stigma polyester biosynthesis; chemical characterizations were performed by the Matsuzaki *et al* (1983a; 1983b; 1983c; 1986; Koiwai & Matsuzaki, 1988), preliminary labeling trials were conducted by Wang *et al* (2003), and the identification of the cytochrome P450 CYP86A22 by Han *et al* (2010) remains the only confirmed enzyme involved in the biosynthesis of wet stigma polyesters.

This work aimed to investigate the mechanism of extracellular glycerolipid polyester assembly and accumulation in tobacco stigmas by examining further the chemical structure of these lipids and by studying the kinetics of [14 C]-labeled substrate incorporation through their metabolic intermediates. Similarities and distinctions between stigma polyesters and the established structures and biochemical pathways of cutin, oilseed TAG, and bayberry wax provide a foundation to furthering the understanding of a potentially novel method for glycerolipid production. Major goals of this work were to identify the compartmentalization of the polyester biosynthesis, the estolide structure of the polyacylglycerols, the possible role of DAG isomers, and whether or not estolide polymerization occurs prior to glycerol esterification. An important characteristic of

stigma lipid polyester is that they accumulate in very large amounts on the tissue surface and they are readily soluble in organic solvents, making them extremely viable candidates for large scale production of industry-important lipids. Identifying the mechanisms involved in their production will help provide an efficient source of alternative bio-based polymers through the engineering of plant surfaces or microorganisms which can have substantial economic and environmental benefits.

4.2 Summary of findings

The techniques used to achieve our objectives in this research involve isolating and characterizing the structures and compositions of developing wet stigma glycerolipids using a combination of thin layer and gas chromatography, as well as kinetic radiolabeling with [^{14}C]-labeled substrates using a novel pulse time course experimental method we developed for *in planta* isotope analysis. Tobacco stigma lipid polyesters accumulated estolides in the form of TAG(n), DAG(n), and free estolides, FFA(n), which consist primarily of 18:1 and 18:2 FAs along with their ω -hydroxy counterparts, such that the ω -hFAs are esterified in a chain that is end-capped by a normal FA to form the estolide; estolide chains with one estolide bond were found to be predominant considering all estolide molecules present in the exudate. Positional estolide analysis of TAG(n) species identified that these estolides can form on any position of the glycerol backbone. This is another unique characteristic of stigma TAG(n) estolides as all identified oilseed TAG estolides were found to occur in either the outer or central carbons of glycerol but not all three positions simultaneously (Mikolajczak & Smith, 1968; Sprecher et al, 1965; Hayes *et al*, 1995; Rajiah *et al*, 1976; Smith *et al*, 2013). The investigation of polyester distribution between surface and internal lipid tissues across the stigma developmental stages demonstrated only traces of polyesters in the surface exudate fraction in the early stages of development, with non-estolide containing lipids, namely TAG(0), DAG(0) and FFA(0), scarcely present in this fraction throughout development. This result suggests that their assembly occurs in the glandular zone and the lipids are then exported to the stigma surface, in agreement with electron microscopy observations (Cresti *et al*, 1986; Konar & Linskens, 1966).

Radioisotope labeling assays showed that [^{14}C]-glycerol and [^{14}C]-acetate were effective substrates for tracking label accumulation across lipid fractions and estolide

chain lengths within lipid species. These experiments showed that the first labeled lipids in each fraction were those that did not contain estolides and the labeling trends between DAG(0), TAG(0), and phosphatidylcholine suggest a mechanism similar to oilseed combined *de novo* DAG/TAG and PC-derived DAG/TAG biosynthesis pathways for the synthesis of non-estolide stigma glycerolipids. Similarly, initial label incorporation occurs exclusively in 18:1 normal FA monomers. Furthermore, label incorporation into estolide lipids showed subsequent rates of initial appearance inversely proportional to estolides chain length, such that (0) > (1) > (2) > (3) > (4) for both FFA(n) and TAG(n). Moreover, the pulse-chase labeling with [¹⁴C]-glycerol substrate demonstrated stepwise precursor-product relationship between these species showing that TAG(n) remodeling occurs to produce TAG(n+1). Thus, the estolide polymerization mechanisms may require TAG(0) as a precursor; while a known hydroxylation reaction is confirmed to be intracellular (Han *et al*, 2010), whether the entirety of polymerization occurs intracellularly or extracellularly is still to be determined. It is possible that a series of lipase, hydroxylase, and acyltransferase enzymes are involved in the estolide production and incorporation into these lipid polyesters which may explain the presence of FFA(n) species and the inconsistent labeling trends seen in the DAG(n) lipid fraction. Labeling and mass quantification of DAG(n) isomers suggests that α,β -DAG(0) is produced initially and isomerized to α,α -DAG(0), but whether α,β -DAG(n) and α,α -DAG(n) are used as intermediates for TAG(n) production remains unclear.

4.3 Unknowns and future experiments

In regard to chemical characterization, it will be important to confirm that the structure of FFA(n) estolides are in fact ω -hFAs end-capped with normal FA as described in TAG(n) and DAG(n) fractions (Matsuzaki *et al*, 1983b; 1986). This can be accomplished by isolating, depolymerizing, comparing the stoichiometric ratios of the normal to hydroxy monomers in each FFA(n) species and diazomethane can be used as a derivative to convert the carboxylic acids into their methyl esters for GC-FID analysis (Gutsche, 2004).

The IPPE fraction is another important group of lipids that may be crucial in identifying potential precursors involved in the process of stigma glycerolipids. Although we were unable to confirm, this fraction has been speculated to consist of

polyacylglycerols containing more polar hydroxyl fatty acyl groups, typically found in cutin or as photo/auto-oxidation products, such as mid-chain hydroxyl groups and peroxides, respectively. Through the presence of these acyl groups, new genes of interest can be identified which elucidate certain mechanisms involved in polyester polymerization and transport. New methods of GC-MS quantification are being considered beyond transmethylation for future endeavors as these IPPE molecules may not be amenable to our standard methods. Hydrogenolysis through lithium aluminum hydride (LiAlH_4) can be used to reduce carboxylic acids and keto-groups (but not acetyls) to alcohols, a method used previously in identifying cutin monomers (Walton & Kolattukudy, 1972) and more recently in analyzing lignin monomer composition, albeit with a different catalyst (van de Pas *et al*, 2014; Wang *et al*, 2021). Combining this with catalytic hydrogenation ($\text{PtO}_2 + \text{H}_2$) to reduce the double bonds and peroxy groups and trimethylsilyl (TMS) derivatization will simplify the identification of these compounds through mass spectroscopy.

While many lipid groups were identified in these analyses, it may be crucial to identify intermediates in known metabolic pathways, such as lysophosphatidic acid (LPA) as used in oilseed TAG production. We did not observe an accumulation of monoacylglycerols (MAG) as seen in the bayberry wax pathways (Simpson & Ohlrogge, 2016), and our chemical approach did not carefully characterize the IPPE and polar fractions where the presence of cutin-like hydroxy-MAG components may have been identified. These molecules could be involved in the polymerization process of stigma polyester estolides. If present, hydroxy-MAG composition would need to be compared to the composition of cutin in the stigma to confirm that such hydroxy-MAG is not just an intermediate of cutin biosynthesis. Nevertheless, any MAG precursor used for stigma estolide biosynthesis would be in much higher proportion than cutin MAG precursors given large flux of lipids into the exudate fraction, which accumulates about 3 mg cm^{-2} , compared to lipids required for cutin biosynthesis, which shows a concentration of 1.5 mg cm^{-2} at anthesis (Dubois, 2020).

As described in Chapter 2, some of the methods used in our analyses yielded inherent inaccuracies in our quantitative results, namely using iodine-staining densitometry, gas chromatography mass spectroscopy, and an internal standard for ω -hFA quantification that may undergo parallel reactions and not represent the actual amount added. Thus, results affected by these issues should be reevaluated.

In regard to labeling experiments, repeating the assays with shorter time courses (i.e. minutes) and more stigma material (e.g. 10-20 stigmas instead of 5 per replicate) will allow for more accurate tracing of labeled metabolites and may yield more accurate reaction kinetics and lag times. With larger sample sizes, the standard error obtained for metabolites with very low label accumulation becomes less significant and more material may allow us to identify more transient metabolites that have gone undetected in these trials. Furthermore, an extended time course for the labeled monomer analysis could also be performed in pulse-chase conditions to view the fate of acyl groups and confirm whether polyester-bound normal FAs are remodeled into hFAs.

Tracing experiments using labeled precursors can reveal new information regarding the metabolic pathways for estolide synthesis. For example, labeled acyl groups with different carbon lengths, degree of unsaturation, and functional groups may identify acyl selectivity for estolide incorporation, or methods and compartmentalization of hydroxylation or estolide polymerization processes. Understanding whether the processes involved in stigma lipid biosynthesis occur intra- or extracellularly is a crucial task for future research. Furthermore, supplying labeled MAG or hydroxy-MAG precursors can identify whether these can be used as acyl suppliers for estolide esterification, as performed by Simpson and Ohlogge (2016) to confirm *sn*-2-MAG as a DAG and TAG precursor. Regiochemical analysis using stable isotope labeling and electrospray ionization mass spectroscopy (ESI-MS) could also be used to infer synthesis mechanisms for stigma polyesters.

Lastly, our research group has identified multiple genes relating to cutin synthesis that are expressed uniquely in the stigmatic tissue of tobacco plants. RNAi mutants of some of these genes have been demonstrated to significantly affect the stigmas' ability to produce estolides (unpublished data). Radiolabeling tracing experiments of select knockdown or overexpression mutants presenting phenotypes in their stigma lipids can be compared to wild type stigmas to identify potential bottlenecks or redundancies in the synthesis process of stigma polyesters.

4.4 Future applications of research

Stigma lipids are sources of oxygenated FAs for the synthesis of bio-based polymers and chemicals, and of estolides that have physicochemical properties suitable for use as biolubricants (Li *et al*, 2018; Soni & Agarwal, 2014; Kajdas *et al*, 2010). The physical properties of estolides have been demonstrated to outperform those of regular vegetable oils in these applications (Hayes & Kleiman, 1995; Isbell *et al*, 2001; Zerkowski, 2008). Free acyl estolides containing both hydroxy and unsaturated FAs were shown to have great potential for a wide range of industrial lubricant applications due to their oxidative stability and useful properties at cold temperatures (Isbell, 2011). Tobacco stigma lipids have been demonstrated to accumulate up to 3 mg cm⁻² (Appendix Table A1) of exudate that is readily extractable with organic solvents and, considering that surface lipids are more resistant to deterioration than internal lipids (Yang & Ohlrogge, 2009), these represent a valuable source for desirable lipids. Furthermore, understanding the metabolic pathways involved in stigma polyester synthesis would allow researchers to engineer alternative pathways producing the same or other high value lipids using either *Yarrowia lipolytica* or *Saccharomyces cerevisiae* yeasts as bio-synthetic lipid factories (Lazar *et al*, 2018; Jiang *et al*, 2022).

References

- Abramovic, H., & Abram, V. (2005). Physico-chemical properties, composition and oxidative stability of *Camelina sativa* oil. *Food technol. biotechnol*, *43*(1), 63-70.
- Allen, D. K., Bates, P. D., & Tjellström, H. (2015). Tracking the metabolic pulse of plant lipid production with isotopic labeling and flux analyses: past, present and future. *Progress in Lipid Research*, *58*, 97-120.
- Aronel, V., Lemieux, B., Hwang, I., Gibson, S., Goodman, H. M., & Somerville, C. R. (1992). Map-based cloning of a gene controlling omega-3 fatty acid desaturation in *Arabidopsis*. *Science*, *258*(5086), 1353-1355.
- Bafor, M., Jonsson, L., Stobart, A. K., & Stymne, S. (1990). Regulation of triacylglycerol biosynthesis in embryos and microsomal preparations from the developing seeds of *Cuphea lanceolata*. *Biochemical Journal*, *272*(1), 31-38.
- Bago, B., Zipfel, W., Williams, R. M., Jun, J., Arreola, R., Lammers, P. J., ... & Shachar-Hill, Y. (2002). Translocation and utilization of fungal storage lipid in the arbuscular mycorrhizal symbiosis. *Plant Physiology*, *128*(1), 108-124.
- Bakan, B., & Marion, D. (2017). Assembly of the cutin polyester: from cells to extracellular cell walls. *Plants*, *6*(4), 57.
- Bates, P. D., & Browse, J. (2011). The pathway of triacylglycerol synthesis through phosphatidylcholine in *Arabidopsis* produces a bottleneck for the accumulation of unusual fatty acids in transgenic seeds. *The Plant Journal*, *68*(3), 387-399.
- Bates, P. D., & Browse, J. (2012). The significance of different diacylglycerol synthesis pathways on plant oil composition and bioengineering. *Frontiers in plant science*, *3*, 147.
- Bates, P. D., Durrett, T. P., Ohlrogge, J. B., & Pollard, M. (2009). Analysis of acyl fluxes through multiple pathways of triacylglycerol synthesis in developing soybean embryos. *Plant Physiology*, *150*(1), 55-72.
- Bates, P. D., Ohlrogge, J. B., & Pollard, M. (2007). Incorporation of newly synthesized fatty acids into cytosolic glycerolipids in pea leaves occurs via acyl editing. *Journal of Biological Chemistry*, *282*(43), 31206-31216.
- Bayer, A., Ma, X., & Stöckigt, J. (2004). Acetyltransfer in natural product biosynthesis—functional cloning and molecular analysis of vinorine synthase. *Bioorganic & medicinal chemistry*, *12*(10), 2787-2795.
- Becker, R., & Knorr, A. (1996). An evaluation of antioxidants for vegetable oils at elevated temperatures. *Lubrication Science*, *8*(2), 95-117.
- Bednarska, E. (1991). Calcium uptake from the stigma by germinating pollen in *Primula officinalis* L. and *Ruscus aculeatus* L. *Sexual Plant Reproduction*, *4*, 36-38.
- Bessire, M., Borel, S., Fabre, G., Carraca, L., Efremova, N., Yephremov, A., ... & Nawrath, C. (2011). A member of the PLEIOTROPIC DRUG RESISTANCE

- family of ATP binding cassette transporters is required for the formation of a functional cuticle in Arabidopsis. *The Plant Cell*, 23(5), 1958-1970.
- Binder, R. G., Applewhite, T. H., Kohler, G. O., & Goldblatt, L. A. (1962). Chromatographie analysis of seed oils. Fatty acid composition of castor oil. *Journal of the American Oil Chemists' Society*, 39, 513-517.
- Bird, D., Beisson, F., Brigham, A., Shin, J., Greer, S., Jetter, R., ... & Samuels, L. (2007). Characterization of Arabidopsis ABCG11/WBC11, an ATP binding cassette (ABC) transporter that is required for cuticular lipid secretion. *The Plant Journal*, 52(3), 485-498.
- Bisht, K. S., Henderson, L. A., Gross, R. A., Kaplan, D. L., & Swift, G. (1997). Enzyme-catalyzed ring-opening polymerization of ω -pentadecalactone. *Macromolecules*, 30(9), 2705-2711.
- Bonaventure, G., Beisson, F., Ohlrogge, J., & Pollard, M. (2004). Analysis of the aliphatic monomer composition of polyesters associated with Arabidopsis epidermis: occurrence of octadeca-cis-6, cis-9-diene-1, 18-dioate as the major component. *The Plant Journal*, 40(6), 920-930.
- Bouyahyi, M., Pepels, M. P., Heise, A., & Duchateau, R. (2012). ω -Pentadecalactone polymerization and ω -pentadecalactone/ ϵ -caprolactone copolymerization reactions using organic catalysts. *Macromolecules*, 45(8), 3356-3366.
- Cahoon, E. B., & Ohlrogge, J. B. (1994). Apparent role of phosphatidylcholine in the metabolism of petroselinic acid in developing Umbelliferae endosperm. *Plant physiology*, 104(3), 845-855.
- Canadian Nuclear Safety Commission. "Licensing: Nuclear Substances and Radiation Devices." *Canadian Nuclear Safety Commission*, 20 June 2022, <https://nuclearsafety.gc.ca/eng/nuclear-substances/licensing-nuclear-substances-and-radiation-devices/index.cfm>.
- Chen, G., Snyder, C. L., Greer, M. S., & Weselake, R. J. (2011). Biology and biochemistry of plant phospholipases. *Critical Reviews in Plant Sciences*, 30(3), 239-258.
- Choi, Y. E., Lim, S., Kim, H. J., Han, J. Y., Lee, M. H., Yang, Y., ... & Kim, Y. S. (2012). Tobacco NtLTP1, a glandular-specific lipid transfer protein, is required for lipid secretion from glandular trichomes. *The Plant Journal*, 70(3), 480-491.
- Christie, W. W., Han, X. (2010). *Lipid Analysis: Isolation Separation and Lipidomic Analysis*, 4th ed. (Bridgewater, UK: The Oily Press).
- Cresti, M., Ciampolini, F., Van Went, J. L., & Wilms, H. J. (1982). Ultrastructure and histochemistry of Citrus limon (L.) stigma. *Planta*, 156, 1-9.
- Cresti, M., Keijzer, C. J., Tiezzi, A., Ciampolini, F., & Focardi, S. (1986). Stigma of Nicotiana: ultrastructural and biochemical studies. *American Journal of Botany*, 73(12), 1713-1722.
- Crossley, A., Freeman, I. P., Hudson, B. J. F., & Pierce, J. H. (1959). 152. Acyl migration in diglycerides. *Journal of the Chemical Society (Resumed)*, 760-764.

- Dahlqvist, A., Ståhl, U., Lenman, M., Banas, A., Lee, M., Sandager, L., ... & Stymne, S. (2000). Phospholipid: diacylglycerol acyltransferase: an enzyme that catalyzes the acyl-CoA-independent formation of triacylglycerol in yeast and plants. *Proceedings of the National Academy of Sciences*, 97(12), 6487-6492.
- DeBono, A., Yeats, T. H., Rose, J. K., Bird, D., Jetter, R., Kunst, L., & Samuels, L. (2009). Arabidopsis LTPG is a glycosylphosphatidylinositol-anchored lipid transfer protein required for export of lipids to the plant surface. *The Plant Cell*, 21(4), 1230-1238.
- Dubois, A. (2020). Compositional analysis of the *Nicotiana tabacum* stigma cuticle [Unpublished bachelor's thesis]. Algoma University.
- Dumas, C., Rougier, M., Zandonella, P., Ciampolini, F., Cresti, M., & Pacini, E. (1978). The secretory stigma in *Lycopersicon peruvianum* Mill.: ontogenesis and glandular activity. *Protoplasma*, 96, 173-187.
- Eastmond, P. J. (2004). Glycerol-insensitive Arabidopsis mutants: gli1 seedlings lack glycerol kinase, accumulate glycerol and are more resistant to abiotic stress. *The Plant Journal*, 37(4), 617-625.
- Edstam, M. M., Viitanen, L., Salminen, T. A., & Edqvist, J. (2011). Evolutionary history of the non-specific lipid transfer proteins. *Molecular plant*, 4(6), 947-964.
- Fabre, G., Garroum, I., Mazurek, S., Daraspe, J., Mucciolo, A., Sankar, M., ... & Nawrath, C. (2016). The ABCG transporter PEC1/ABCG32 is required for the formation of the developing leaf cuticle in Arabidopsis. *New Phytologist*, 209(1), 192-201.
- Fahn, A. (1988). Secretory tissues in vascular plants. *New phytologist*, 108(3), 229-257.
- Fich, E. A., Segerson, N. A., & Rose, J. K. (2016). The plant polyester cutin: biosynthesis, structure, and biological roles. *Annual review of plant biology*, 67, 207-233.
- Folch, J., Lees, M., & Sloane Stanley, G. H. (1957). A simple method for the isolation and purification of total lipids from animal tissues. *J Biol Chem*, 226(1), 497-509.
- Gaydou, E. M., Lozano, Y., & Ratovohery, J. (1987). Triglyceride and fatty acid compositions in the mesocarp of *Persea americana* during fruit development. *Phytochemistry*, 26(6), 1595-1597.
- Girard, A. L., Mounet, F., Lemaire-Chamley, M., Gaillard, C., Elmorjani, K., Vivancos, J., ... & Bakan, B. (2012). Tomato GDSL1 is required for cutin deposition in the fruit cuticle. *The Plant Cell*, 24(7), 3119-3134.
- Goldman, M. D., Pezzotti, M., Seurinck, J., & Mariani, C. (1992). Developmental expression of tobacco pistil-specific genes encoding novel extensin-like proteins. *The Plant Cell*, 4(9), 1041-1051.
- Graca, J., & Lamosa, P. (2010). Linear and branched poly (ω -hydroxyacid) esters in plant cutins. *Journal of agricultural and food chemistry*, 58(17), 9666-9674.

- Graça, J., Schreiber, L., Rodrigues, J., & Pereira, H. (2002). Glycerol and glyceryl esters of ω -hydroxyacids in cutins. *Phytochemistry*, 61(2), 205-215.
- Gray, G. M. (1967). Chromatography of lipids. II. The quantitative isolation of the minor (acidic) phospholipids and of phosphatidylethanolamine from the lipid extracts of mammalian tissues. *Biochimica et Biophysica Acta (BBA)-Lipids and Lipid Metabolism*, 144(3), 519-524.
- Griffiths, G., & Harwood, J. L. (1991). The regulation of triacylglycerol biosynthesis in cocoa (*Theobroma cacao*) L. *Planta*, 184, 279-284.
- Griffiths, G., Stymne, S., & Stobart, A. K. (1988). Phosphatidylcholine and its relationship to triacylglycerol biosynthesis in oil-tissues. *Phytochemistry*, 27(7), 2089-2093.
- Gutsche, C. D. (2004). The reaction of diazomethane and its derivatives with aldehydes and ketones. *Organic Reactions*, 8, 364-430.
- Hamberg, M., Liepinsh, E., Otting, G., & Griffiths, W. (1998). Isolation and structure of a new galactolipid from oat seeds. *Lipids*, 33(4), 355-363.
- Han, J., Clement, J. M., Li, J., King, A., Ng, S., & Jaworski, J. G. (2010). The cytochrome P450 CYP86A22 is a fatty acyl-CoA ω -hydroxylase essential for estolide synthesis in the stigma of *Petunia hybrida*. *Journal of Biological Chemistry*, 285(6), 3986-3996.
- Hara, A., & Radin, N. S. (1978). Lipid extraction of tissues with a low-toxicity solvent. *Analytical biochemistry*, 90(1), 420-426.
- Harlow, R. D., Litchfield, C., Fu, H. C., & Reiser, R. (1965). The triglyceride composition of *Myrica carolinensis* fruit coat fat (bayberry tallow). *Journal of the American Oil Chemists Society*, 42, 747-750.
- Hayes, D. G., & Kleiman, R. (1995). Lipase-catalyzed synthesis and properties of estolides and their esters. *Journal of the American Oil Chemists' Society*, 72, 1309-1316.
- Hayes, D. G., Kleiman, R., & Phillips, B. S. (1995). The triglyceride composition, structure, and presence of estolides in the oils of *Lesquerella* and related species. *Journal of the American Oil Chemists' Society*, 72(5), 559-569.
- Heslop-Harrison, Y., & Shivanna, K. R. (1977). The receptive surface of the angiosperm stigma. *Annals of botany*, 41(6), 1233-1258.
- Higgins, C. F. (1992). ABC transporters: from microorganisms to man. *Annual review of cell biology*, 8(1), 67-113.
- Hoffmann-Benning, S., & Kende, H. (1994). Cuticle biosynthesis in rapidly growing internodes of deepwater rice. *Plant Physiology*, 104(2), 719-723.
- Holloway, P. J. (1982). Chemical constitution of plant cutins. In *Linnean Society symposium series*.

- Hong, L., Brown, J., Segerson, N. A., Rose, J. K., & Roeder, A. H. (2017). CUTIN SYNTHASE 2 maintains progressively developing cuticular ridges in Arabidopsis sepals. *Molecular Plant*, 10(4), 560-574.
- Isbell, T. A. (2011). Chemistry and physical properties of estolides. *grasas y aceites*, 62(1), 8-20.
- Isbell, T. A., Edgcomb, M. R., & Lowery, B. A. (2001). Physical properties of estolides and their ester derivatives. *Industrial Crops and Products*, 13(1), 11-20.
- Isbell, T. A., Lowery, B. A., DeKeyser, S. S., Winchell, M. L., & Cermak, S. C. (2006). Physical properties of triglyceride estolides from lesquerella and castor oils. *Industrial crops and products*, 23(3), 256-263.
- Jakobson, L., Lindgren, L. O., Verdier, G., Laanemets, K., Brosché, M., Beisson, F., & Kollist, H. (2016). BODYGUARD is required for the biosynthesis of cutin in Arabidopsis. *New Phytologist*, 211(2), 614-626.
- Jeffree, C. E. (2006). The fine structure of the plant cuticle. In 'Biology of the plant cuticle'. (Eds M Riederer, C Müller) pp. 11–125.
- Jenkin, S., & Molina, I. (2015). Isolation and compositional analysis of plant cuticle lipid polyester monomers. *JoVE (Journal of Visualized Experiments)*, (105), e53386.
- Jetter, R., Kunst, L., & Samuels, A. L. (2006). Composition of plant cuticular waxes. *Annual plant reviews volume 23: Biology of the plant cuticle*, 145-181.
- Jiang, W., Li, C., Li, Y., & Peng, H. (2022). Metabolic Engineering Strategies for Improved Lipid Production and Cellular Physiological Responses in Yeast *Saccharomyces cerevisiae*. *Journal of Fungi*, 8(5), 427.
- Kajdas, C., Karpińska, A., & Kulczycki, A. (2010). Industrial lubricants. Chemistry and technology of lubricants, 239-292.
- Kalla, R., Shimamoto, K., Potter, R., Nielsen, P. S., Linnestad, C., & Olsen, O. A. (1994). The promoter of the barley aleurone-specific gene encoding a putative 7 kDa lipid transfer protein confers aleurone cell-specific expression in transgenic rice. *The Plant Journal*, 6(6), 849-860.
- Koiwai, K., & Matsuzaki, T. (1988). Hydroxy and normal fatty acid distribution in stigmas of *Nicotiana* and other plants. *Phytochemistry*, 27(9), 2827-2830.
- Kolattukudy, P. T. (1981). Structure, biosynthesis, and biodegradation of cutin and suberin. *Annual Review of plant physiology*, 32(1), 539-567.
- Konar, R. N., & Linskens, H. F. (1966). The morphology and anatomy of the stigma of *Petunia hybrida*. *Planta*, 71, 356-371.
- Kotapati, H. K., & Bates, P. D. (2021). 14C-Tracing of Lipid Metabolism Lipid metabolism. In *Plant Lipids: Methods and Protocols* (pp. 59-80). New York, NY: Springer US.

- Kumar, A., Kalra, B., Dekhterman, A., & Gross, R. A. (2000). Efficient Ring-Opening Polymerization and Copolymerization of ϵ -Caprolactone and ω -Pentadecalactone Catalyzed by *Candida antarctica* Lipase B. *Macromolecules*, 33(17), 6303-6309.
- Kunst, L., Jetter, R., & Samuels, A. L. (2008). Biosynthesis and transport of plant cuticular waxes. *Annual Plant Reviews*, 23, 182-215.
- Kurdyukov, S., Faust, A., Nawrath, C., Bar, S., Voisin, D., Efremova, N., ... & Yephremov, A. (2006). The epidermis-specific extracellular BODYGUARD controls cuticle development and morphogenesis in *Arabidopsis*. *The Plant Cell*, 18(2), 321-339.
- Lal, K., & Carrick, V. (1994). Performance testing of lubricants based on high oleic vegetable oils. *Journal of synthetic lubrication*, 11(3), 189-206.
- Landgraf, R., Smolka, U., Altmann, S., Eschen-Lippold, L., Senning, M., Sonnewald, S., ... & Rosahl, S. (2014). The ABC transporter ABCG1 is required for suberin formation in potato tuber periderm. *The Plant Cell*, 26(8), 3403-3415.
- Lashbrooke, J., Cohen, H., Levy-Samocho, D., Tzfadia, O., Panizel, I., Zeisler, V., ... & Aharoni, A. (2016). MYB107 and MYB9 homologs regulate suberin deposition in angiosperms. *The Plant Cell*, 28(9), 2097-2116.
- Lazar, Z., Liu, N., & Stephanopoulos, G. (2018). Holistic approaches in lipid production by *Yarrowia lipolytica*. *Trends in biotechnology*, 36(11), 1157-1170.
- Lee, J., Welti, R., Schapaugh, W. T., & Trick, H. N. (2011). Phospholipid and triacylglycerol profiles modified by PLD suppression in soybean seed. *Plant biotechnology journal*, 9(3), 359-372.
- Lee, S. B., Go, Y. S., Bae, H. J., Park, J. H., Cho, S. H., Cho, H. J., ... & Suh, M. C. (2009). Disruption of glycosylphosphatidylinositol-anchored lipid transfer protein gene altered cuticular lipid composition, increased plastoglobules, and enhanced susceptibility to infection by the fungal pathogen *Alternaria brassicicola*. *Plant Physiology*, 150(1), 42-54.
- Li, X., Teitgen, A. M., Shirani, A., Ling, J., Busta, L., Cahoon, R. E., ... & Cahoon, E. B. (2018). Discontinuous fatty acid elongation yields hydroxylated seed oil with improved function. *Nature plants*, 4(9), 711-720.
- Li, Y., Beisson, F., Koo, A. J., Molina, I., Pollard, M., & Ohlrogge, J. (2007). Identification of acyltransferases required for cutin biosynthesis and production of cutin with suberin-like monomers. *Proceedings of the National Academy of Sciences*, 104(46), 18339-18344.
- Li, Y., Beisson, F., Pollard, M., & Ohlrogge, J. (2006). Oil content of *Arabidopsis* seeds: the influence of seed anatomy, light and plant-to-plant variation. *Phytochemistry*, 67(9), 904-915.
- Li-Beisson, Y., Shorrosh, B., Beisson, F., Andersson, M. X., Arondel, V., Bates, P. D., ... & Ohlrogge, J. (2013). Acyl-lipid metabolism. *The Arabidopsis book/American Society of Plant Biologists*, 11.

- Lin, J. T., Arcinas, A., Harden, L. R., & Fagerquist, C. K. (2006). Identification of (12-ricinoleoylricinoleoyl) diricinoleoylglycerol, an acylglycerol containing four acyl chains, in castor (*Ricinus communis* L.) oil by LC-ESI-MS. *Journal of agricultural and food chemistry*, 54(10), 3498-3504.
- Lin, J. T., Turner, C., Liao, L. P., & McKeon, T. A. (2003). Identification and quantification of the molecular species of acylglycerols in castor oil by HPLC using ELSD. *Journal of liquid chromatography & related technologies*, 26(5), 773-780.
- Lu, C., Xin, Z., Ren, Z., Miquel, M., & Browse, J. (2009). An enzyme regulating triacylglycerol composition is encoded by the ROD1 gene of Arabidopsis. *Proceedings of the National Academy of Sciences*, 106(44), 18837-18842.
- Ma, X., Koepke, J., Panjekar, S., Fritsch, G., & Stöckigt, J. (2005). Crystal structure of vinorine synthase, the first representative of the BAHD superfamily. *Journal of Biological Chemistry*, 280(14), 13576-13583.
- Mackenzie, S. M., Howells, A. J., Cox, G. B., & Ewart, G. D. (2000). Sub-cellular localisation of the white/scarlet ABC transporter to pigment granule membranes within the compound eye of *Drosophila melanogaster*. *Genetica*, 108, 239-252.
- Maharjan, S. (2022). Microscopic characterization of lipid polyesters in developing stigmas of *Nicotiana tabacum* and *Petunia hybrida* [Unpublished bachelor's thesis]. Algoma University.
- Matsuzaki, T., Koiwai, A., & Kawashima, N. (1983a). Changes in stigma-specific lipids of tobacco plant during flower development. *Plant and Cell Physiology*, 24(2), 207-213.
- Matsuzaki, T., Koiwai, A., & Kawashima, N. (1983b). Isolation of tetra-, penta-, hexa- and heptaacyl glycerides from stigmas of *Nicotiana tabacum*. *Agricultural and Biological Chemistry*, 47(1), 77-82.
- Matsuzaki, T., Koiwai, A., & Kawashima, N. (1983c). Total fatty acid and polar lipid content in developing flower of *Nicotiana tabacum*. *Plant and cell physiology*, 24(2), 199-206.
- Matsuzaki, T., Koiwai, A., & Kubo, S. (1986). 1, 3-diacylglycerol and 1, 2-diacylglycerol types of multiacylglycerol in stigma lipids of tobacco. *Agricultural and biological chemistry*, 50(6), 1581-1587.
- Matsuzaki, T., Koiwai, A., Iwai, S., & Yamada, Y. (1984). In vitro proliferation of stigma-like, style-like structures of *Nicotiana tabacum* and its fatty acid composition. *Plant and cell physiology*, 25(2), 197-203.
- Mattson, F. H., & Volpenhein, R. A. (1962). Synthesis and properties of glycerides. *Journal of Lipid Research*, 3(3), 281-296.
- McDowell, S. C., Lopez-Marques, R. L., Poulsen, L. R., Palmgren, M. G., & Harper, J. F. (2013). Loss of the Arabidopsis thaliana P4-ATPase ALA3 reduces adaptability to temperature stresses and impairs vegetative, pollen, and ovule development. *PLoS One*, 8(5), e62577.

- McFarlane, H. E., Watanabe, Y., Yang, W., Huang, Y., Ohlrogge, J., & Samuels, A. L. (2014). Golgi-and trans-Golgi network-mediated vesicle trafficking is required for wax secretion from epidermal cells. *Plant physiology*, *164*(3), 1250-1260.
- Miklaszewska, M., Zienkiewicz, K., Inchana, P., & Zienkiewicz, A. (2021). Lipid metabolism and accumulation in oilseed crops. *OCL*, *28*, 50.
- Mikolajczak, K. L., & Smith Jr, C. R. (1968). Penta-acid triglycerides of *Chamaepeuce afra* seed oil. *Biochimica et Biophysica Acta (BBA)-Lipids and Lipid Metabolism*, *152*(2), 244-254.
- Miwa, T. K. (1971). Jojoba oil wax esters and derived fatty acids and alcohols: gas chromatographic analyses. *Journal of the American Oil Chemists' Society*, *48*(6), 259-264.
- Molina I, Bourgault R. Poster presentation at the International Symposium on Plant Lipids, Goettingen, Germany, July 8-13 2016.
- Molina, I., Bonaventure, G., Ohlrogge, J., & Pollard, M. (2006). The lipid polyester composition of *Arabidopsis thaliana* and *Brassica napus* seeds. *Phytochemistry*, *67*(23), 2597-2610.
- Moreau, R. A., & Stumpf, P. K. (1981). Recent studies of the enzymic synthesis of ricinoleic acid by developing castor beans. *Plant Physiology*, *67*(4), 672-676.
- Moreau, R. A., Doehlert, D. C., Welti, R., Isaac, G., Roth, M., Tamura, P., & Nunez, A. (2008). The identification of mono-, di-, tri-, and tetragalactosyl-diacylglycerols and their natural estolides in oat kernels. *Lipids*, *43*, 533-548.
- Morris, L. J., & Hall, S. W. (1966). The structure of the glycerides of ergot oils. *Lipids*, *1*(3), 188-196.
- Nakai, K., & Horton, P. (1999). PSORT: a program for detecting sorting signals in proteins and predicting their subcellular localization. *Trends in biochemical sciences*, *24*(1), 34-35.
- Neumann, J., Rose-Sperling, D., & Hellmich, U. A. (2017). Diverse relations between ABC transporters and lipids: An overview. *Biochimica et Biophysica Acta (BBA)-Biomembranes*, *1859*(4), 605-618.
- Nuyken, O., & Pask, S. D. (2013). Ring-opening polymerization—an introductory review. *Polymers*, *5*(2), 361-403.
- Ohlrogge, J., & Browse, J. (1995). Lipid biosynthesis. *The Plant Cell*, *7*(7), 957.
- Okuley, J., Lightner, J., Feldmann, K., Yadav, N., Lark, E., & Browse, J. (1994). *Arabidopsis* FAD2 gene encodes the enzyme that is essential for polyunsaturated lipid synthesis. *The Plant Cell*, *6*(1), 147-158.
- Ollivier, D., Artaud, J., Pinatel, C., Durbec, J. P., & Guèrère, M. (2003). Triacylglycerol and fatty acid compositions of French virgin olive oils. Characterization by chemometrics. *Journal of agricultural and food chemistry*, *51*(19), 5723-5731.

- Otsu, C. T., Dasilva, I., De Molfetta, J. B., Da Silva, L. R., de Almeida-Engler, J., Engler, G., ... & Goldman, M. H. S. (2004). NtWBC1, an ABC transporter gene specifically expressed in tobacco reproductive organs. *Journal of experimental botany*, *55*(403), 1643-1654.
- Panikashvili, D., Shi, J. X., Schreiber, L., & Aharoni, A. (2009). The Arabidopsis DCR encoding a soluble BAHD acyltransferase is required for cutin polyester formation and seed hydration properties. *Plant physiology*, *151*(4), 1773-1789.
- Panikashvili, D., Shi, J. X., Schreiber, L., & Aharoni, A. (2011). The Arabidopsis ABCG13 transporter is required for flower cuticle secretion and patterning of the petal epidermis. *New Phytologist*, *190*(1), 113-124.
- Philippe, G., De Bellis, D., Rose, J. K., & Nawrath, C. (2022). Trafficking processes and secretion pathways underlying the formation of plant cuticles. *Frontiers in Plant Science*, 2817.
- Piffanelli, P., Ross, J. H., & Murphy, D. J. (1997). Intra- and extracellular lipid composition and associated gene expression patterns during pollen development in *Brassica napus*. *The Plant Journal*, *11*(3), 549-562.
- Pollard, M., Beisson, F., Li, Y., & Ohlrogge, J. B. (2008). Building lipid barriers: biosynthesis of cutin and suberin. *Trends in plant science*, *13*(5), 236-246.
- Pollard, M., Delamarter, D., Martin, T. M., & Shachar-Hill, Y. (2015). Lipid labeling from acetate or glycerol in cultured embryos of *Camelina sativa* seeds: a tale of two substrates. *Phytochemistry*, *118*, 192-203.
- Pryde, E. H. (1980). Composition of soybean oil. *Handbook of soy oil processing and utilization*, 13-31.
- Pyee, J., Yu, H. S., & Kolattukudy, P. E. (1994). Identification of a lipid transfer protein as the major protein in the surface wax of broccoli (*Brassica oleracea*) leaves. *Archives of Biochemistry and Biophysics*, *311*(2), 460-468.
- Rajiah, A., Subbaram, M. R., & Achaya, K. T. (1976). Contribution towards the glyceride structure of Kamala seed oil. *Lipids*, *11*(2), 87-92.
- Rautengarten, C., Ebert, B., Ouellet, M., Nafisi, M., Baidoo, E. E., Benke, P., ... & Scheller, H. V. (2012). Arabidopsis deficient in cutin ferulate encodes a transferase required for feruloylation of ω -hydroxy fatty acids in cutin polyester. *Plant Physiology*, *158*(2), 654-665.
- Roughan, P. G., Holland, R., & Slack, C. R. (1980). The role of chloroplasts and microsomal fractions in polar-lipid synthesis from [1-¹⁴C] acetate by cell-free preparations from spinach (*Spinacia oleracea*) leaves. *Biochemical Journal*, *188*(1), 17-24.
- Samuels, L., Kunst, L., & Jetter, R. (2008). Sealing plant surfaces: cuticular wax formation by epidermal cells. *Annu. Rev. Plant Biol.*, *59*, 683-707.
- Schaff, J. E., Mbeunkui, F., Blackburn, K., Bird, D. M., & Goshe, M. B. (2008). SILIP: a novel stable isotope labeling method for in planta quantitative proteomic analysis. *The Plant Journal*, *56*(5), 840-854.

- Schmitz, G., Langmann, T., & Heimerl, S. (2001). Role of ABCG1 and other ABCG family members in lipid metabolism. *Journal of lipid research*, 42(10), 1513-1520.
- Shakya, R., & Bhatla, S. C. (2010). A comparative analysis of the distribution and composition of lipidic constituents and associated enzymes in pollen and stigma of sunflower. *Sexual plant reproduction*, 23, 163-172.
- Sharma, B., & Bhatla, S. C. (2014). Elemental and biochemical markers of stigma receptivity in sunflower. *Acta Physiologiae Plantarum*, 36, 1299-1311.
- Sharma, S., Gangal, S., & Rauf, A. (2009). Lipase mediated hydrolysis of *Mimusops elengi* and *Parkinsonia aculeata* seed oils for the determination of positional distribution of fatty acids. *Industrial Crops and Products*, 30(2), 325-328.
- Shepherd, R. W., Bass, W. T., Houtz, R. L., & Wagner, G. J. (2005). Phylloplanins of tobacco are defensive proteins deployed on aerial surfaces by short glandular trichomes. *The Plant Cell*, 17(6), 1851-1861.
- Simpson, J. P., & Ohlrogge, J. B. (2016). A novel pathway for triacylglycerol biosynthesis is responsible for the accumulation of massive quantities of glycerolipids in the surface wax of bayberry (*Myrica pensylvanica*) fruit. *The Plant Cell*, 28(1), 248-264.
- Simpson, J. P., Thrower, N., & Ohlrogge, J. B. (2016). How did nature engineer the highest surface lipid accumulation among plants? Exceptional expression of acyl-lipid-associated genes for the assembly of extracellular triacylglycerol by Bayberry (*Myrica pensylvanica*) fruits. *Biochimica et Biophysica Acta (BBA)-Molecular and Cell Biology of Lipids*, 1861(9), 1243-1252.
- Slack, C. R., Bertaud, W. S., Shaw, B. D., Holland, R., Browse, J., & Wright, H. (1980). Some studies on the composition and surface properties of oil bodies from the seed cotyledons of safflower (*Carthamus tinctorius*) and linseed (*Linum usitatissimum*). *Biochemical Journal*, 190(3), 551-561.
- Slack, C. R., Campbell, L. C., Browse, J. A., & Roughan, P. G. (1983). Some evidence for the reversibility of the cholinephosphotransferase-catalysed reaction in developing linseed cotyledons in vivo. *Biochimica et Biophysica Acta (BBA)-Lipids and Lipid Metabolism*, 754(1), 10-20.
- Slack, C. R., Roughan, P. G., & Balasingham, N. (1978). Labelling of glycerolipids in the cotyledons of developing oilseeds by [1-14C] acetate and [2-3H] glycerol. *Biochemical Journal*, 170(2), 421-433.
- Slack, C. R., Roughan, P. G., & Balasingham, N. A. T. H. A. N. (1977). Labelling studies in vivo on the metabolism of the acyl and glycerol moieties of the glycerolipids in the developing maize leaf. *Biochemical Journal*, 162(2), 289-296.
- Slack, C. R., Roughan, P. G., Browse, J. A., & Gardiner, S. E. (1985). Some properties of cholinephosphotransferase from developing safflower cotyledons. *Biochimica et Biophysica Acta (BBA)-Lipids and Lipid Metabolism*, 833(3), 438-448.
- Smirnov, B. P. (1960). Biosynthesis of higher fatty acids from acetate in isolated chloroplasts of *Spinacia oleracea* leaves. *Biochimica*, 25.

- Smith, M. A., & Zhang, H. (2016). Apocynaceae seed lipids: characterization and occurrence of isoricinoleic acid and triacylglycerol estolides. *Journal of the American Oil Chemists' Society*, 93, 105-114.
- Smith, M. A., Zhang, H., Forseille, L., & Purves, R. W. (2013). Characterization of novel triacylglycerol estolides from the seed oil of *Mallotus philippensis* and *Trewia nudiflora*. *Lipids*, 48, 75-85.
- Soni, S., & Agarwal, M. (2014). Lubricants from renewable energy sources—a review. *Green Chemistry letters and reviews*, 7(4), 359-382.
- Sperling, P., Linscheid, M., Stöcker, S., Mühlbach, H. P., & Heinz, E. (1993). In vivo desaturation of cis-delta 9-monounsaturated to cis-delta 9, 12-diunsaturated alkenylether glycerolipids. *Journal of Biological Chemistry*, 268(36), 26935-26940.
- Sprecher, H. W., Maier, R., Barber, M., & Holman, R. T. (1965). Structure of an optically active allene-containing tetraester triglyceride isolated from the seed oil of *Sapium sebiferum*. *Biochemistry*, 4(9), 1856-1863.
- Stahl, U., Banas, A., & Stymne, S. (1995). Plant microsomal phospholipid acyl hydrolases have selectivities for uncommon fatty acids. *Plant Physiology*, 107(3), 953-962.
- Stymne, S., & Stobart, A. K. (1984). Evidence for the reversibility of the acyl-CoA: lysophosphatidylcholine acyltransferase in microsomal preparations from developing safflower (*Carthamus tinctorius* L.) cotyledons and rat liver. *Biochemical Journal*, 223(2), 305-314.
- Suh, M. C., Samuels, A. L., Jetter, R., Kunst, L., Pollard, M., Ohlrogge, J., & Beisson, F. (2005). Cuticular lipid composition, surface structure, and gene expression in *Arabidopsis* stem epidermis. *Plant physiology*, 139(4), 1649-1665.
- van de Pas, D. J., Nanayakkara, B., Suckling, I. D., & Torr, K. M. (2014). Comparison of hydrogenolysis with thioacidolysis for lignin structural analysis. *Holzforschung*, 68(2), 151-155.
- Verrier, P. J., Bird, D., Burla, B., Dassa, E., Forestier, C., Geisler, M., ... & Theodoulou, F. L. (2008). Plant ABC proteins—a unified nomenclature and updated inventory. *Trends in plant science*, 13(4), 151-159.
- Vogel, G., & Browse, J. (1996). Cholinephosphotransferase and diacylglycerol acyltransferase (substrate specificities at a key branch point in seed lipid metabolism). *Plant Physiology*, 110(3), 923-931.
- Vogt, T., Pollak, P., Tarlyn, N., & Taylor, L. P. (1994). Pollination-or wound-induced kaempferol accumulation in petunia stigmas enhances seed production. *The Plant Cell*, 6(1), 11-23.
- Wagner, G. J. (1991). Secreting glandular trichomes: more than just hairs. *Plant physiology*, 96(3), 675-679.
- Wakelin, A. M., & Leung, D. W. M. (2009). β -1, 3-Glucanase activity in the stigma of healthy petunia flowers. *Biologia plantarum*, 53, 69-74.

- Walton, T. J., & Kolattukudy, P. E. (1972). Determination of the structures of cutin monomers by a novel depolymerization procedure and combined gas chromatography and mass spectrometry. *Biochemistry*, 11(10), 1885-1897.
- Wang, E., Wang, R., DeParasis, J., Loughrin, J. H., Gan, S., & Wagner, G. J. (2001). Suppression of a P450 hydroxylase gene in plant trichome glands enhances natural-product-based aphid resistance. *Nature biotechnology*, 19(4), 371-374.
- Wang, G., Cho, Y.-H., Keifer, J., Ohlrogge, J. & Pollard, M. The structure and biosynthesis of the lipid polyesters in stigma exudates of tobacco and petunia. *Symposium on the Biochemistry and Molecular Biology of Plant Fatty acids and Glycerolipids*. Fallen Leaf Lake, California, USA (2003).
- Wang, K., Durrett, T. P., & Benning, C. (2019). Functional diversity of glycerolipid acylhydrolases in plant metabolism and physiology. *Progress in Lipid Research*, 75, 100987.
- Wang, Y., Zhu, Z., Xia, Y., Zhong, M., Ma, R., Zhao, Y., ... & Zhou, Y. (2021). Accessing the position-specific 18O/16O ratios of lignin monomeric units from higher plants with highly selective hydrogenolysis followed by GC/Py/IRMS analysis. *Analytica Chimica Acta*, 1171, 338667.
- Weiss, S. B., & Kennedy, E. P. (1956). The enzymatic synthesis of triglycerides. *Journal of the American Chemical Society*, 78(14), 3550-3550.
- Weiss, S. B., Kennedy, E. P., & Kiyasu, J. Y. (1960). The enzymatic synthesis of triglycerides. *Journal of Biological Chemistry*, 235(1), 40-44.
- Wilson, J. A., Hopkins, S. A., Wright, P. M., & Dove, A. P. (2014). 'Immortal' ring-opening polymerization of ω -pentadecalactone by Mg (BHT) 2 (THF) 2. *Polymer Chemistry*, 5(8), 2691-2694.
- Wolters-Arts, M., Lush, W. M., & Mariani, C. (1998). Lipids are required for directional pollen-tube growth. *Nature*, 392(6678), 818-821.
- Wu, Z., Zhang, Q., Li, N., Pu, Y., Wang, B., & Zhang, T. (2017). Comparison of critical methods developed for fatty acid analysis: A review. *Journal of separation science*, 40(1), 288-298.
- Xiao, F., Mark Goodwin, S., Xiao, Y., Sun, Z., Baker, D., Tang, X., ... & Zhou, J. M. (2004). Arabidopsis CYP86A2 represses *Pseudomonas syringae* type III genes and is required for cuticle development. *The EMBO journal*, 23(14), 2903-2913.
- Xin, A., & Fry, S. C. (2021). Cutin: xyloglucan transacylase (CXT) activity covalently links cutin to a plant cell-wall polysaccharide. *Journal of Plant Physiology*, 262, 153446.
- Yadav, V., Molina, I., Ranathunge, K., Castillo, I. Q., Rothstein, S. J., & Reed, J. W. (2014). ABCG transporters are required for suberin and pollen wall extracellular barriers in Arabidopsis. *The Plant Cell*, 26(9), 3569-3588.
- Yang, W., Pollard, M., Li-Beisson, Y., & Ohlrogge, J. (2016). Quantitative analysis of glycerol in dicarboxylic acid-rich cutins provides insights into Arabidopsis cutin structure. *Phytochemistry*, 130, 159-169.

- Yang, Z., & Ohlrogge, J. B. (2009). Turnover of fatty acids during natural senescence of Arabidopsis, Brachypodium, and switchgrass and in Arabidopsis β -oxidation mutants. *Plant Physiology*, 150(4), 1981-1989.
- Yanni, J. (2023). Regiochemical Analysis of Nicotiana tabacum Stigma Lipid Polyesters to Determine Estolide Position [Unpublished bachelor's thesis]. Algoma University.
- Yeats, T. H., Howe, K. J., Matas, A. J., Buda, G. J., Thannhauser, T. W., & Rose, J. K. (2010). Mining the surface proteome of tomato (*Solanum lycopersicum*) fruit for proteins associated with cuticle biogenesis. *Journal of Experimental Botany*, 61(13), 3759-3771.
- Yeats, T. H., Martin, L. B., Viart, H. M., Isaacson, T., He, Y., Zhao, L., ... & Rose, J. K. (2012). The identification of cutin synthase: formation of the plant polyester cutin. *Nature Chemical Biology*, 8(7), 609-611.
- Yen, C. L. E., & Farese, R. V. (2003). MGAT2, a monoacylglycerol acyltransferase expressed in the small intestine. *Journal of Biological Chemistry*, 278(20), 18532-18537.
- Yen, C. L. E., Stone, S. J., Cases, S., Zhou, P., & Farese Jr, R. V. (2002). Identification of a gene encoding MGAT1, a monoacylglycerol acyltransferase. *Proceedings of the National Academy of Sciences*, 99(13), 8512-8517.
- Zaderimowski, R., & Sosulski, F. (1978). Composition of total lipids in rapeseed. *Journal of the American Oil Chemists' Society*, 55(12), 870-872.
- Zerkowski, J. A. (2008). Estolides: From structure and function to structured and functionalized. *Lipid technology*, 20(11), 253-256.
- Zhong, Z., Dijkstra, P. J., & Feijen, J. (2000). Controlled ring-opening polymerization of ω -pentadecalactone with yttrium isopropoxide as an initiator. *Macromolecular chemistry and physics*, 201(12), 1329-1333.